Ferrocene-containing β-diketones derived from lactones: Synthesis, complexation with rhodium(I), electrochemistry and substitution kinetics

A dissertation submitted in accordance with the requirements for the degree

Magister Scientiae

in the

Department of Chemistry
Faculty of Natural and Agricultural Sciences

at the

University of the Free State

by

Lydia Siegert

Supervisor

Prof. J.C. Swarts

Acknowledgments

I would hereby like to thank all the people who made this project possible:

- My supervisor, Prof. J.C. Swarts for his guidance throughout my studies, his support and motivation in both scientific and personal matters and the time devoted to my project.

- My husband, Uwe Siegert, for all your help with the project and support during my studies. Thank you for all the hours you spent collecting all my NMR data, helping so much with structures and always giving advice when I was stuck. Thank you for your unwavering love and patience.

- The Physical Chemistry Group who helped me through my studies. Thanks for your friendship and support.

- My family and friends for motivation and support.

- Dr. M. Landman from the Chemistry Department of the University of Pretoria for the data collection and refinement of the crystal structure.

- The Chemistry department and the University of the Free State for available facilities.

- The National Research Foundation for funding.

Abstract

New ferrocene-containing β-diketones of the form $FcCOCH_2CO(CH_2)_nOH$ (Fc = ferrocenyl) where n = 3 [pK_a' = 5.97], 4 [pK_a' = 8.01] and 5 [pK_a' = 10.44] were prepared by the Claisen condensation of acetyl ferrocene and the appropriate cyclic ester under the influence of lithium diisopropylamide. The rate of conversion of $FcCOCH_2CO(CH_2)_5OH$ from the enol to the keto form and *vice versa* was studied and the kinetic parameters determined. All β-diketones were also reacted with $[Rh_2(COD)_2Cl_2]$ to yield the [Rh(β-diketonato)(COD)] complexes $[Rh(FcCOCHCO(CH_2)_nOH)(COD)]$ where n = 3, 4 and 5.

The group electronegativity of the alcohol side chains was determined by the linear relationship between the methyl or ethyl ester (RCOOMe or RCOOEt) infrared carbonyl stretching frequencies and the group electronegativities of known R groups, R = CF_3, CCl_3, CH_3, C_6H_5 and Fc.

A cyclic voltammetry study of the free β-diketones showed chemical and quasi-electrochemically reversible behaviour for the iron core in the free β-diketones with side-chain lengths of 3, 4 and 5 carbons with $E^{0'}$ = 197 mV, 174 mV and 151 mV respectively. Electrochemical and chemical reversibility were observed for the ferrocene moiety during the study of the [Rh(β-diketonato)(COD)] complexes. It was found that the rhodium centre of the rhodium complexes exhibited two coordination numbers. A 4-coordinate rhodium redox centre was observed with $i_{pc}/i_{pa.}$ >1 and ΔE < 100 mV. Electrochemical evidence of a 5-coordinate rhodium centre by virtue of interaction between the OH-endgroups of the side-chain of the β-diketonato ligand and the rhodium centre, was observed.

Substitution of the β-diketonato ligand from the [Rh(β-diketonato)(COD)] complexes with 1,10-phenanthroline in methanol was also studied and the kinetic parameters determined. Large negative activation entropy values were obtained; these suggested an associative substitution mechanism. All substitution reactions had observable mechanistic solvent pathway contributions.

Keywords: metallocenes, β-diketones, rhodium, isomerization kinetics, cyclic voltammetry, substitution kinetics

Opsomming

Deur middel van Claisen-kondensasie van asetielferroseen met die ooreenstemmende sikliese esters onder die invloed van litiumdiisopropielamied, is nuwe ferroseen-bevattende β-diketone, $FcCOCH_2CO(CH_2)_nOH$ (Fc=ferroseniel) waar n = 3 [pK_a' = 5.97], 4 [pK_a' = 8.01] en 5 [pK_a' = 10.44], gesintetiseer. Die reaksie tempo van omskakeling vanaf die enol vorm na die keto toestand en ook omgekeerd is betudeer vir $FcCOCH_2CO(CH_2)_5OH$ met behulp van ^1H KMR spektroskopie. Kinetiese parameters is dus bereken. Die rhodium komplekse, [$Rh(FcCOCHCO(CH_2)_nOH)(COD)$] waar n = 3, 4 en 5, is berei deur die ooreenstemmende β-diketoon met [$Rh_2(COD)_2Cl_2$] te reageer.

Die skynbare groep elektronegatiwiteite van die alkohol sy-kettings is bepaal vanaf die lineêre verband tussen die metiel of etiel esters (RCOOMe of RCOOEt) se infrarooi karbonielstrekkingsfrekwensies en die groep elektronegatiwiteit van bekende R groepe, R = CF_3, CCl_3, CH_3, C_6H_5 en Fc.

Die sikliese voltammetries bepaalde formele reduksiepotensiale, $E^{0'}$, vir die ferrosenielgroep van die β-diketone met sy-ketting lengtes van 3, 4 en 5 koolstowwe is gevind as $E^{0'}$ = 197 mV, 174 mV en 151 mV onderskeidelik. Chemiese en quasi-elektrochemiese omkeerbaarheid is bevind. Tydens die elektrochemiese studie van die [Rh(β-diketonato)(COD)] komplekse, is chemiese en elektrochemiese omkeerbaarheid vir die ferroseniel groep opgemerk. Dit is gevind dat die rhodium kern in die rhodium komplekse twee verskillende koördinasie getalle openbaar: ‘n 4-gekoördineerde rhodium redoks paar is waargeneem met $i_{pc}/i_{pa.}$ >1 en ΔE < 100 mV, en as gevolg van interaksie tussen die OH terminale groep en die rhodium kern, is ‘n 5-gekoördineerde rhodium redoks paar ook waargeneem.

Substitusiekinetika van die bidentate β-diketone in die [Rh(β-diketonato)(COD)] komplekse met behulp van 1,10-fenantrolien is spektrofotometries (UV/vis) ondersoek. Relatiewe groot aktiveringsentropie dui op ‘n assoiatiewe meganisme. Alle substitusie reaksies het ‘n beduidende oplosmiddelroete komponent in die meganisme getoon.

Table of Contents

List of Structures

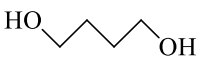

1

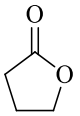

2

3

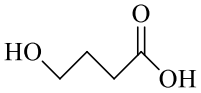

4

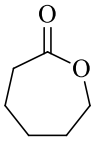

5

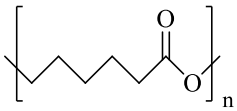

6

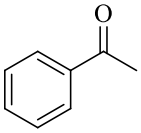

7

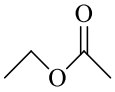

8

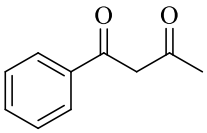

9

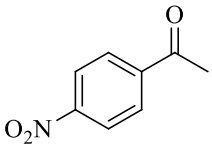

10

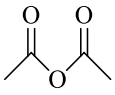

11

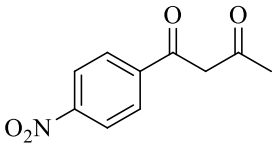

12

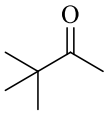

13

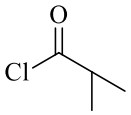

14

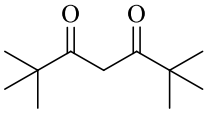

15

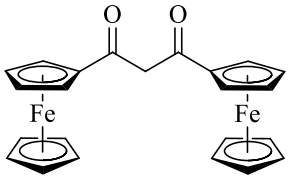

16

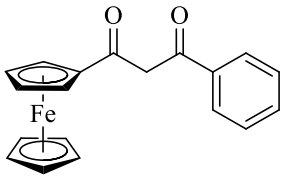

17

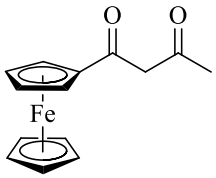

18

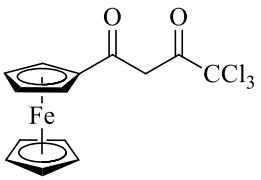

19

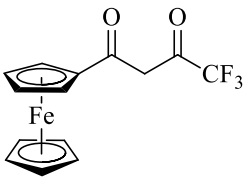

20

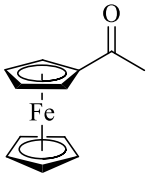

21

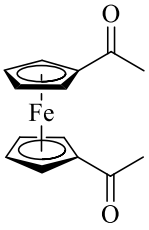

22

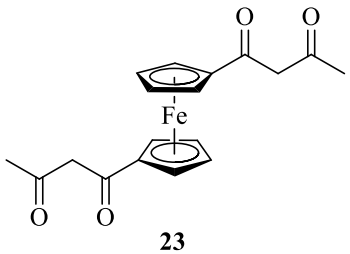

23

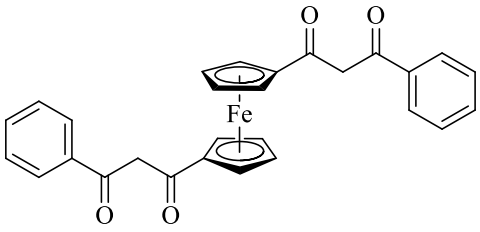

24

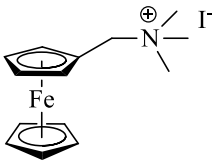

25

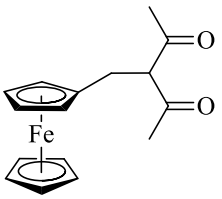

26

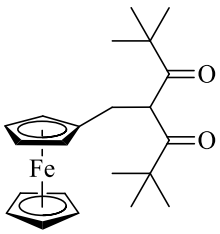

27

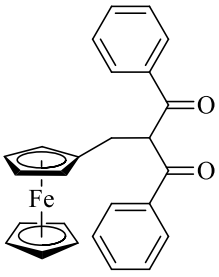

28

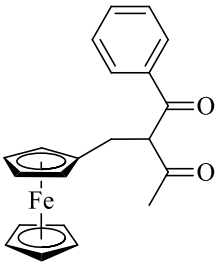

29

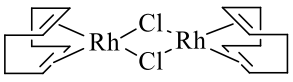

30

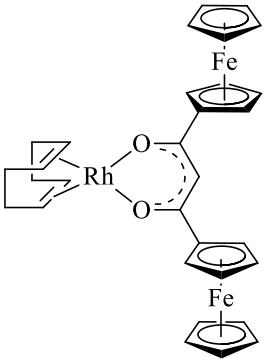

31

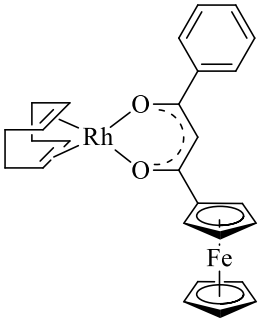

32

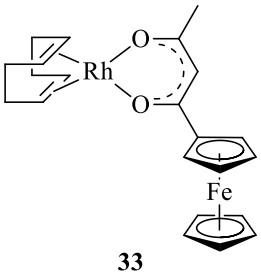

33

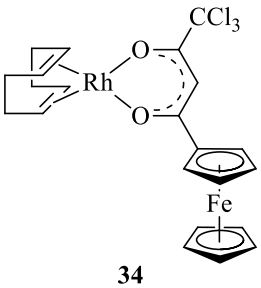

34

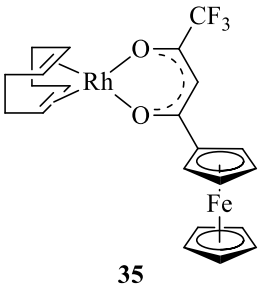

35

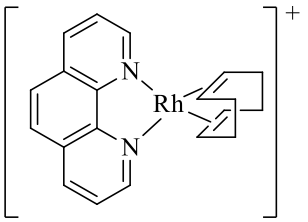

36

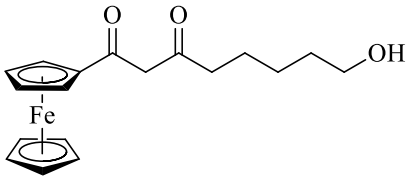

37

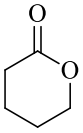

38

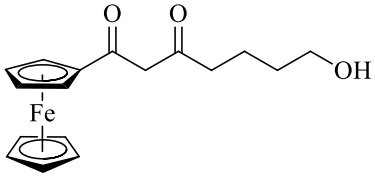

39

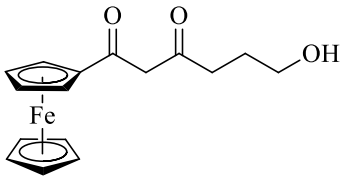

40

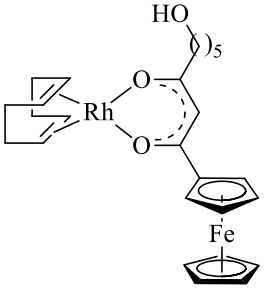

41

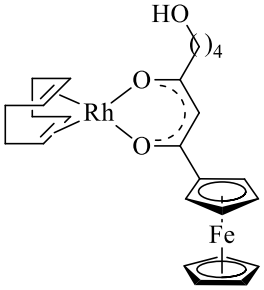

42

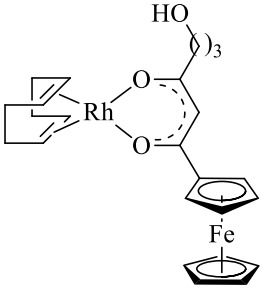

43

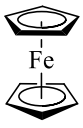

44

List of Abbreviations

A	associative mechanism
CMOS	complementary metal-oxide semiconductor
COD	1,5-cyclooctadiene
Cp	cyclopentadienyl, (C_5H_5)
CV	cyclic voltammogram/voltammetry
D	dissosiative mechanism
DCM	dichloromethane
DMF	dimethylformamide
DMSO	dimethyl sulfoxide
$E^{0'}$	formal reduction potential
E_{pa}	peak anodic potential
E_{pc}	peak cathodic potential
Fc	ferrocenyl, $Fe^{II}(\eta^5\text{-}C_5H_5)(\eta^5\text{-}C_5H_4)$
Fc^+	ferrocenium, $[Fe^{III}(\eta^5\text{-}C_5H_5)_2]^+$
FcH	ferrocene, $Fe^{II}(\eta^5\text{-}C_5H_5)_2$
^{1}H NMR	proton nuclear magnetic resonance
i_{pa}	peak anodic current
i_{pc}	peak cathodic current
IR	infrared
LDA	lithium diisopropylamide
LSV	linear sweep voltammogram/voltammetry
NHE	normal hydrogen electrode
phen	1,10-phenanthroline
SCE	saturated calomel electrode
SWV	square wave voltammogram/voltammetry
TBAHFP	tetrabuthylammonium hexafluorophosphate
X	substitution leaving ligand
Y	substitution entering ligand
ΔE	difference between anodic and cathodic peak potentials
μ	ionic strength

λ_{exp}	wavelength at which experiment is performed
λ_{max}	wavelength with maximum absorption

1 Introduction and aims to this study

1.1 Introduction

In this project, alcohol-functionalized ferrocene-containing β-diketones and their complexes with rhodium(I) were studied.

Since the first characterization of ferrocene in 1952, it has become a well-known and widely used organometallic compound.[1] Ferrocene and the derivatives thereof have many uses such as catalysts,[2] anticancer drugs[3] and as fuel additives.[4]

β-diketones with a ferrocenyl moiety have been well studied and were found to have a wide range of uses ranging from biomedical applications to being used as ligands in metal complexes for catalysis.[5] β-diketones easily coordinate as ligands to metal centres and these complexes have potential for various uses. One such metal is rhodium.

Rhodium compounds are widely used as catalysts[6] and for biomedical purposes.[7] In the Monsanto process methanol is converted to acetic acid with the aid of a rhodium catalyst.[8] Rhodium(I) complexes are used in the hydrogenation of alkenes[9] and rhodium(I) complexes of ferrocene containing β-diketonates have been extensively studied for use as anticancer drugs.[10]

Most neutral organometallic compounds are poorly soluble in aqueous medium,[11] and therefore a need arose to synthesize better soluble compounds if used in biological environments. β-diketones containing a hydroxy group could potentially show better solubility[12] as well as providing an additional reactive site through the O donor atom.

1.2 Aims

With this background, the following goals were set for this study:

1. Optimized synthesis of new ferrocenyl β-diketones $FcCOCH_2CO(CH_2)_nOH$ where n = 3, 4 and 5.
2. Complexation of these β-diketones with rhodium(I) to obtain complexes of the type $[Rh(FcCOCHCO(CH_2)_nOH)(COD)]$ where n = 3, 4 and 5.
3. Solving the single crystal X-ray structure of $FcCOCH_2CO(CH_2)_3OH$.
4. Determination of the rates of conversion between the enol and keto isomers of the new β-diketones of goal 1 by means of NMR spectroscopy.
5. Determining the pK_a' values of the β-diketones of goal 1.
6. Performing an electrochemical study on the new β-diketones and the corresponding rhodium(I) complexes.
7. Determination of the mechanism of substitution of the β-diketonato ligand in [Rh(β-diketonato)(COD)] with 1,10-phenantroline by means of a stopped flow kinetic study.

Bibliography

(1) Wilkinson, G.; Rosenblum, M.; Whiting, M. C.; Woodward, R. B. *J. Am. Chem. Soc.* **1952**, *74* (8), 2125–2126.

(2) Sinditskii, V. P.; Chernyi, A. N.; Marchenkov, D. A. *Combust. Explos. Shock Waves* **2014**, *50* (2), 158–167.

(3) Ornelas, C. *New J. Chem.* **2011**, *35* (10), 1973–1985.

(4) Emel'yanov, V. E.; Simonenko, L. S.; Skvortsov, V. N. *Chem. Technol. Fuels Oils* **2001**, *37* (4), 224–228.

(5) Conradie, J.; Lamprecht, G. J.; Roodt, A.; Swarts, J. C. *Polyhedron* **2007**, *26* (17), 5075–5087.

(6) Cullen, W. R.; Wickenheiser, E. B. *J. Organomet. Chem.* **1989**, *370* (1–3), 141–154.

(7) McCully, K. S.; Vezeridis, M. P. *Cancer Invest.* **1987**, *5* (1), 25–30.

(8) Forster, D. In *Advances in Organometallic Chemistry*; West, F. G. A. S. and R., Ed.; Catalysis and Organic Syntheses; Academic Press, 1979; Vol. 17, pp 255–267.

(9) Osborn, J. A.; Jardine, F. H.; Young, J. F.; Wilkinson, G. *J. Chem. Soc. Inorg. Phys. Theor.* **1966**, 1711–1732.

(10) Swarts, J. C.; Vosloo, T. G.; Cronje, S. J.; Plessis, W. C. (Ina) D.; Rensburg, C. E. J. V.; Kreft, E.; Lier, J. E. V. *Anticancer Res.* **2008**, *28* (5A), 2781–2784.

(11) Breno, K. L.; Ahmed, T. J.; Pluth, M. D.; Balzarek, C.; Tyler, D. R. *Coord. Chem. Rev.* **2006**, *250* (9–10), 1141–1151.

(12) Horváth, I. T.; Joó, F. *Aqueous Organometallic Chemistry and Catalysis*; Springer Science & Business Media, 2012.

2 Literature survey

2.1 Introduction

This chapter provides a short literature review on the topics relevant to this study. The synthesis of β-diketones, complexation with rhodium and characteristics of these types of compounds are covered in this chapter. Some aspects of kinetics and electrochemistry are also discussed.

2.2 Synthesis

2.2.1 Chemistry of lactones

Lactones are cyclic esters of hydrocarboxylic acids that occur in nature.[1] This group of compounds includes a large number of well-known chemical compounds such as vitamin C,[2] perfume ingredients such as pentadecanolide and ambrettolide[3] and it is even the building blocks for numerous antibiotics.[4] Simple lactones such as γ-butyrolactone are also often used as solvent.[2]

Lactones can be synthesized (Scheme 2.1) by dehydrogenation of a diol,[5] oxidation of a cyclic ether[6] or the intramolecular esterification of an hydroxycarboxylic acid.[7] Lactones are synthesized by enzymes in nature[8] and can also be synthesized by modified enzymes.[7]

Lactones can be broken down in various ways, the easiest being hydrolization in the presence of a base such as sodium hydroxide that will yield an aliphatic hydroxyl acid.[9] In an acidic solution the lactone will only partially cleave leading to polimerization[10] and in the case of the presence of a non-nucleophylic base such as lithium diisopropylamide the carbon α to the carbonyl is deprotonated and a polyester is formed.[11] One well known polymer of lactones is polycaprolactone made of ε-caprolactone (Scheme 2.2).[10]

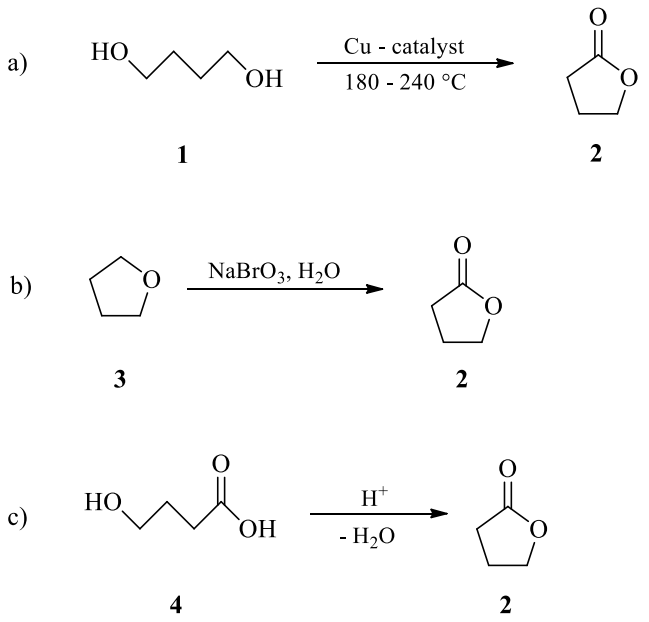

Scheme 2.1: Methods of synthesizing lactones; a) Dehydrogenation of a diol with a copper catalyst,[5] b) Oxidation of a cyclic ether with the aid of a base; [6] c) Acid catalyzed esterification of a hydroxycarboxylic acid[7]

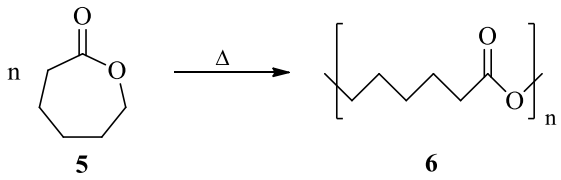

Scheme 2.2: Thermal polymerisation of ε-caprolactone [12]

2.2.2 β-diketones

β-diketone compounds, such as acetyl acetone, have a number of interesting and specific properties due to the presence of two β-positioned carbonyl groups causing them to be

valuable substrates in many chemical syntheses.[13] Substituents can be introduced without lowering the activity of the compound in further synthesis, making it an easy method of introducing different active groups in a complex.[14] Owing to their properties, β-diketones and their complexes have been used both in science and in industry, such as polymer chemistry,[15] healthcare[16] and environmental protection due to the chelating properties.[17]

β-diketones can be synthesized by a number of methods such as the acylation of ketones with esters,[18] acid anhydrides[19] or acid chlorides[20] in the presence of a base or Lewis acid (Scheme 2.3).

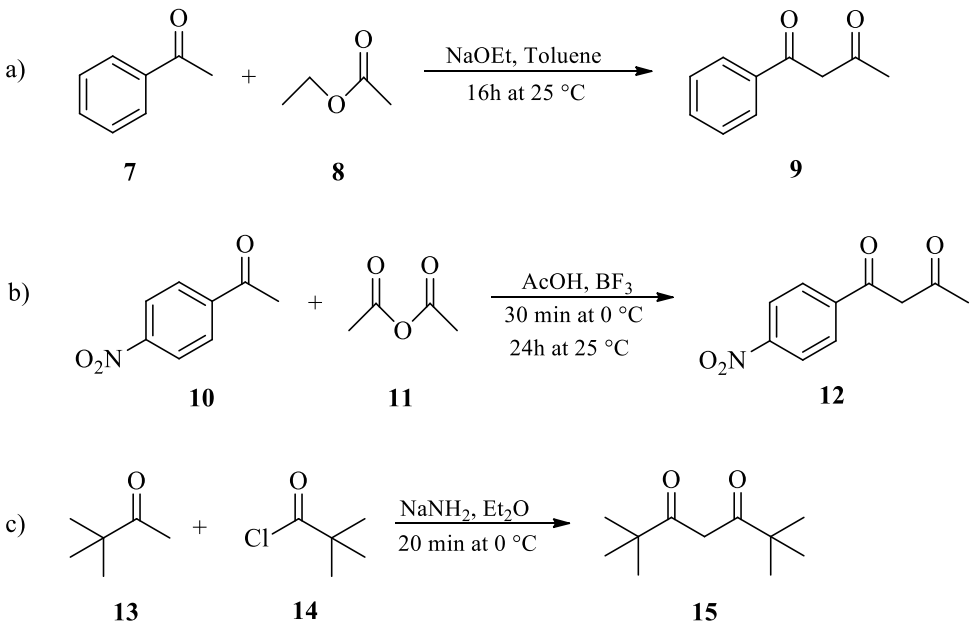

Scheme 2.3: Synthesis of β-diketones using different methods; a) Reaction of a ketone with an ester in the presence of a base;[18] b) The reaction between a ketone and an acid anhydride;[19] c) Reaction of a ketone with an acid chloride[20]

The most common method of synthesis of β-diketones is Claisen condensation where the ketone is reacted with a suitable acylation reagent in the presence of a base. The mechanism consists of three steps, as shown in Scheme 2.4.[21]

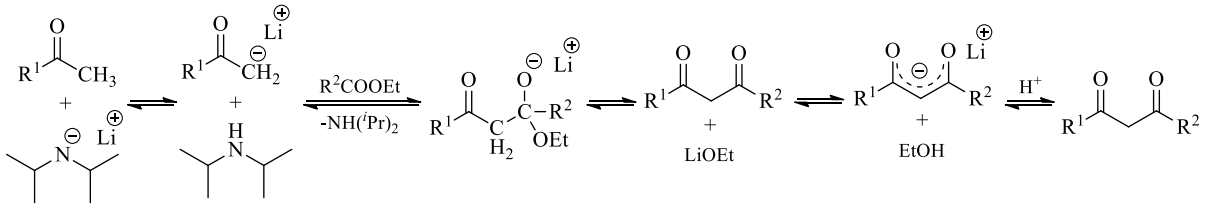

Scheme 2.4: The mechanism for the formation of β-diketones by the acylation of a ketone with an ester in the presence of lithium diisopropylamide

This mechanism involves the removal of a proton from the α-carbon of the ketone by the base to form a carbanion stabilized by Li^+. This negatively charged CH_2 species then attacks the carbonyl carbon of the ester, and a β-diketone is formed as well as LiOEt. The LiOEt in the solution then reacts with the diketone to form a β-diketonato anion and only after acidifying the solution can the β-diketone be isolated (Scheme 2.4).

2.2.3 Metallocene β-diketones

A sandwiched metallocene is an organometallic molecule where two negatively charged cyclopentadienyl rings are bound to a metallic cation.[22] Of these, the most well-know example is ferrocene, as it and derivatives thereof have many uses as a ligand on catalysts,[23] anticancer drugs[24] and as fuel additives.[25]

β-diketones containing a ferrocene moiety have been extensively studied, varying the functional groups on the β-diketone as shown in Scheme 2.5.[26]

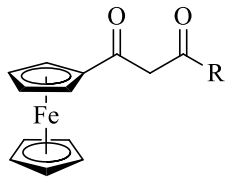

R = ferrocenyl (**16**)
phenyl (**17**)
CH_3 (**18**)
CCl_3 (**19**)
CF_3 (**20**)

Scheme 2.5: A few ferrocene containing β-diketones with different side functionalities[26]

The above mentioned β-diketones have been studied as anticancer drugs with positive results,[27] as well as used as ligands on catalysts such as square planar rhodium catalysts for the Monsanto process of converting methanol to acetic acid.[28,29]

Ferrocene containing β-diketones are usually formed by reacting acetyl ferrocene with the suitable ester *via* Claisen condensation,[26] or reacting a di-acetyl ferrocene with an ester to form a bis-β-diketone, see Scheme 2.6.[30,31]

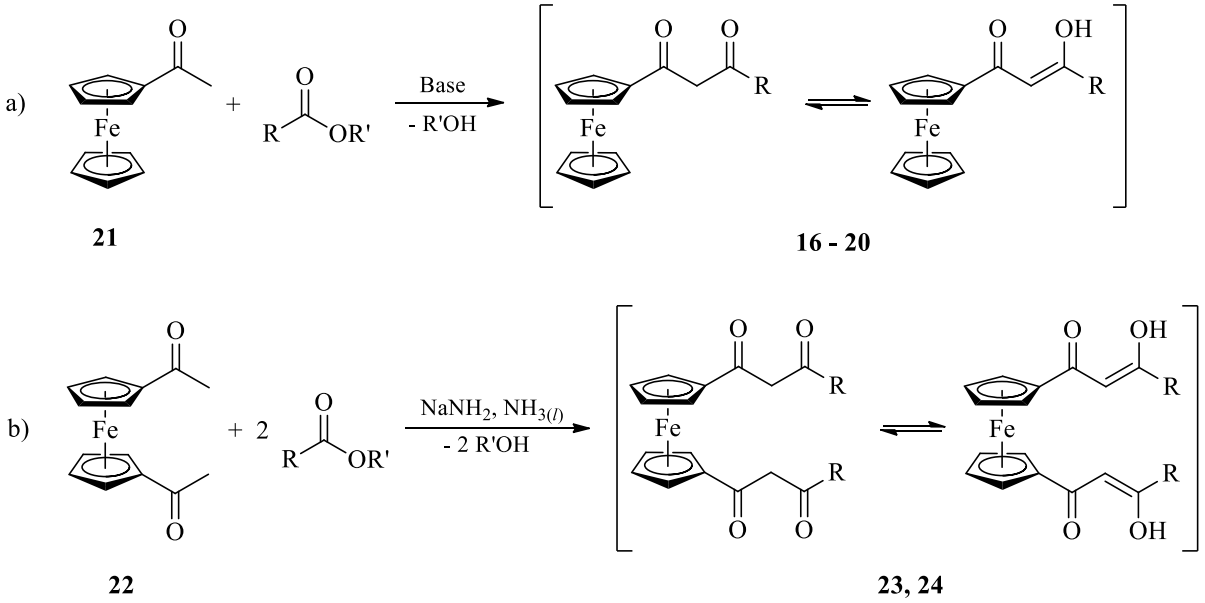

Scheme 2.6: Synthesis of β-diketones containing ferrocene; a) Mono-substituted ferrocene β-diketones *via* a basic route where R is ferrocene **(16)**, phenyl **(17)**, methyl **(18)**, trichloromethyl **(19)** or trifluoromethyl **(20)**; [26] b) Di-substituted ferrocene β-diketone synthesis where R is methyl **(23)** or phenyl **(24)**[30,31]

Other methods of introducing ferrocene into the β-diketone pseudo-aromatic backbone exists such as ferrocenyl substitution in the methine or α-position.[32] This is done by reacting (ferrocenylmethyl)-trimethylammonium iodide with salts of different β-diketones.

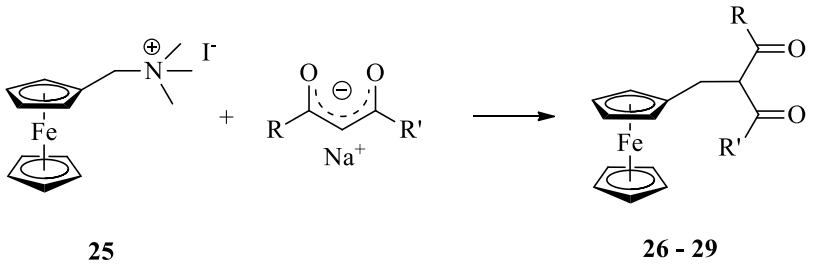

Scheme 2.7: Synthesis of α-substituted β-diketones where R=R′ is CH_3 **(26)**; $C(CH_3)_3$ **(27)**; Ph **(28)** or R is Ph and R′ is CH_3 **(29)**.

2.2.4 Metal complexes of β-diketones

The strong chelating tendency of β-diketone ligands led to the synthesis of a number of neutral coordinated complexes.[33] These bidentate ligands react with metals of different oxidation states as shown in Scheme 2.8.

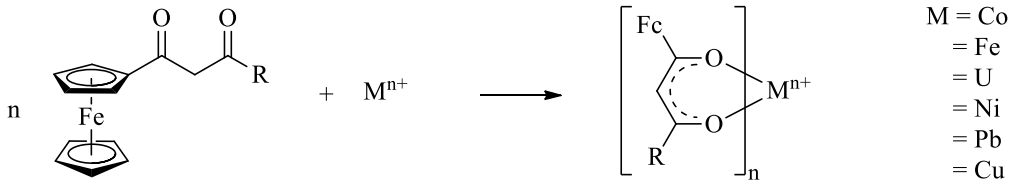

Scheme 2.8: Examples of complexes with β-diketones containing ferrocene where n can be 1,2,3 or 4[34]

β-diketonato complexes with rhodium are easy to prepare and have many uses in many different fields.[35] Rhodium is of the platinum group metals, and is well known for many uses in industry.[36] Rhodium exists in a number of oxidative states, 0, I, II and III being the most common. Rhodium complexes are often used as catalysts such as $[RhH(CO)(PPh_3)_3]$ as a hydroformylation catalyst,[37] $[RhCl(PPh_3)_3]$ as a hydrogenation catalyst[38] and $[Rh(CO)_2I_2]^-$ as a carbonylation catalyst.[39] Rhodium complexes also have uses in medicinal areas, and have been mainly used against cancer.[40]

Rhodium (I) complexes containing β-diketonato ligands and cyclooctadiene can easily and in good yield be synthesized from $[Rh_2Cl_2(COD)_2]$ as shown in Scheme 2.9. This is usually an intermediate for synthesis of $[Rh(\beta\text{-diketonato})(CO)_2]$ complexes. The cyclooctadiene ligand can easily be displaced by two carbon monoxide molecules.[41]

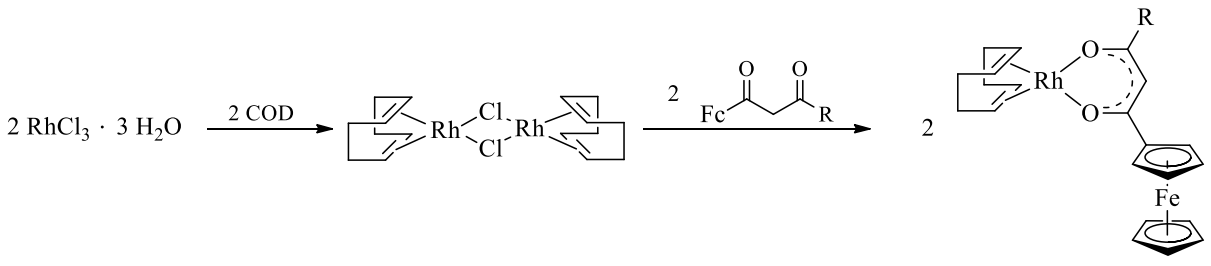

30 **31 - 35**

Scheme 2.9: Synthetic route for the synthesis of [Rh(β-diketonato)(COD)] complexes where R is ferrocene **(31)**, phenyl **(32)**, methyl **(33)**, trichloromethyl **34)** or trifluoromethyl **(35)**

2.3 Keto-enol tautomerism of β-diketones

β-diketones display an equilibrium between keto and enol isomers.[42] It has been found that although two enol forms are possible, the isomer with the OH-group furthest from the ferrocene moiety is dominant for ferrocene containing β-diketones.[7]

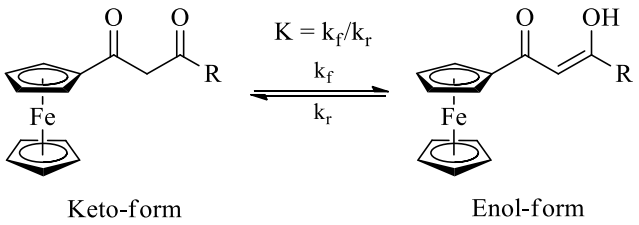

Scheme 2.10: Keto-enol tautomerism of ferrocene-containing β-diketones

The proportion of tautomers present is greatly influenced by electronic properties of the substituents, the size of the substituents, thus steric effect, as well as solvent and temperature.[26]

The equilibrium constant associated with this equilibrium can be determined with a range of methods, such as bromine titration,[43] ultraviolet spectroscopy,[44] infrared spectroscopy[45] etc., but the easiest method is by NMR as this can be done without affecting the equilibrium itself.[46] For such a study the β-diketone can be reacted with a base such as NaOH. The resulting β-diketonato anion will be predominantly in the keto form. After acidification the formation of the enol form of the neutralized β-diketone can then be monitored.[47] This method is not suitable for β-diketones that are sensitive to prolonged basic conditions. It also was found that in the solid state, the β-diketone will be converted mainly to the enol form given enough time.[47] When dissolved, the formation of the keto form can be monitored over time utilizing NMR until equilibrium is reached. For compounds where both the acidic and basic approach can be used, the resulting rate constants may be used to determine the equilibrium constant, K, of the keto-enol equilibrium.[47]

$$forward\ rate = reverse\ rate$$

$$k_f[keto] = k_r[enol]$$

$$\frac{[enol\ ]}{[keto\ ]} = \frac{k_f}{k_r}$$

$$K = \frac{[enol\ form\ ]}{[keto\ form]} = \frac{k_f}{k_r}$$

eq. 2.1

At equilibrium, the forward rate and reverse rate will be the same. In equation 2.1, k_f is the rate constant for the forward reaction in Scheme 2.10, and k_r is the rate constant for the reverse reaction.

In recent years computational chemistry has been implemented to study equilibrium constants by calculating the theoretical constant based on the structure and electronic properties of the β-diketone and comparing it with the experimental results.[48]

2.4 Acid dissociation constants

2.4.1 Introduction

When a weak acid is ionized, the acid will be in equilibrium with the corresponding conjugated base. This reaction's equilibrium constant is also known as the acid dissociation constant or K_a[49] The acid dissociation constant is applicable to the following reaction:

$$HA_{(aq)} + H_2O_{(l)} \rightleftharpoons H_3O^+{}_{(aq)} + A^-{}_{(aq)}$$

From equilibrium principle, a general equilibrium constant K_c may be defined as:

$$K_c = \frac{[H_3O^+][A^-]}{[HA][H_2O]}$$

By assigning $K_a = K_c\,[H_2O]$, it follows that

$$K_a = \frac{[H^+][A^-]}{[HA]}$$

By operating logarithms on both side of the equation, we obtain:

$$logK_a = \log[H^-] + log\frac{[A^-]}{[HA]}$$

As log K_a can be expressed as pK_a and log[H^+] as pH, it follows that

$$pK_a = pH + log\frac{[HA]}{[A^-]}$$

eq. 2.2

The pK_a value of a compound yields valuable information regarding the form the compound will be in at a given pH. pK_a values are especially vital for medicinal compounds, as pH in the body varies from blood to cells and therefor the molecule will be in different forms depending on the area of the body it is introduced to.[50] Ionization of any compound will increase the solubility in water, but decrease the lipophilicity.[51] In pharmaceutical cases the concentration of a compound in the blood can be adjusted by choosing derivatives with different pK_a's of an ionizable group, and drug availability can thus be controlled.[52] pK_a values are also important when synthesising complexes. The pK_a value of a ligand can influence the ease of complexation and also affects the most suitable pH at which the reaction will take place.[53]

2.4.2 Methods of determining acid dissociation constants

The most common method of determining an acid dissociation constant is to monitor an acid base titration by spectroscopy and potentiometry.[54] The absorbance data is collected as a function of the pH, and a least square fitting of the absorbance/pH data by equation 2.3 yields the pK_a value.[55]

$$A_T = \frac{A_{HA}10^{-pH} + A_A10^{-pK_a}}{10^{-pH} + 10^{-pK_a}}$$

eq. 2.3

In equation 2.3, A_T = total absorption, A_{HA} = absorption of the free acid and A_A = absorption of the deprotonated species.

2.4.3 β-diketone acid dissociation constants

pK_a values of β-diketone keto- and enol-tautomers are difficult to separate, and due to this the symbol pK_a' is rather used implying that it is the observed pK_a of a solution consisting of a mixture of keto and enol isomers.[56] The reaction that takes place is shown in Scheme 2.11.

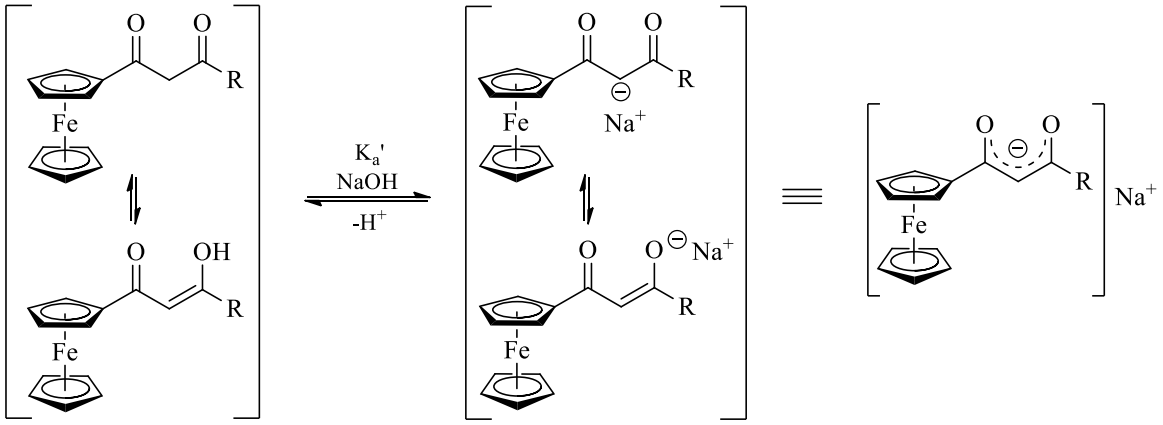

Scheme 2.11: The reaction that takes place during base titrations of β-diketones or acid titrations of β-diketonates.

pK_a' values of ferrocene containing β-diketones **16-19** were determined as shown in Figure 2.1 and listed in Table 2.1.

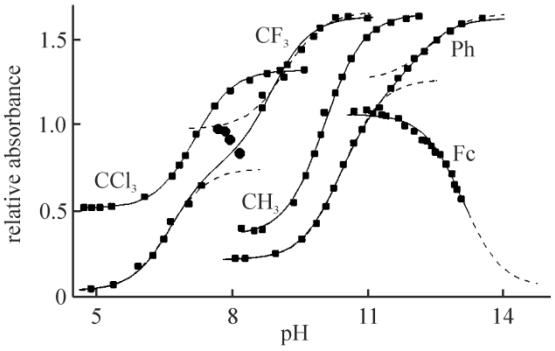

Figure 2.1: S-curves for the change of absorbance due to change in pH for ferrocene containing β-diketones[26]

Table 2.1: pK_a' values (In water containing 10% acetonitrile, I = 0.1 mol.dm^{-3} ($NaClO_4$)) and % enol tautomer (determined in $CDCl_3$) of ferrocene β-diketones **16-19**[26]

R-group	% Enol	pK_a
Fc	>99	13.1
Ph	≈95	10.41
CH_3	86	10.01
CCl_3	≈95	7.13
CF_3	>99	6.56

2.5 Electroanalytical chemistry

2.5.1 Introduction

By understanding a compound's electrochemical behaviour, much can be learned about possible reactions and how the compound will behave in oxidative or reductive environments.[57] In this study cyclic voltammetry (CV), square wave voltammetry (SW) and linear sweep voltammetry (LSV) was utilized to determine the electrochemical nature of the compounds. These methods are summarized in Figure 2.2.

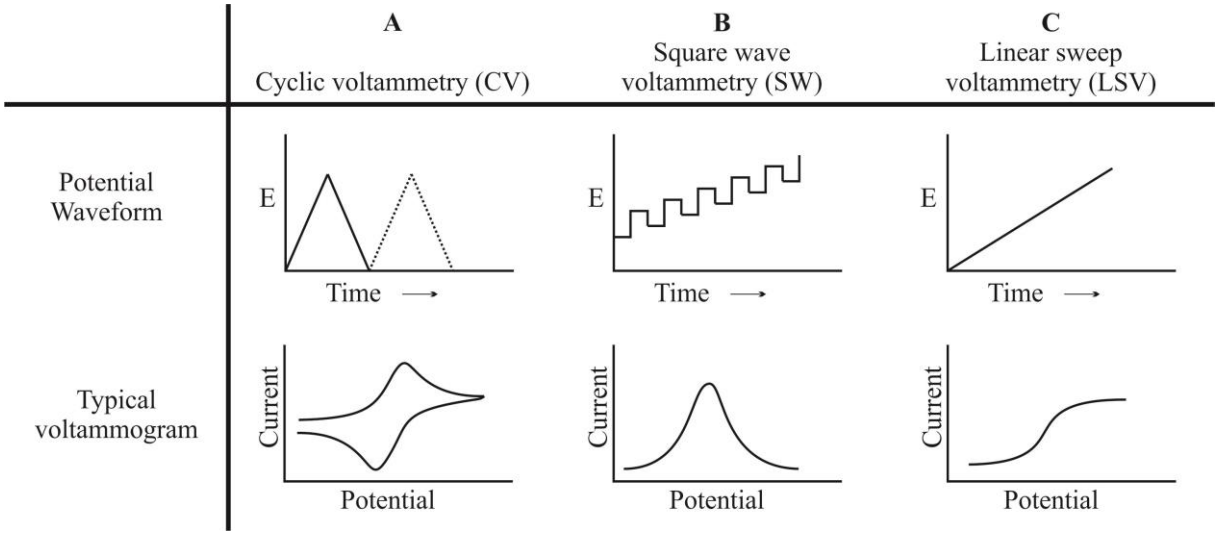

Figure 2.2: Methods used in voltammetry

2.5.2 Cyclic voltammetry

Cyclic voltammetry is an easy, but versatile method of studying electro-active species. This is due to the ability to view the behaviour of the specie over a wide potential range in a very short period of time, especially if the oxidised and reduced forms are relatively unstable over long periods of time.[58]

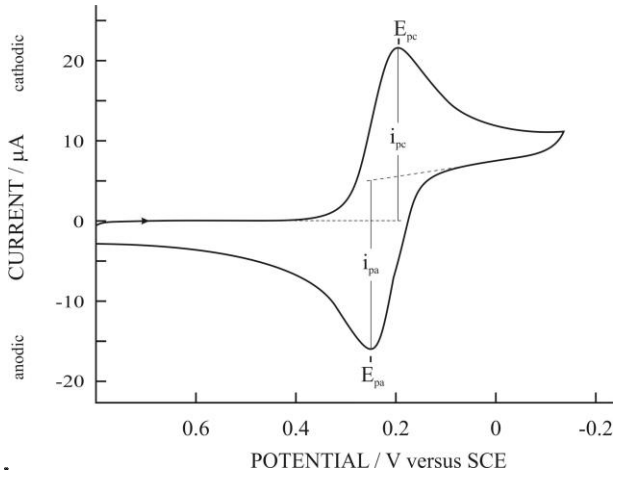

Figure 2.3: Cyclic voltammogram of 6 mM $K_3Fe(CN)_6$ in 1 M aqueous KNO_3. Scan initiated at 0.8 V versus SCE in anegative direction at 50 mV/s utilizing a platinum workingelectrode

Cyclic voltammetry implies the measuring of the current that flows due to the changing of the potential of an electrode (the working electrode) in a solution. The potential of the working electrode is referenced against a reference electrode such as a saturated calomel electrode

(SCE), silver/silver chloride electrode (Ag/AgCl) or a silver or platinum wire. A voltammogram such as shown in Figure 2.3 is then obtained.[58]

The peak anodic potential (E_{pa}), peak cathodic potential (E_{pc}) and the peak anodic current (i_{pa}) and peak cathodic current (i_{pc}) are the crucial parameters to be obtained from a voltammogram as shown in Figure 2.3.[58] For a one-electron electrochemical reversible redox couple the difference in peak potentials (ΔE_p) should theoretically be 59 mV at 25 °C. n in the equation below is the number of electrons involved in the redox process.

$$\Delta E_p = E_{pa} - E_{pc} \approx \frac{0.059\,V}{n}$$

and the formal reduction potential is midway between the two peak potentials,

$$E^{o'} = \frac{(E_{pa} + E_{pc})}{2}$$

For a chemically reversible processes exhibiting fast electron transfer kinetics between electrode and substrate, i.e. electrochemically reversible couple, i_{pa} and i_{pc} should be equal. This implies

$$\frac{i_{pa}}{i_{pc}} = 1$$

2.5.3 Aspects that influence voltammograms

2.5.3.1 Solvent system

Traditionally $(CH_3)_2SO$ (DMSO) and CH_3CN were favourite solvents for non-aqueous electrochemical experimentation, but as both can coordinate to metals to form new species, favour has moved to other solvents.[28] This interaction can be reduced by using the non-coordinating CH_2Cl_2 (DCM), but this has a drawback since the solvent potential window does not tolerate strong oxidizing or reducing conditions (See Figure 2.4).[59]

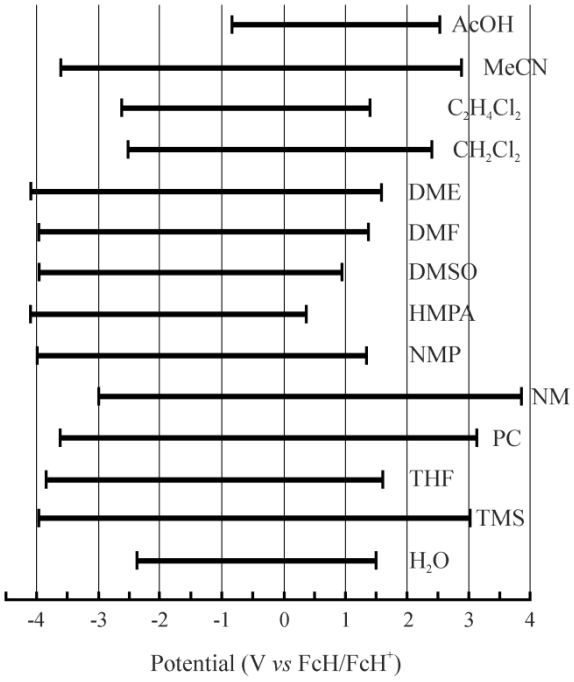

Figure 2.4: Potential windows in various solvents referenced against FcH/FcH^+ [60]

2.5.3.2 Supporting electrolyte

Ion pairs can form between oxidized analyte and the supporting electrolyte cations and anions. This unwanted side effect results in poor resolution of closely overlapping processes and even false redox potentials. To minimize this ion pair formation, it is advantageous to spread the charge of the electrolyte cation and anion over as large an area as possible to reduce the charge density. One such electrolyte is tetrabutylammonium tetrakis(pentafluorophenyl)borate (see Scheme 2.12). With $[N(^nBu)_4][B(C_6F_5)_4]$ as supporting electrolyte, better peak resolution can be obtained,[59] but as it is very expensive, $[N(^nBu)_4][PF_6]$ is rather used when sufficient resolution is achieved with this electrolyte.

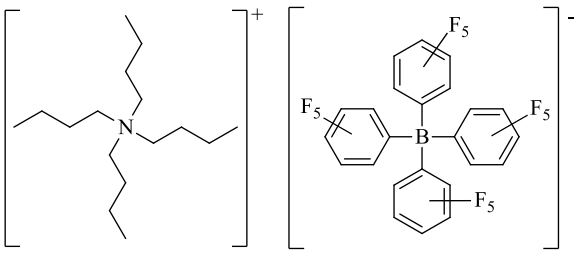

Scheme 2.12: Structure of $[N(^{n}Bu)_4][B(C_6F_5)_4]$

2.5.3.3 Reference electrode

Potentials are specified *vs* a reference electrode such as normal hydrogen electrode (NHE), saturated calomel electrode (SCE) or Ag/Ag^+ electrode. However, IUPAC now recommend that all electrochemical studies performed in organic media be reported *vs* ferrocene/ferrocenium (FcH/FcH^+) couple as an internal standard.[61] In cases where this is not possible, *i.e.* when the ferrocene oxidation/reduction peak potentials overlap with the analyte peak potentials, another reference such as decamethylferrocene may be required. This reference compound is then referenced against FcH/FcH^+, and the data of the analyte is manipulated to be as if referenced against the FcH/FcH^+ couple. From an experimental view it is advantageous to use ferrocene or decamethylferrocene as an internal standard in the same solution as that of the analyte to be studied. This eases the data manipulation to be expressed as referenced to FcH/FcH^+.

2.5.4 Examples of relevant electrochemical studies

An electrochemical study was performed on a series of ferrocene containing β-diketones **(16-19)** using CH_3CN as solvent and $[NBu_4][PF_6]$ as supporting electrolyte.[56] All redox peaks showed chemical and electrochemical reversibility (explained in paragraph 2.5.2) as shown by Figure 2.5 and the data in Table 2.2.

It should be noted that the processes associated with two ferrocene groups in compound **16** could be resolved thus showing a good communication (intramolecular charge transfer)

though the β-diketone. This communication can also be observed for the other compounds where a higher electronegativity led to a higher oxidation potential for the ferrocene.

Table 2.2: Electrochemical data obtained from cyclic voltammograms performed at 50 mVs^{-1}. [56]

R-group	ΔE_p/mV	E^0/mV	i_{pc}/i_{pa}
Fc	74; 71	106; 271	0.88; 1.09
Ph	81	231	1,01
CH_3	92	236	0.97
CCl_3	83	293	0.97
CF_3	74	317	0.97

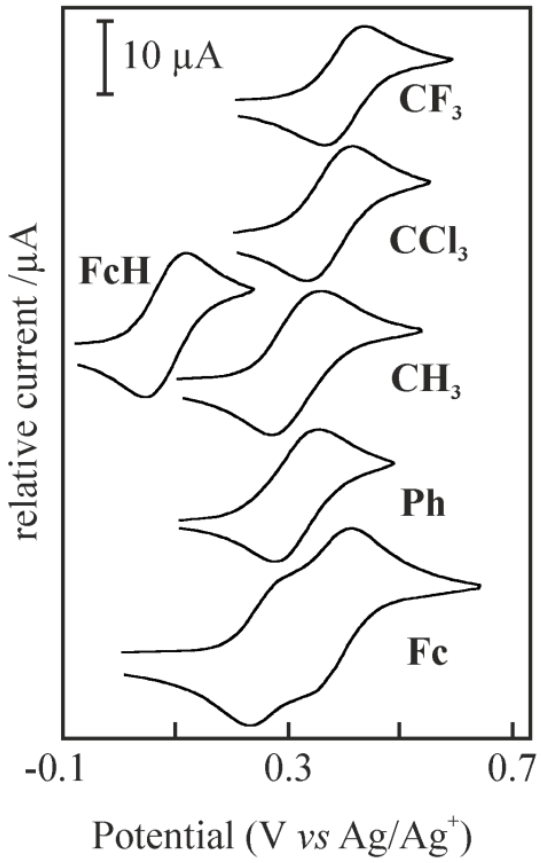

Figure 2.5: Cyclic voltammograms of compounds **16-19** in CH_3CN as solvent, $[N(^nBu)_4][PF_6]$ as supporting electrolyte and 50 mVs^{-1} as scanrate with FcH as reference[56]

An electrochemical study was also performed on the rhodium complexes of the form [Rh(FcCOCHCOCR)(COD)] where R is ferrocenyl **(31)**, phenyl **(32)**, methyl **(33)**, trichloromethyl **(34)** or trifluoromethyl **(35)**.[62] In all cases the CV's showed an electrochemically irreversible oxidation peak assigned to the oxidation of rhodium(I) to

rhodium(III) followed by a reversible redox couple of the ferrocenyl group. In the case of the complex with two ferrocenyl groups **(31)**, two one-electron reversible peaks corresponding to the ferrocenyl groups were observed as was the case with the free β-diketone. It was observed that the ease of oxidation of the metal centres of these compounds increased as the R-group group electronegativity decreased as can be seen from the values in Table 2.3

Table 2.3: 0.1 mol dm^{-3} $[N(^nBu)_4]PF_6]/CH_3CN$ on a glassy carbon electrode at 25°C and a scan rate of 100 mV s^{-1}

		Ferrocenyl group			Rhodium
R-group	χ_R	ΔE_p/mV	E^0/mV	i_{pc}/i_{pa}	E_{pa}/mV
Fc	1.87	64;81	203;302	0.88; 1.09	135
Ph	2.21	67	237	1,01	184
CH_3	2.34	71	232	0.97	177
CCl_3	2.97	92	312	0.97	256
CF_3	3.01	75	329	0.97	269

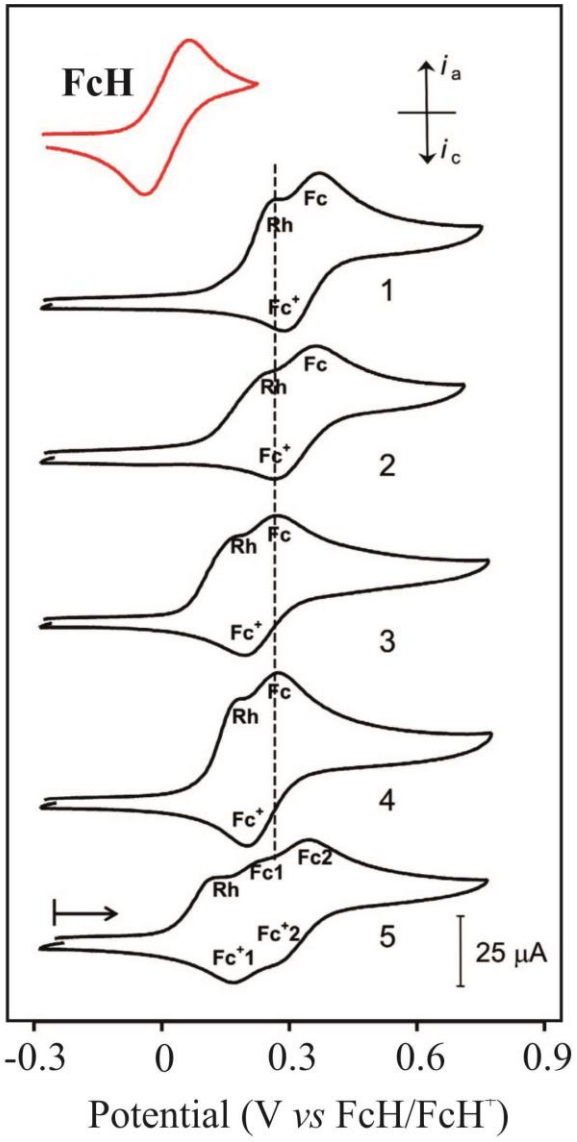

Figure 2.6: Cyclic Voltammograms of compounds **31-35** in CH_3CN as solvent, $[N(^nBu)_4][PF_6]$ as supporting electrolyte and 100 mV s^{-1} as scanrate with FcH as reference[62]

2.6 Substitution kinetics

2.6.1 Introduction

Kinetics involves the study of reaction mechanisms, reaction rate and the changes the rate undergoes due to changes in the environment. These changes can be in concentration of reagents, temperature, solvent and pressure.[63]

Generally a substitution reaction can follow one of three mechanisms; a dissociative (D), associative (A) or interchange mechanism.[53] Dissociative substitution resembles an S_N1 reaction. This means that the leaving ligand first detaches from the metal and the incoming ligand thus reacts with the transition state to form the final product.[64]

Slow step:

$$[L_3MX] \underset{\rightleftharpoons}{k_2, slow} [L_3M] + [X]$$

Fast step:

$$[L_3M] + [Y] \underset{\rightleftharpoons}{fast} [L_3MY]$$

The rate law associated with this process can be expressed as such:

$$Rate = k_2[L_3MX]$$

This shows that the reaction is independent of the concentration of the entering ligand and $\Delta S^{\ddagger}$ for this type of reaction is positive.

It is found that most square planar substitution occurs *via* an associative mechanism. This means that an entering ligand attacks the metal centre to form a 5-coordinate intermediate species.[64]

Slow step:

$$[L_3MX] + [Y] \underset{\rightleftharpoons}{k_2, slow} [L_3MXY]$$

Fast step:

$$[L_3MXY] \underset{\rightleftharpoons}{fast} [L_3MY] + [X]$$

The rate law associated with this process can be expressed as such:

$$Rate = k_2[L_3MX][Y]$$

This shows that the reaction is dependant of the concentration of the entering ligand. $\Delta S^{\ddagger}$ for this type of reaction is always negative.

If the solvent interferes, it can also form a 5-coordinate intermediate *via* a solvent pathway. The rate law for such a reaction can be expressed as

$$\frac{-d[ML_3X]}{dt} = \left[k_s + k_y[Y]\right][ML_3X]$$

$$= k_{obs}[ML_3X]$$

$$k_{obs} = k_s + k_y[Y]$$

eq. 2.4

Here k_s is the rate constant due to the solvent pathway, k_y is the rate constant of the path independent of the solvent and $k_{obs}$is the observed rate constant. If k_{obs} is plotted against [Y], the y-intercept will represent k_s, and if this is not 0, a solvent pathway contributed to the overall reaction.[63]

2.6.2 Activation parameters

The Eyring equation can be derived from the Arrenius equation as

$$ln\frac{k}{T} = ln\frac{k}{h} - \frac{\Delta H^{\ddagger}}{RT} + \frac{\Delta S^{\ddagger}}{R}$$

eq. 2.5

The mathematical solution of this is well known and this study will thus only focus on the application of this equation.

If $ln\frac{k}{T}$ is plotted against $ln\frac{1}{T}$, it usually yields a straight line, and from this $\Delta H^{\ddagger}$ and $\Delta S^{\ddagger}$ can be found as the slope = $-\frac{\Delta H^{\ddagger}}{RT}$ and the y-intercept= $ln\frac{k}{h} + \frac{\Delta S^{\ddagger}}{R}$ as shown in Figure 2.7. Much can be deduced about the mechanism from $\Delta H^{\ddagger}$ and $\Delta S^{\ddagger}$. $\Delta H^{\ddagger}$ is the enthalpy of activation and $\Delta S^{\ddagger}$ is the enthropy of activation. A large negative $\Delta S^{\ddagger}$ implies an associative mechanism.

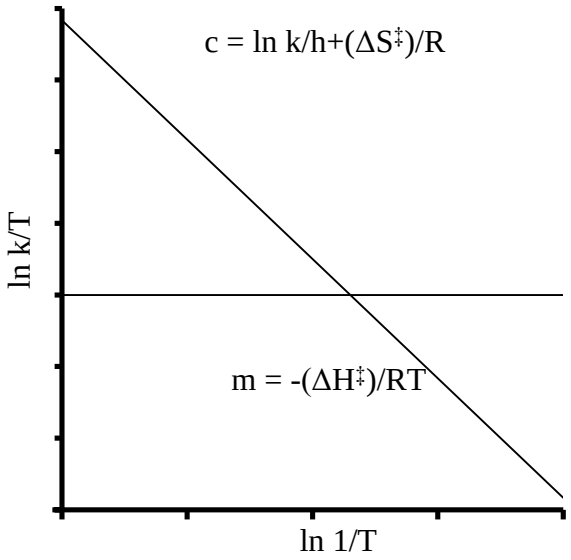

Figure 2.7: A typical example of an Eyring graph where there is a linear relationship between $ln\frac{k}{T}$ and $ln\frac{1}{T}$, and the enthalpy and entropy can be calculated as shown.

2.6.3 [Rh(β-diketonato)(COD)] substitution kinetics

Rhodium(I) β-diketonato cyclooctadiene complexes can undergo substitution reactions to replace either of the ligands as shown in Scheme 2.13. 1,10-Phenanthroline is a strong σ-donating ligand and thus replace the strong σ-donating β-diketonato ligand, while in the case of phosphines which are π-accepting, cyclooctadiene, which is π-donating, will be replaced.

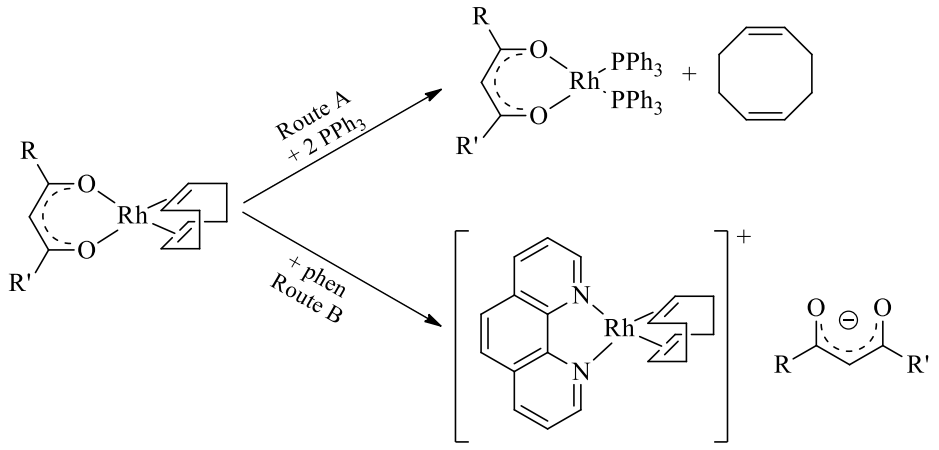

Scheme 2.13: [Rh(β-diketonato)(COD)] can undergo substitution at either of the coordinated ligands. Route A: the cyclooctadiene group is substituted and Route B: the β-diketone is substituted.

Compounds **31-35** were studied where the rates of substitution of the β-diketonato ligand with 1,10-pheneanthroline were measured.[26] Large negative entropies of activation were obtained, indicating an associative mechanism and only the phenyl containing complex substitution reaction occurred via a solvent pathway. It was also found that the reaction rate increased as the pK_a' values of the free β-diketone decreased. Data is summarized in Table 2.4.

Table 2.4: pK_a'values (in water containing 10% acetonitrile, μ = 0.1 mol dm^{-3} ($NaClO_4$)) of ferrocene-containing β-diketones **16-19**[26] compared with to the data obtained from substitution reactions of the corresponding [Rh(β-diketonato)(COD)] with 1,10-phenanthroline

R-group	χ_R	pK_a'	k_y (dm^3 mol^{-1} s^{-1})	$\Delta S^{\ddagger}$ (J K^{-1} mol^{-1})
Fc	1.87	13.1	7.0	-162
Ph	2.21	10.41	30	-113
CH_3	2.34	10.01	29	-123
CCl_3	2.76	7.13	1375	-81
CF_3	3.01	6.56	558	-107

2.7 Group electronegativities

Electronegativity can be described as the measure of the tendency of an atom to attract a bonding pair of electrons.[65] A trend can be seen over the periodic table with atoms with large electronegativity in the top right-hand corner and smallest electronegativity in the bottom left-hand corner.[66] This property of elements has been quantified in numerous ways, though the Pauling scale is the most commonly used.[67] Electronegativity can be calculated using thermodynamic properties (Pauling),[68] ionization potentials (Mulliken)[69] and through distances in covalent bonds (Wilmshurst).[70]

A more practical approach to electronegativity was proposed by Gordy.[71] That is to correlate electronegativity to bond stretching frequencies, thus infrared-spectrometry. By calculating certain group electronegativities and plotting it against the stretching frequencies, the apparent group electronegativities can be extrapolated as shown in Table 2.5 and Figure 2.8.

Table 2.5: Carbonyl stretching frequencies and apparent group electronegativities (Gordy scale) of methyl and ethyl esters[72]

Ester	$\nu_{(C=O)}$ (cm^{-1})	χ_R (Gordy scale)
HCOOMe	1717	2.13
$H_3CCOOMe$	1738	2.34
$(CHCl_2)COOMe$	1755	2.62
$(CCl_3)COOMe$	1768	2.76
ClCOOMe	1780	2.97
FcCOOMe	1700	1.87[26]

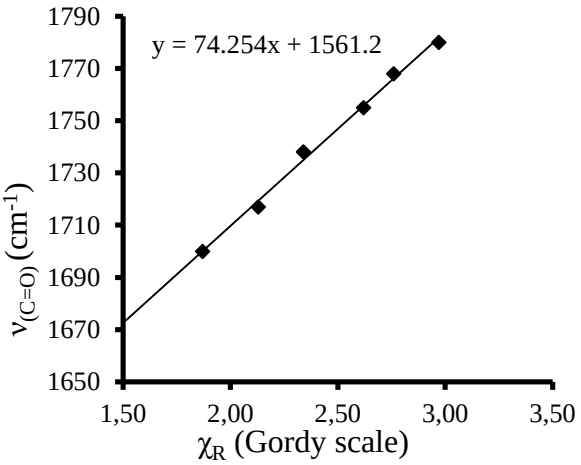

Figure 2.8: The relationship between carbonyl stretching frequencies and apparent group electronegativities (Gordy scale) of methyl and ethyl esters.

Group electronegativity is quite useful when determining the nature of a compound. Structure, pK_a, keto-enol isomers, electrochemistry and substitution kinetics have direct correlations to electronegativity.[67]

This concludes a short literature survey covering topics relevant to this study.

Bibliography

(1) Svendsen, A.; Boll, P. M. *J. Org. Chem.* **1975**, *40* (13), 1927–1932.

(2) Elvers, B.; Hawkins, S.; Russey, W. E. *Ullmann's encyclopedia of industrial chemistry*; Wiley-VCH: Weinheim; Cambridge, 2003.

(3) McGinty, D.; Letizia, C. S.; Api, A. M. *Food Chem. Toxicol. Int. J. Publ. Br. Ind. Biol. Res. Assoc.* **2011**, *49 Supplement 2*, S207–S211.

(4) Janecki, T. *Natural Lactones and Lactams: Synthesis, Occurrence and Biological Activity*, 1st ed.; Wiley-VCH Verlag GmbH & Co. KGaA, 2013.

(5) Schwarz, W.; Schossig, J.; Rossbacher, R.; Höke, H. In *Ullmann's Encyclopedia of Industrial Chemistry*; Wiley-VCH Verlag GmbH & Co. KGaA, 2000.

(6) Metsger, L.; Bittner, S. *Tetrahedron* **2000**, *56* (13), 1905–1910.

(7) Choi, S.; Kim, H. U.; Kim, T. Y.; Kim, W. J.; Lee, M. H.; Lee, S. Y. *Metab. Eng.* **2013**, *20*, 73–83.

(8) Ferraz, H. M. C.; Bombonato, F. I.; Sano, M. K.; Longo Jr., L. S. *Quím. Nova* **2008**, *31* (4), 885–900.

(9) Paryzek, Z.; Skiera, I. *Org. Prep. Proced. Int.* **2007**, *39* (3), 203–296.

(10) Woodruff, M. A.; Hutmacher, D. W. *Prog. Polym. Sci.* **2010**, *35* (10), 1217–1256.

(11) Labet, M.; Thielemans, W. *Chem. Soc. Rev.* **2009**, *38* (12), 3484–3504.

(12) Natta, F. J. van; Hill, J. W.; Carothers, W. H. *J. Am. Chem. Soc.* **1934**, *56* (2), 455–457.

(13) Lukehart, C. M. *Acc. Chem. Res.* **1981**, *14* (4), 109–116.

(14) Bertolasi, V.; Ferretti, V.; Gilli, P.; Yao, X.; Li, C.-J. *New J Chem* **2008**, *32* (4), 694–704.

(15) Qu, S.; Wang, X.; Tong, C.; Wu, J. *J. Chromatogr. A* **2010**, *1217* (52), 8205–8211.

(16) Sheikh, J.; Juneja, H.; Ingle, V.; Ali, P.; Hadda, T. B. *J. Saudi Chem. Soc.* **2013**, *17* (3), 269–276.

(17) Wai, C. M.; Wang, S.; Liu, Y.; Lopez-Avila, V.; Beckert, W. F. *Talanta* **1996**, *43* (12), 2083–2091.

(18) Perez, J. A.; Montoya, V.; Ayllon, J. A.; Font-Bardia, M.; Calvet, T.; Pons, J. *Inorganica Chim. Acta* **2013**, *394*, 21–30.

(19) Cravero, R. M.; González-Sierra, M.; Olivieri, A. C. *J. Chem. Soc. Perkin Trans. 2* **1993**, *6*, 1067–1071.

(20) Linn, B. O.; Hauser, C. R. *J. Am. Chem. Soc.* **1956**, *78* (23), 6066–6070.

(21) Hauser, C. R.; Swamer, F. W.; Adams, J. T. In *Organic Reactions*; John Wiley & Sons, Inc., 2004.

(22) Pauson, P. L. *J. Organomet. Chem.* **2001**, *637–639*, 3–6.

(23) Sinditskii, V. P.; Chernyi, A. N.; Marchenkov, D. A. *Combust. Explos. Shock Waves* **2014**, *50* (2), 158–167.

(24) Ornelas, C. *New J. Chem.* **2011**, *35* (10), 1973–1985.

(25) Emel'yanov, V. E.; Simonenko, L. S.; Skvortsov, V. N. *Chem. Technol. Fuels Oils* **2001**, *37* (4), 224–228.

(26) du Plessis, W. C. (Ina); Vosloo, T. G.; Swarts, J. C. *J. Chem. Soc. Dalton Trans.* **1998**, *15*, 2507–2514.

(27) Swarts, J. C.; Vosloo, T. G.; Cronje, S. J.; Plessis, W. C. (Ina) D.; Rensburg, C. E. J. V.; Kreft, E.; Lier, J. E. V. *Anticancer Res.* **2008**, *28* (5A), 2781–2784.

(28) Conradie, J.; Cameron, T. S.; S. Aquino, M. A.; Lamprecht, G. J.; Swarts, J. C. *Inorganica Chim. Acta* **2005**, *358* (8), 2530–2542.

(29) Conradie, J.; Lamprecht, G. J.; Roodt, A.; Swarts, J. C. *Polyhedron* **2007**, *26* (17), 5075–5087.

(30) Cain, C. E.; Mashburn, T. A.; Hauser, C. R. *J. Org. Chem.* **1961**, *26* (4), 1030–1034.

(31) Hauser, C. R.; Cain, C. E. *J. Org. Chem.* **1958**, *23* (8), 1142–1146.

(32) Zakaria, C. M.; Morrison, C. A.; McAndrew, D.; Bell, W.; Glidewell, C. *J. Organomet. Chem.* **1995**, *485* (1–2), 201–207.

(33) Mehrotra, R. C. *Pure Appl. Chem.* **1988**, *60* (8).

(34) J, P. C.; Weinmayr, V. Dicyclopentadienyliron derivatives. US2875223 A, February 24, 1959.

(35) Bonati, F.; Wilkinson, G. *J. Chem. Soc.***1964**, 3156–3160.

(36) Hunt, L. B.; Lever, F. M. *Platin. Met. Rev.* **1969**, *13* (4), 126.

(37) Evans, D.; Yagupsky, G.; Wilkinson, G. *J. Chem. Soc. Inorg. Phys. Theor.* **1968**, 2660–2665.

(38) Osborn, J. A.; Jardine, F. H.; Young, J. F.; Wilkinson, G. *J. Chem. Soc. Inorg. Phys. Theor.* **1966**, 1711–1732.

(39) Forster, D. In *Advances in Organometallic Chemistry*; West, F. G. A. S. and R., Ed.; Catalysis and Organic Syntheses; Academic Press, 1979; Vol. 17, pp 255–267.

(40) McCully, K. S.; Vezeridis, M. P. *Cancer Invest.* **1987**, *5* (1), 25–30.

(41) Conradie, J.; Lamprecht, G. J.; Otto, S.; Swarts, J. C. *Inorg. Chim. Acta* **2002**, *328* (1), 191–203.

(42) Alagona, G.; Ghio, C. *Int. J. Quantum Chem.* **2008**, *108* (10), 1840–1855.

(43) Bell, R. P.; Davis, G. G. *J. Chem. Soc.* **1965**, 353–361.

(44) Mills, S. G.; Beak, P. *J. Org. Chem.* **1985**, *50* (8), 1216–1224.

(45) Lowe, J. U.; Ferguson, L. N. *J. Org. Chem.* **1965**, *30* (9), 3000–3003.

(46) Burdett, J. L.; Rogers, M. T. *J. Am. Chem. Soc.* **1964**, *86* (11), 2105–2109.

(47) du Plessis, W. C. (Ina); Davis, W. L.; Cronje, S. J.; Swarts, J. C. *Inorg. Chim. Acta* **2001**, *314* (1–2), 97–104.

(48) Gomes, J. R. B.; Ribeiro da Silva, M. A. V. *J. Phys. Chem. A* **2006**, *110* (51), 13948–13955.

(49) Albert, A.; Serjeant, E. P. *The Determination of Ionization Constants*; Springer Netherlands: Dordrecht, 1984.

(50) Paradkar, D. A. R. *Biopharmaceutics & Pharmacokinetics*; Pragati Books Pvt. Ltd., 2008.

(51) Lemke, T. L.; Williams, D. A. *Foye's Principles of Medicinal Chemistry*; Lippincott Williams & Wilkins, 2012.

(52) Diaz, D.; Ford, K. A.; Hartley, D. P.; Harstad, E. B.; Cain, G. R.; Achilles-Poon, K.; Nguyen, T.; Peng, J.; Zheng, Z.; Merchant, M.; Sutherlin, D. P.; Gaudino, J. J.; Kaus, R.; Lewin-Koh, S. C.; Choo, E. F.; Liederer, B. M.; Dambach, D. M. *Toxicol. Appl. Pharmacol.* **2013**, *266* (1), 86–94.

(53) Braterman, P. S. *Reactions of Coordinated Ligands*; Springer Science & Business Media, 2012.

(54) Cookson, R. F. *Chem. Rev.* **1974**, *74* (1), 5–28.

(55) Schmitt, G.; Ozman, S. *J. Org. Chem.* **1976**, *41* (20), 3331–3332.

(56) du Plessis, W. (Ina); Erasmus, J. J.; Lamprecht, G. J.; Conradie, J.; Cameron, T. S.; Aquino, M. A.; Swarts, J. C. *Can. J. Chem.* **1999**, *77* (3), 378–386.

(57) Mabbott, G. A. *J. Chem. Educ.* **1983**, *60* (9), 697.

(58) Kissinger, P. T.; Heineman, W. R. *J. Chem. Educ.* **1983**, *60* (9), 702–706.

(59) Gericke, H. J.; Barnard, N. I.; Erasmus, E.; Swarts, J. C.; Cook, M. J.; Aquino, M. A. S. *Inorg. Chim. Acta* **2010**, *363* (10), 2222–2232.

(60) Izutsu, K. *Electrochemistry in Nonaqueous Solutions*; John Wiley & Sons, 2009.

(61) Gritzner, G.; Kuta, J. *Pure Appl. Chem.* **1984**, *56* (4).

(62) Conradie, J.; Swarts, J. C. *Dalton Trans.* **2011**, *40*, 5844–5851.

(63) Alberta, R. B. J. P. of C. U. of. *Reaction Mechanisms of Inorganic and Organometallic Systems*; Oxford University Press, 2007.

(64) Atwood, J. D.; Wovkulich, M. J.; Sonnenberger, D. C. *Acc. Chem. Res.* **1983**, *16* (9), 350–355.

(65) Maksic, Z. B.; Orville-Thomas, W. J. *Pauling's Legacy: Modern Modelling of the Chemical Bond*; Elsevier, 1999.

(66) Wulfsberg, G. *Inorganic Chemistry*; University Science Books, 2000.

(67) Smith, M. B.; March, J. *March's Advanced Organic Chemistry: Reactions, Mechanisms, and Structure*; John Wiley & Sons, 2007.

(68) Pauling, L. *J. Am. Chem. Soc.* **1932**, *54* (9), 3570–3582.

(69) Mulliken, R. S. *J. Chem. Phys.* **1934**, *2* (11), 782–793.

(70) Wilmshurst, J. K. *J. Chem. Phys.* **1957**, *27* (5), 1129–1131.

(71) Gordy, W. *Phys. Rev.* **1946**, *69* (11-12), 604–607.

(72) Kagarise, R. E. *J. Am. Chem. Soc.* **1955**, *77* (5), 1377–1379.

3 Results and Discussion

3.1 Introduction

In this study a series of ferrocene-containing β-diketones with a hydroxyl group as well as their complexes with rhodium were synthesized. These compounds were characterized by infrared (IR), ultra violet (UV/vis) and nuclear magnetic resonance (^{1}H NMR and ^{13}C NMR) spectroscopy. pK_a values for the free β-diketones were determined, a kinetic study was performed to determine the rate of keto-enol tautomerism of one of the β-diketones, and substitution kinetics were studied on all the rhodium complexes. Electrochemical analysis was performed on all compounds.

3.2 Synthetic Aspects

3.2.1 β-diketones

Three new ferrocene-containing β-diketones were synthesized by Claisen condensation during this study by reacting acetyl ferrocene with a suitable cyclic ester in the presence of LDA (lithium diisopropylamide). The esters used in this study were ε-caprolactone, δ-valerolactone and γ-butyrolactone and the β-diketones formed are as shown in Scheme 3.1.

Sodium ethoxide was also investigated as a base as this was used successfully for the synthesis of other ferrocene containing β-diketones,[1] but it was found to be ineffective in the

case where a lactone is used as the ester. A large number of side reactions occurred during these reactions. It was found that an excess of acetyl ferrocene caused less unwanted reactions and thus simplified purification. An excess of 2:1 acetyl ferrocene to lactone was found to be convenient.

The resulting β-diketones, $FcCOCH_2CO(CH_2)_nOH$, with n = 5 **(37)**, n = 4 **(39)** and n = 3 **(40)** could be purified by column chromatography with eluent hexane:ethylacetate (1:1) to yield 58.6% of product for **37**, 40.4% for **39** and 35.1% for **40**. Both the longer chain β-diketones are deep red liquids and only the shortest chain compound was a solid at room temperature.

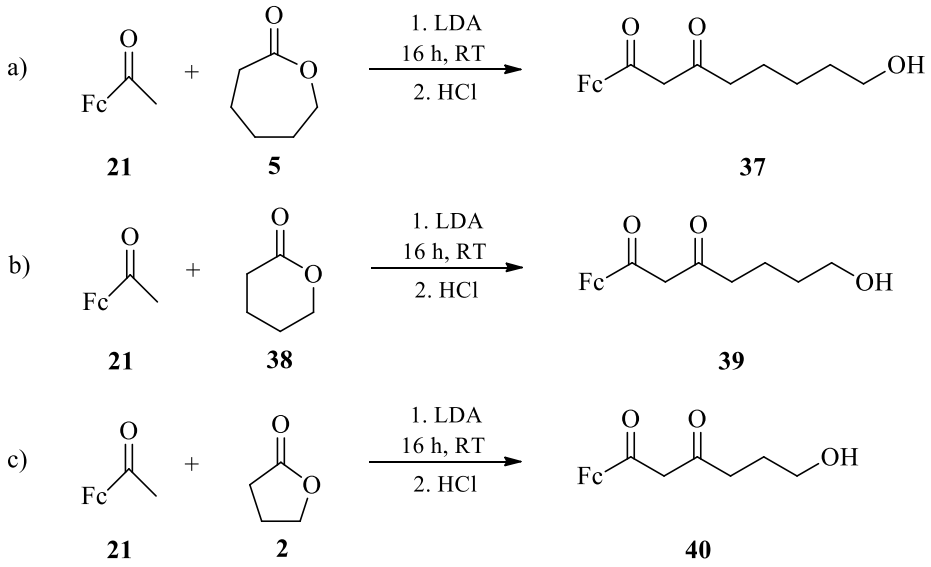

Scheme 3.1: Synthesis of hydroxylated β-diketones **37**, **39** and **40** by reacting acetyl ferrocene with an appropriate lactone

Through ^{1}H NMR, compound **37** was found to exist in a keto- and one enol isomer in equilibrium. Keto-enol tautomerism was also observed for compounds **39** and **40**, but both showed two enol isomers in solution. However, in the solid state only one enol form was observed (see crystal structure of **40**). Below are the ^{1}H NMR spectra of **37** and **40 (**Figure 3.1). The ^{1}H NMR spectra for **37** is easily assigned, but the NMR spectra for **40** is troublesome in that the two CH_2 peaks at 2.95 – 3.15 ppm and 3.85 – 4.05 ppm as well as the

Cp-CH peak at 4.68 and 4.75 appear to be split into two components. This is typical of a cyclic structure, although at this stage the exact structure of such a configuration can only be speculated on. Further study is required to understand this spectrum fully.

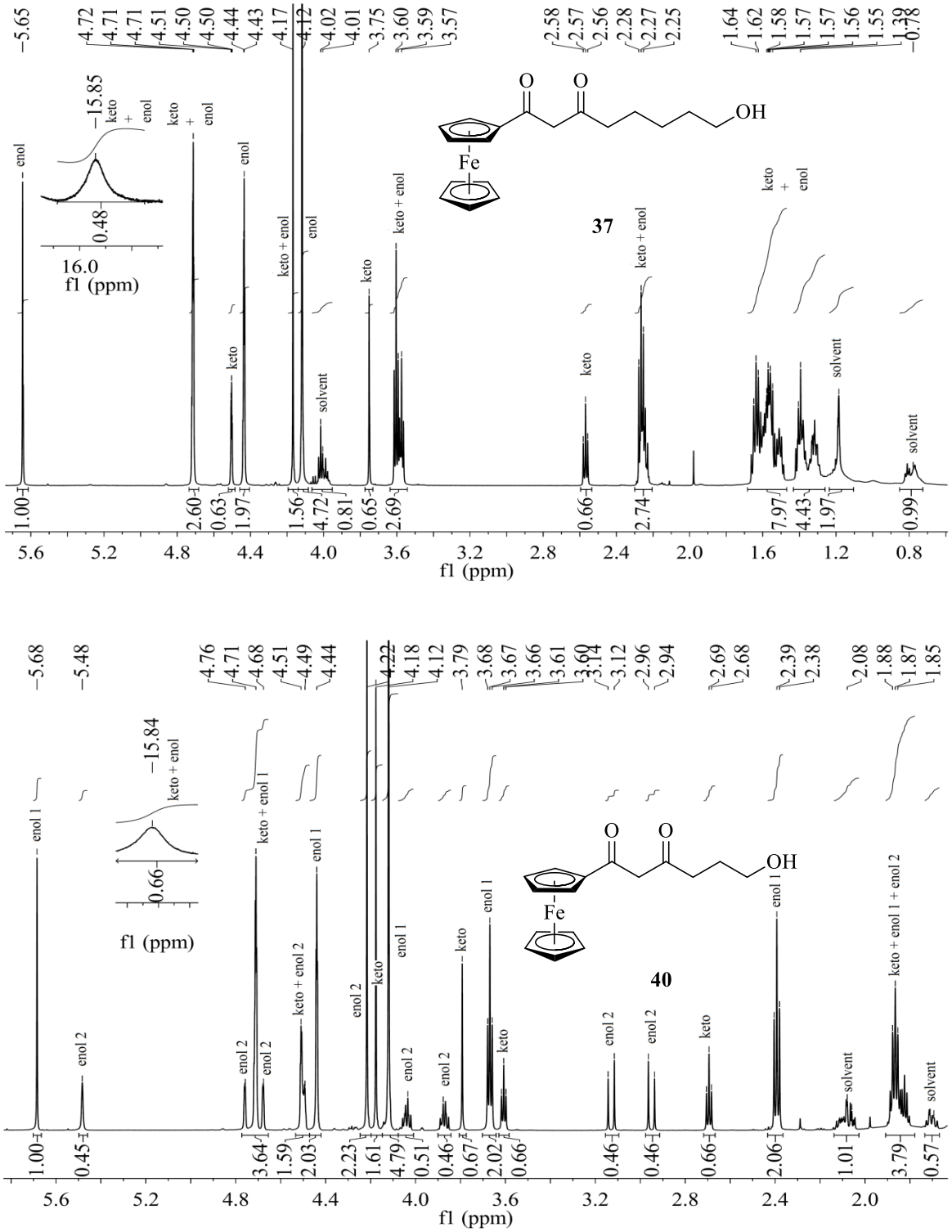

Figure 3.1: ^{1}H NMR spectra of **37** and **40** in $CDCl_3$ at 293 K

Table 3.1: Infrared stretching frequencies of the β-diketones as a function of n

n	$\nu_{(C=O)}$ (cm^{-1})	$\nu_{(O-H)}$ (cm^{-1})	$\nu_{(aliphatic\ C-H)}$ (cm^{-1})	$\nu_{(aromatic\ C-H)}$ (cm^{-1})
5 **(37)**	1548; 1609	3110-3560	2860; 2931	3094
4 **(39)**	1547; 1604	3150-3530	2868; 2933	3096
3 **(40)**	1542; 1602	3140-3550	2873; 2928	3097

Table 3.1 summarizes the most prominent IR bands. The $\nu_{(C=O)}$ stretching frequency was observed as two bands (symmetric and asymmetric) at 1542 – 1548 cm^{-1} and 1602 – 1609 cm^{-1} respectively. This leads to an average $\Delta\ \nu_{(C=O)} = \nu_{(C=O)asym} - \nu_{(C=O)sym} = 59\ cm^{-1}$. The O-H vibration was observed as a broad band in the region 3100 – 3600 cm^{-1} . The aliphatic C-H vibrations were observed as two strong bands in the region of 2800 - 3000 cm^{-1} and the aromatic C-H vibrations of the ferrocenyl group at 3094 – 3097 cm^{-1}. Normally aliphatic C-O vibrations of primary alcohols are observed at ν = 1050 cm^{-1}. However, in **37**, **39** and **40**, this band could not uniquely be identified, probably due to the C⋯O character of the pseudo-aromatic β-diketone core. These bands can be observed for **37** in Figure 3.2.

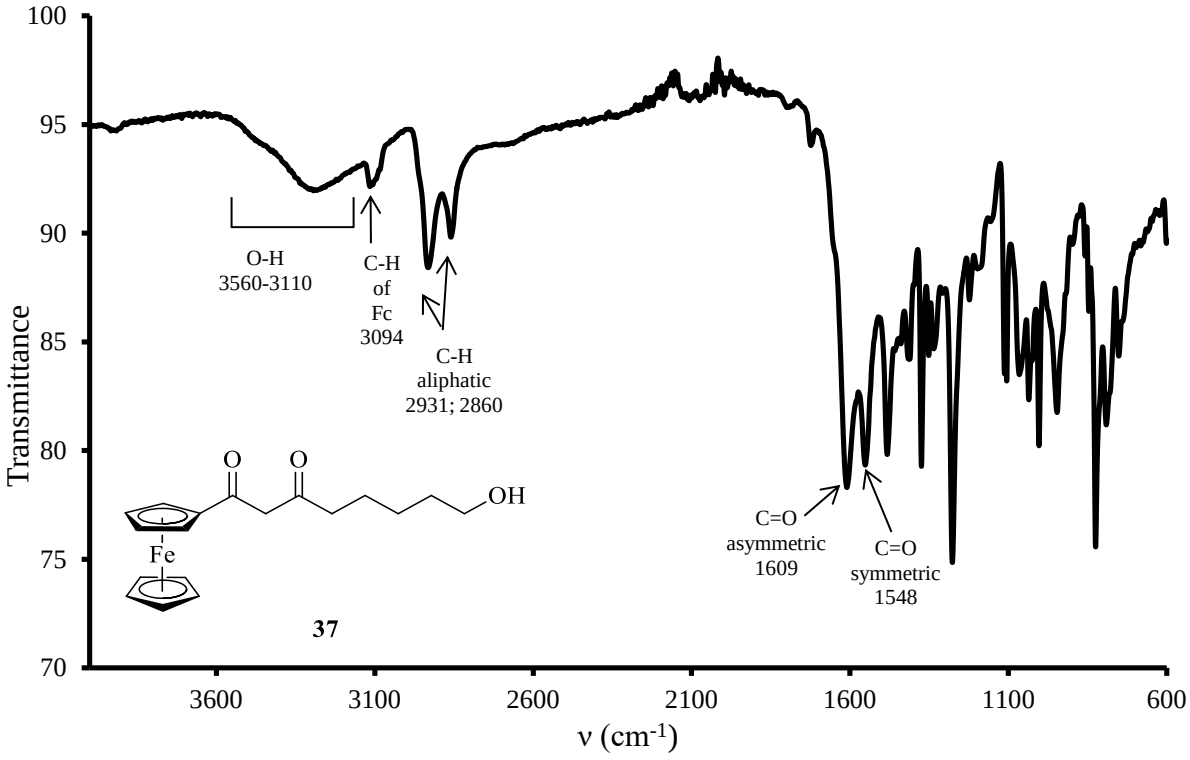

Figure 3.2: Infrared spectrum for β-diketone **37**

3.2.2 Rhodium complexation

The β-diketones $FcCOCH_2CO(CH_2)_nOH$, were reacted with di-μ-chloro-bis[(1,2,5,6-η)1,5-cyclooctadiene]dirhodium(I) to form $Rh[FcCOCHCO(CH_2)_nOH(COD)]$ complexes as shown in Scheme 3.2.

The complexes, $Rh[FcCOCHCO(CH_2)_nOH(COD)]$ with n = 5 **(41)**, n = 4 **(42)** and n = 3 **(43)**, were easily synthesized at room temperature to yield 87.0% of **41**, 82.9% of **42** and 71.7% of **43**. Purification was done by washing the precipitate with cold water and drying under reduced pressure.

All three complexes formed a reddish brown glass-like solid after drying.

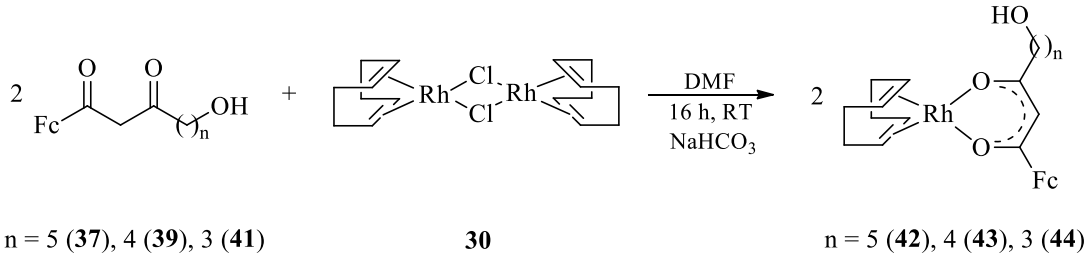

n = 5 (**37**), 4 (**39**), 3 (**41**) **30** n = 5 (**42**), 4 (**43**), 3 (**44**)

Scheme 3.2: Complexation of β-diketones **37**, **39** and **40** with $[RhCl_2(COD)_2]$ to form $Rh[FcCOCHCO(CH_2)_nOH(COD)]$ where n = 5, 4 and 3

Table 3.2: Infrared stretching frequencies of the rhodium complexes as a function of n

n	$\nu_{(C=O)}$ (cm^{-1})	$\nu_{(O-H)}$ (cm^{-1})	$\nu_{(aliphatic\ C-H)}$ (cm^{-1})	$\nu_{(aromatic\ C-H)}$ (cm^{-1})
5 **(41)**	1507; 1541	3130-3600	2868; 2926	3094
4 **(42)**	1508; 1540	3130-3600	2857; 2925	3093
3 **(43)**	1510; 1542	3130-3570	2852; 2921	3095

The prominent IR data are summarized in Table 3.2. Notably are the lowering of the $\nu_{(C=O)}$ stretching frequencies wave numbers by ca. 38 (symmetric) and 61 cm^{-1} for the asymmetric C=O band. The $\nu_{(O-H)}$ and $\nu_{(C-H)}$ bands did not shift substantially from the positions of the equivalent bands in the IR spectra of the free β-diketones (Table 3.1). These bands can be observed for **41** in Figure 3.3.

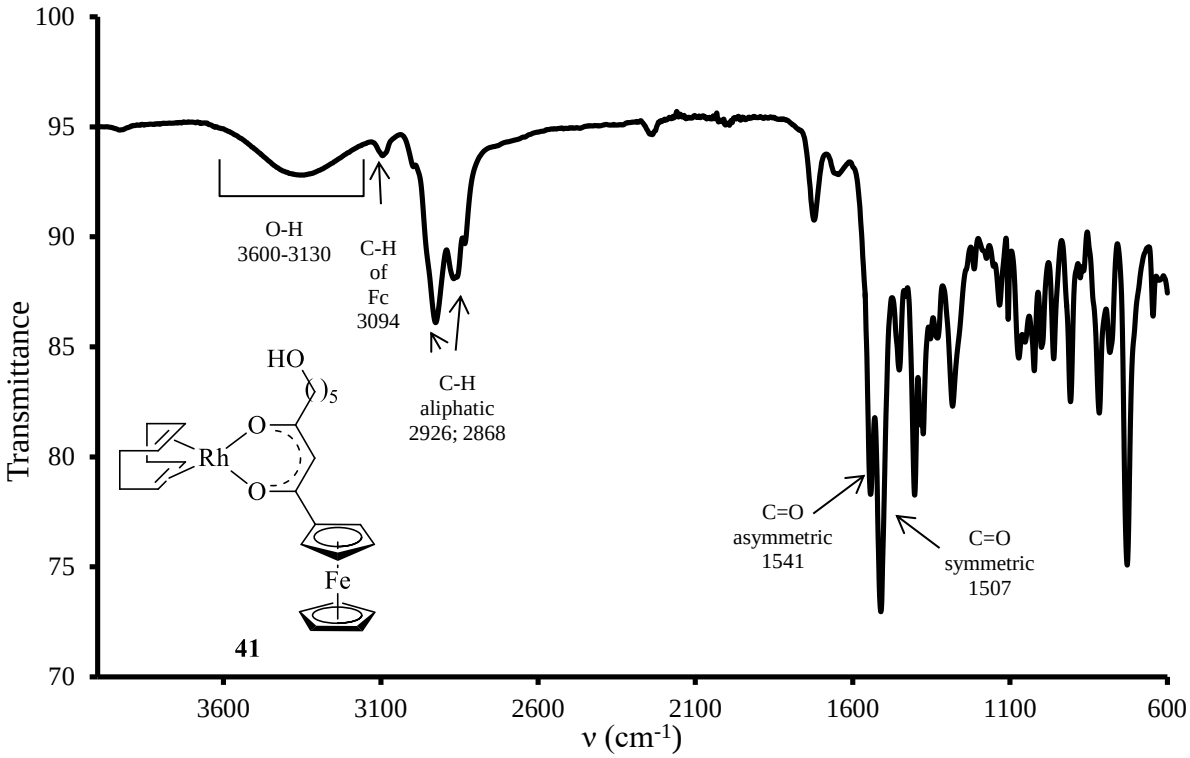

Figure 3.3: Infrared spectrum for rhodium complex **41**

3.3 Crystal structure of $FcCOCH_2CO(CH_2)_3OH$ (40)

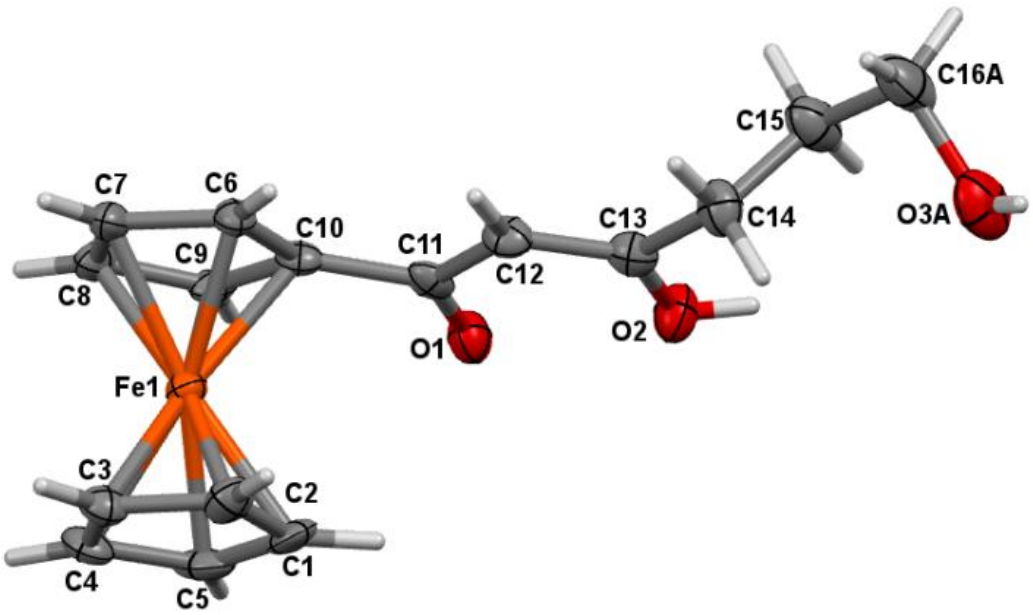

Figure 3.4: Labelled molecular structure of $FcCOCH_2CO(CH_2)_3OH$ (**40**). Only one of two disordered positions for atoms C(16) and O(3) are shown. Figure 3.5 highlights both of the disordered positions

Single crystal X-ray diffraction (XRD) studies were performed on $FcCOCH_2CO(CH_2)_3OH$ **(40)**. The crystal data and structure refinement are summarized in Table 3.3 and Figure 3.4 shows the molecular diagram with atom labelling.

Table 3.3: Crystal structure and data refinement for $FcCOCH_2CO(CH_2)_3OH$ (**40**)

Empirical formula	$C_{16}H_{18}Fe_1O_3$
Formula weight	314.15
Temperature	150(2) K
Wavelength	1.54178 Å
Crystal system	Monoclinic
Space group	$P\ 2_1$
Unit cell dimensions	a = 5.752(6) Å b = 46.39(5) Å c = 21.17(2) Å
Volume	5643(10) $Å^3$
Z	8
Density (calculated)	1.479 mg m^{-3}
Absorption coefficient	8.609 mm^{-1}
F(000)	2624
Crystal size	0.380 x 0.090 x 0.030 mm^3
Theta range for data collection	2.089 to 68.239°.
Index ranges	-6<=h<=6 -55<=k<=55 -25<=l<=25
Reflections collected	154088
Independent reflections	20406 [R(int) = 0.1418]
Completeness to theta = 67.679°	99.6 %
Refinement method	Full-matrix least-squares on F^2
Data / restraints / parameters	20406 / 649 / 1533
Goodness-of-fit on F^2	1.113
Final R indices [I>2sigma(I)]	R1 = 0.0791, wR2 = 0.1592 [a)]
R indices (all data)	R1 = 0.0977, wR2 = 0.1682
Absolute structure parameter	0.5
Largest diff. peak and hole	0.989 and -0.644 e.$Å^{-3}$

a) R1 = 0.0791 value is larger than what was expected, but is attributed to the multiple positions the $(CH_2)_3OH$ side chain of the eight molecules occupy.

β-diketones in solution or gas phase are an equilibrium mixture of keto- and enol tautomers. However, in solid phase the β-diketones are usually found in the enol form.[2] For $FcCOCH_2CO(CH_2)_3OH$, a large number, eight, of independent molecules were found per unit cell (Z = 8), and all were found to be in the enol form with enolization furthest from the

ferrocenyl group. The long side chain, $(CH_2)_3OH$, was not rigid and assumed different positions in each molecule.

For **40**, the compound shown in Figure 3.4, the C(11)-O(1) and C(13)-O(2) bonding lengths are not equivalent. This was found in all 8 molecules. In every case the C-O bond furthest from the ferrocenyl moiety is longer (0.004–0.053 Å) than the other C-O bond (Table 3.4). This corresponds to a double C-O bond for the shorter bond adjacent to the ferrocenyl group and a single C-O bond for the other carbon-oxygen bond.[3]

Enolization was also confirmed by the β-diketone backbone C-C bonds. Bond C(11)-C(12) was found to be substantially longer than bond C(12)-C(13). This indicates that C(11)-C(12) has a single bond character (closer to the value of a pure single bond such as C(14)-C(15)) and C(12)-C(13) a double bond character (1.31-1.34 Å for a pure double bond).[4] This confirms that the molecule crystalized in enol form with enolization furthest from the ferrocenyl group.

The methine C-C-C angle was found in all cases to be ~120°, indicating sp^2 rather than the tetrahedral value of 109° for sp^3 as shown in Table 3.5 by the sp^3 angle of C(14)-C(15)-C(16).

Table 3.4: Selected bond lengths for $FcCOCH_2CO(CH_2)_3OH$ of all eight molecules in the unit cell

Molecule	C(11)-C(12) bond lengths (Å)	C(12)-C(13) bond lengths (Å)	C(11)-O(1) bond lengths (Å)	C(13)-O(2) bond lengths (Å)	C(14)-C(15) bond lengths (Å)
1	1.441(17)	1.407(18)	1.254(16)	1.310(16)	1.510(18)
2	1.427(17)	1.388(18)	1.289(15)	1.311(17)	1.51(2)
3	1.422(17)	1.413(18)	1.285(15)	1.316(16)	1.48(2)
4	1.430(17)	1.381(18)	1.296(15)	1.300(16)	1.50(2)
5	1.457(17)	1.340(18)	1.257(15)	1.328(15)	1.541(18)
6	1.381(18)	1.379(18)	1.297(15)	1.337(17)	1.47(2)
7	1.422(18)	1.347(17)	1.279(16)	1.332(16)	1.534(17)
8	1.399(17)	1.378(19)	1.294(15)	1.313(18)	1.49(2)

Table 3.5: Selected bond angles for $FcCOCH_2CO(CH_2)_3OH$ of all eight molecules in the unit cell

Molecule	C(11)-C(12)-C(13) Bond Angles (°)	C(14)-C(15)-C(16) Bond Angles (°)
1	118.2(12)	113.4(12)
2	119.0(13)	114.4(13)
3	121.8(12)	116.0(13)
4	119.7(12)	114.9(13)
5	119.9(12)	112.4(12)
6	121.2(13)	115.4(14)
7	122.9(12)	111.4(12)
8	121.0(14)	115.0(15)

The dihedral angle between the Cp rings of the ferrocenyl moiety is very small for all molecules, the largest was found to be 2.54°, thus the cyclopentadienyl rings can be considered parallel. Torsion angles were also found to be small meaning that there is only a slight deviation from eclipsed conformation of the Cp rings. All of these angles are listed in Table 3.6 and Figure 3.5 shows the deviations in visual form.

Table 3.6: Dihedral and torsion angles for $FcCOCH_2CO(CH_2)_3OH$

Molecule	Deviation from eclipsed conformation (°)	Deviation from planarity of two Cp rings on Fc (°)
1	1.64	2.54
2	2.28	1.95
3	2.00	1.87
4	-1.40	0.78
5	1.23	2.30
6	-0.57	1.27
7	-1.01	1.80
8	-4.00	1.30
Mod Average	1.77	1.73

It was also noted that the C-C bonds of the substituted Cp ring were substantially longer than that of the unsubstituted Cp ring as shown in Table 3.7.

Table 3.7: Average C-C bond lengths for the unsubstituted and substituted Cp rings

Atoms	Average bond lengths (Å)
Substituted Cp ring	
C(6)-C(7)	1.433(17)
C(7)-C(8)	1.419(19)
C(8)-C(9)	1.423(18)
C(9)-C(10)	1.438(17)
C(10)-C(6)	1.432(18)
Unsubstituted Cp ring	
C(1)-C(2)	1.410(19)
C(2)-C(3)	1.430(18)
C(3)-C(4)	1.429(19)
C(4)-C(5)	1.413(19)
C(5)-C(1)	1.416(19)

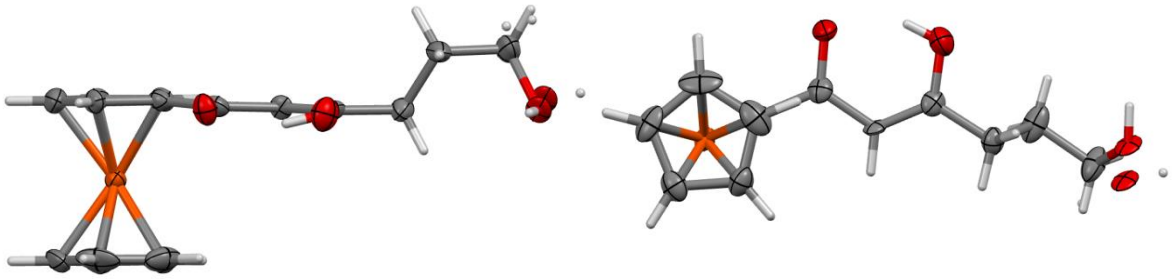

Figure 3.5: Molecular structure of $FcCOCH_2CO(CH_2)_3OH$ showing how the Cp rings are parallel and eclipsed with the terminal OH group in two positions

The O(3) atom of **40** was observed in two disordered positions, indicated by O(3)A and O(3)B, and can be seen in Figure 3.4. All other bond lengths and bond angles are tabulated in the appendix.

3.4 Isomerization kinetics of 37

The synthesized β-diketones exist in equilibrium mixtures of keto and enol tautomers. These tautomers can be differentiated by ^1H NMR and thus the formation of keto isomers from an enol enriched solution could be studied by monitoring the disappearance of the methine proton signal in FcCOCH=COH-R and the appearance of the CH_2 signal of $FcCOCH_2CO$-R

with time. In this study, isomerization kinetics of $FcCOCH_2CO(CH_2)_5OH$ was studied. An enol rich solution of **37** was obtained by dissolving a sample of older than 3 months, and measurements were immediately initiated. Figure 3.6 shows ^1H NMR spectra of the ferrocenyl group in the enol enriched state and also at equilibrium in $CDCl_3$.

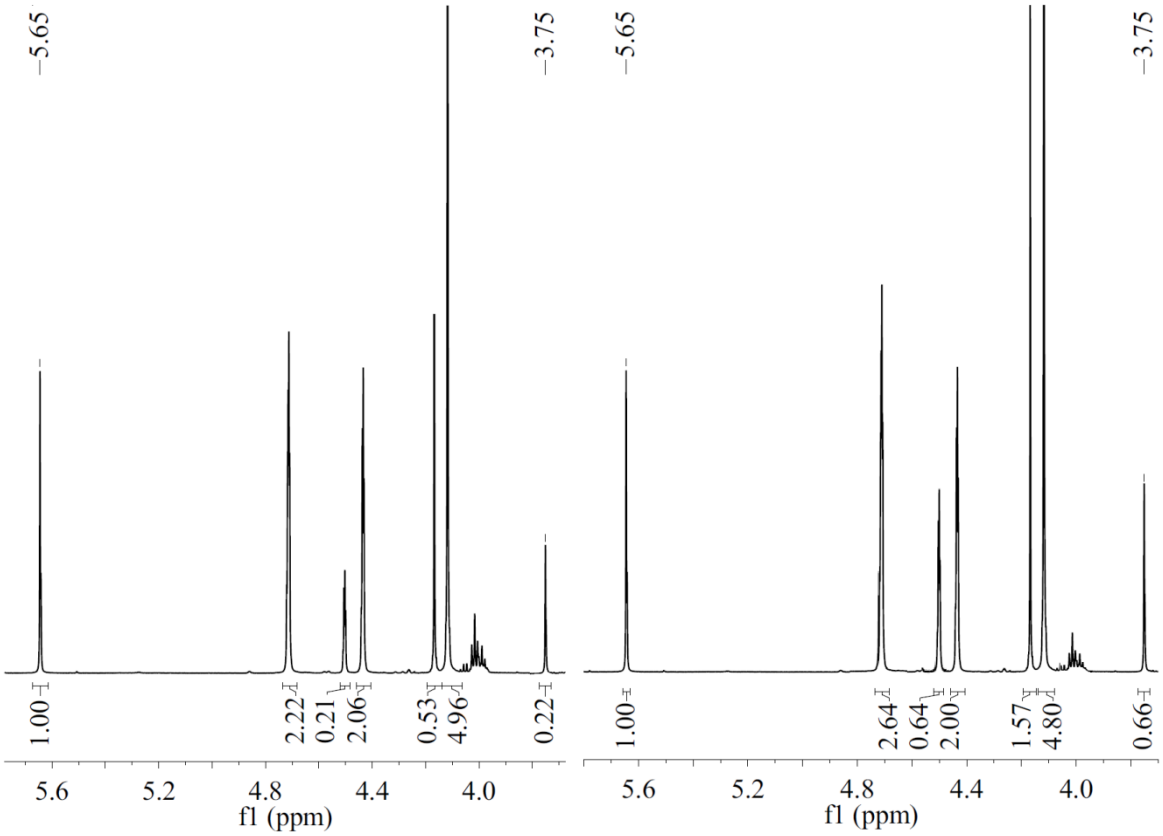

Figure 3.6: A section of the ^1H NMR spectra of **37** in the enol-enriched state (left) and at equilibrium (right) at 293 K in $CDCl_3$.

The methine signal was assigned an integral value of 1, and the percentage keto isomer was calculated as follows:[5]

$$\%\ keto\ isomer\ = \frac{I\ of\ keto\ signal}{I\ of\ keto\ signal + 2(I\ of\ enol\ signal)} \times 100$$

eq. 3.1

The % enol isomer = 100 - % keto isomer. Once the percentages of the isomers were known, K_c, the equilibrium constant could be calculated using equation 3.2.

$$K_c = \frac{\%\ keto\ isomer}{\%\ enol\ isomer} = \frac{\%\ keto\ isomer}{100 - \%\ keto\ isomer} = \frac{k_1}{k_{-1}}$$

eq. 3.2

Equation 3.2 is valid for the reaction as shown in Scheme 3.3:

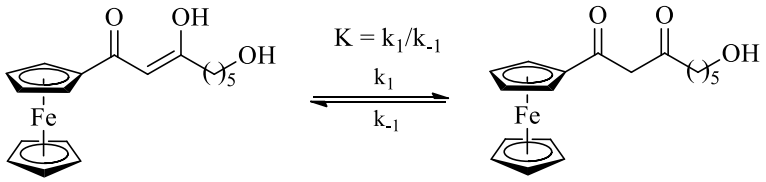

Scheme 3.3: Equilibrium reaction between the enol- and keto isomers of **37**

The data was fitted to Equation 3.3 and plotted as $ln\frac{C_0 - C_\infty}{C_t - C_\infty}$ against time.[6]

$$ln\frac{C_0 - C_\infty}{C_t - C_\infty} = (k_1 + k_{-1})t = k_{obs}t$$

eq. 3.3

The observed rate constant, $k_{obs} = k_1 + k_{-1}$, could be determined from the slope of the plot. k_1, the rate constant for the conversion of the enol to the keto form, and k_{-1}, the rate constant for the conversion of keto to enol form, could be determined through simultaneously solving $K_c = \frac{k_1}{k_{-1}}$ and $k_{obs} = k_1 + k_{-1}$.

A time-dependant ^{1}H NMR study performed on compound **37** indicates, by comparing the relative intensities of the CH_2 (keto) and CH (enol) signals, that the enol form dominates in solution at 75.1% when equilibrium is reached. Experimental results are listed in Table 3.8. In a separate set of reactions, a solution of compound **37** in $CDCl_3$ was reacted with NaOH, thus creating a keto-enriched solution, and a ^{1}H NMR time study was performed on this solution. This time, the formation of the enol isomer could be monitored. Figure 3.7 shows reaction profiles of enol-keto as well as keto-enol conversions of **37**. Also shown in Figure 3.7 is a linear, first-order plot of kinetic data to obtain $k_{obs} = k_1 + k_{-1} = 1.74 \times 10^{-4}\ s^{-1}$ from the

slope of the linear relationship. The half-life of isomer conversion, $t_{1/2} = \frac{ln2}{k_{obs}}$, is approximately 4000 s.

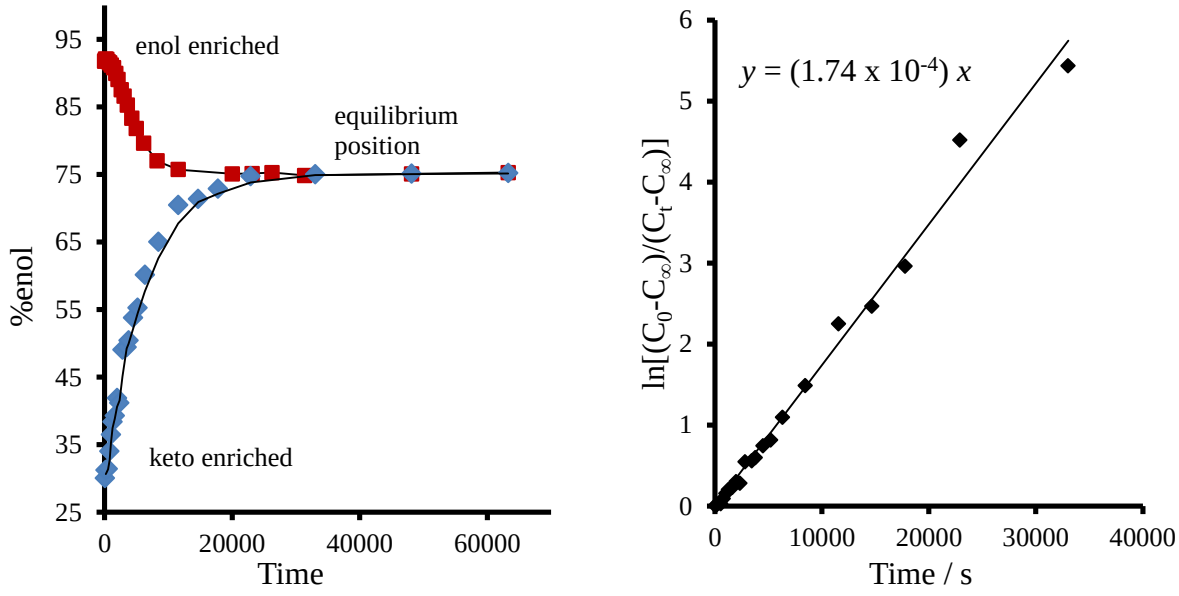

Figure 3.7: Left: determination of the equilibrium ratio of tautomers of compound **37**. Red: reaching equilibrium from an enol-enriched solution; blue: reaching equilibrium from a keto-enriched solution. Right: a ln-time plot of kinetic data giving a slope of the observed rate constant $k_{obs} = k_1 + k_{-1} = 1.74 \times 10^{-4}$ s^{-1}

k_1, the rate constant for the conversion of the enol to the keto form, and k_{-1}, the rate constant for the conversion of keto to enol form, could be determined through simultaneously solving $K_c = \frac{k_1}{k_{-1}}$ and $k_{obs} = k_1 + k_{-1}$. All rate constants obtained are listed in Table 3.8.

Table 3.8: Constants for tautomer equilibrium of **37** at 293 K

K_c	3.02
k_{obs} (s^{-1})	1.74 x 10^{-4}
k_1 (s^{-1})	4.33 x 10^{-5}
k_{-1} (s^{-1})	1.31 x 10^{-4}

3.5 Observed pK_a' values

Observed pK_a' values were obtained for all three β-diketones that were synthesized. The reaction that takes place during pK_a' value determination is as follows:

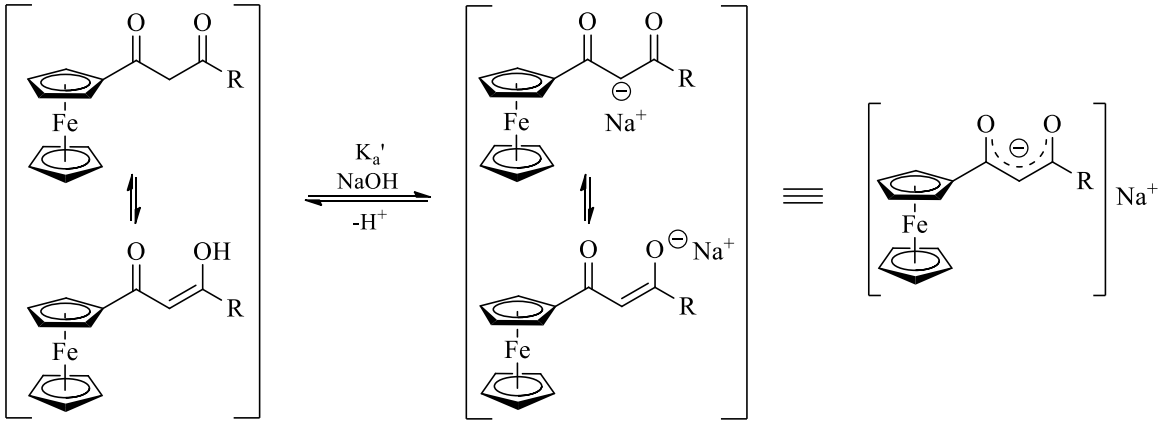

Scheme 3.4: The reaction that takes place during base titrations of β-diketones (forward reaction) or acid titrations of β-diketonates (reverse reaction)

The observed (or apparent) pK_a' values for compounds **37**, **39** and **40** were determined by spectroscopically monitoring acid-base titrations. A solvent system of water with 10% acetonitrile was used to help solubility. Although the β-diketones dissolve in water, precipitation occurs at low pH. Thus if only water is used as solvent, the analyte concentration will vary tremendously during titration. Acetonitrile in this concentration was proven before to have a small effect on the pK_a' determination as demonstrated by acetylacetone (pK_a' = 8.83 in water, pK_a' = 8.93 in water with 10% acetonitrile).[1]

The solution was brought to a high pH by the addition of NaOH, and then titrated with $HClO_4$; $NaClO_4 \cdot H_2O$ was thus a suitable salt to set the ionic strength at 0.100 mol dm^{-1}.

Absorbance data was collected as a function of the pH. A wavelength at which the largest absorbance difference between the basic and acidic solutions occurred was used for

measurements. In all cases this was λ_{max} for the enolate, $FcCO^{\ominus}CHNa^{\oplus}CO(CH_2)_nOH$, and is listed in Table 3.9.

While varying the pH between ~2 and ~13, a change in absorbance in the UV spectra of **37**, **39** and **40** was observed as shown in Figures 3.8.-3.10. For all three compounds the S curve exhibited approximately 2 pH units between absorption minima and maxima. A least square fitting of the absorbance/pH data to equation 3.4 yielded the pK_a' values.

$$A_T = \frac{A_{HA}10^{-pH} + A_A10^{-pK_a}}{10^{-pH} + 10^{-pK_a}}$$

eq.3.4

In equation 3.4 A_T = total absorption, A_{HA} = absorption of the protonated β-diketone (acidic) and A_A = absorption of the deprotonated β-diketonate species (basic).

Table 3.9: pK_a' values for β-diketones $FcCOCH_2CO(CH_2)_nOH$ with n = 5,4 and 3.

β-diketone	λ_{exp} / nm (basic) [ε / $dm^3\,mol^{-1}\,cm^{-1}$]	λ_{exp} / nm (acidic) [ε / $dm^3\,mol^{-1}\,cm^{-1}$]	β-diketone concentration (mol dm^{-3})	pK_a'
37 (n=5)	327 [28072]	327 [4925]	8.77×10^{-5}	10.44
39 (n=4)	320 [15426]	320 [4540]	9.14×10^{-5}	8.01
40 (n=3)	317 [12146]	317 [2513]	9.55×10^{-5}	5.97

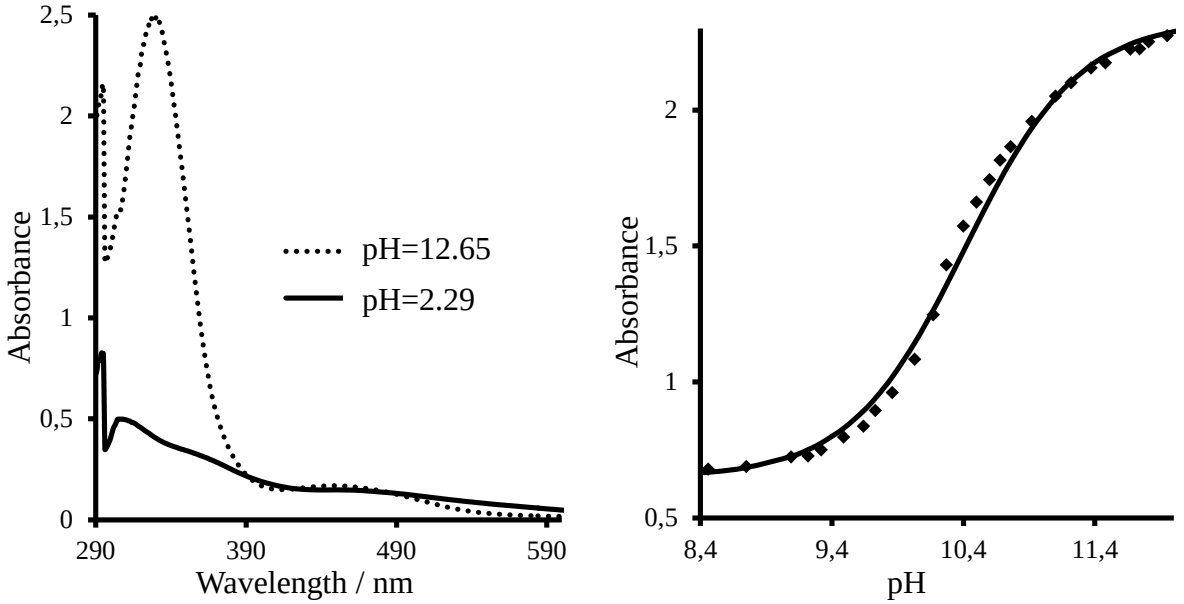

Figure 3.8: pK_a' determination for $FcCOCH_2CO(CH_2)_5OH$ **37**. [**37**] = 8.77 x 10^{-5} mol dm^{-3}. Left: Spectra of protonated and deprotonated β-diketone in 10% CH_3CN. The solid line represents the acidic form at pH = 2.29 and the dotted line the basic form at pH = 12.65. Right: The change in absorbance as a function of pH in water/acetonitrile (9:1) at 25 °C.

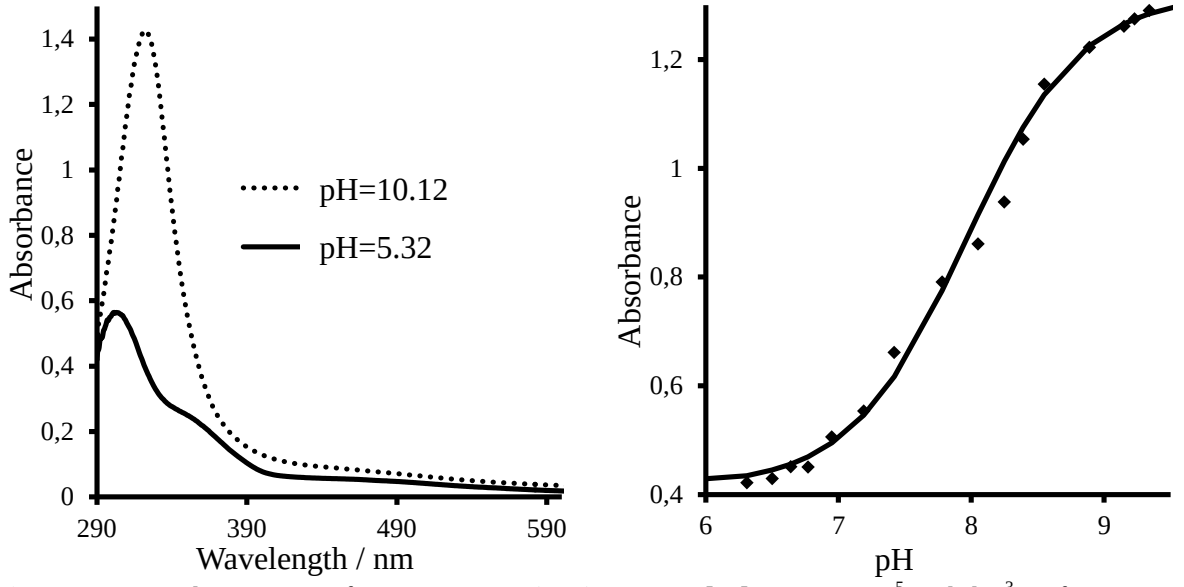

Figure 3.9: pK_a' determination for $FcCOCH_2CO(CH_2)_4OH$ **39**. [**39**] = 9.14 x 10^{-5} mol dm^{-3}. Left: Spectra of protonated and deprotonated β-diketone in 10% CH_3CN. The solid line represents the acidic form at pH = 5.32 and the dotted line the basic form at pH = 10.12. Right: The change in absorbance as a function of pH in water/acetonitrile (9:1) at 25 °C.

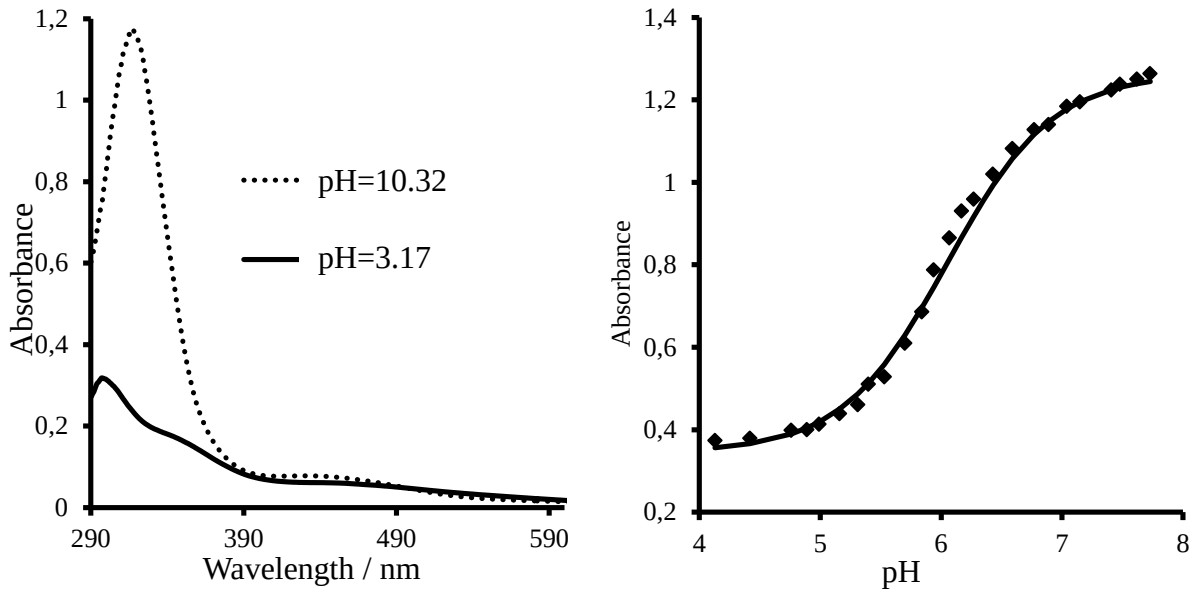

Figure 3.10: pK_a' determination for $FcCOCH_2CO(CH_2)_3OH$ **40**. [**40**] = 9.55 x 10^{-5} mol dm^{-3}. Left: Spectra of protonated and deprotonated β-diketone in 10% CH_3CN. The solid line represents the acidic form at pH = 3.17 and the dotted line the basic form at pH = 10.32. Right: The change in absorbance as a function of pH in water/acetonitrile (9:1) at 25 °C.

There exists a linear relationship between and pK_a' and the sidechain length (n) of the β-diketones $FcCOCH_2CO(CH_2)_nOH$. From Figure 3.11, this relationship is $pK_a' = 2.235\ n - 0.8$. Data summarized in Table 3.9 suggests the addition of each CH_2 group in $FcCOCH_2CO(CH_2)_nOH$ increased the pK_a' by more than two pH units.

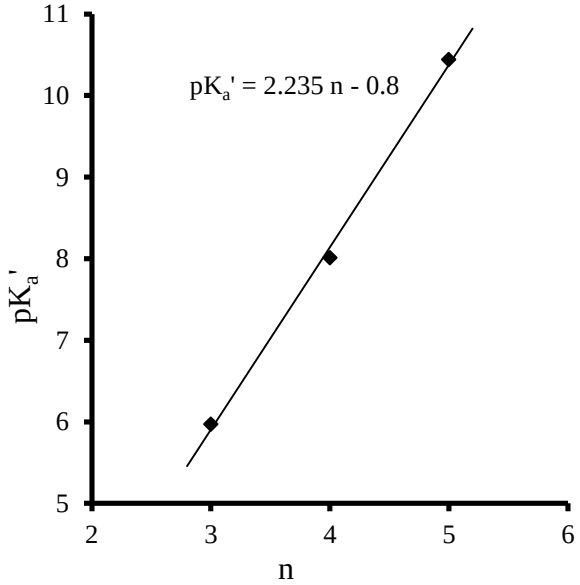

Figure 3.11: Correlating of chain length of β-diketones **37**, **39** and **40** with pK_a'

3.6 Electrochemistry

Electrochemistry was performed on all three β-diketones as well as their rhodium complexes. The formal reduction potentials of all these compounds were thus determined and from that the electronic influence of the different β-diketones on the rhodium centre could be determined. In all cases the ferrocenyl group undergoes a one-electron transfer process as shown in Scheme 3.4.

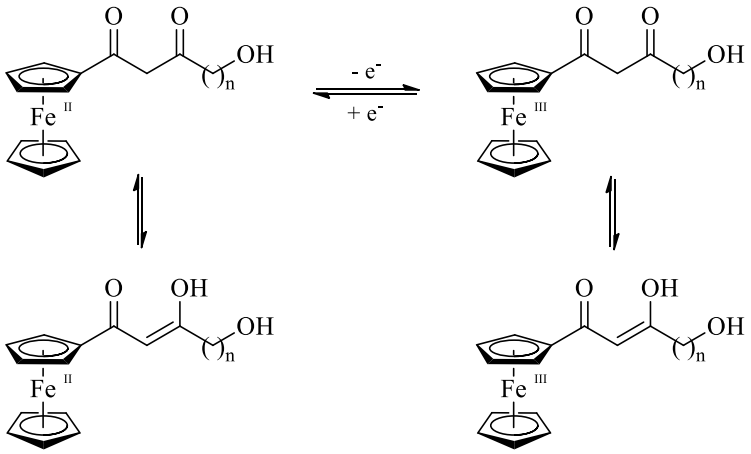

n = 5(**37**), 4(**39**), 3(**40**)

Scheme 3.5: Redox behaviour of β-diketones **37**, **39** and **40** where Fe^{II} is the active redox centre

Cyclic voltammograms of the free β-diketones were measured at 5 different scan rates. The results obtained from these experiments are summarized in Table 3.10. The redox reaction for the ferrocene moiety was shown to be chemically and quasi-electrochemically reversible for all three β-diketones **37**, **39** and **40** by virtue of i_{pc}/i_{pa} ratios that approach 1 in all cases and $\Delta E = E_{pa} - E_{pc} = 91 - 111$ mV (Table 3.10). Electrochemical reversibility is characterized by $\Delta E = 59$ mV. Normally the Fc/Fc^+ couple exhibits electrochemical reversibility, but in the case of **37**, **39** and **40**, the presence of the OH functionality impairs electrochemical reversible behaviour for the ferrocenyl group. Another reason for the larger than expected ΔE values for the ferrocenyl functionality comes from the keto-enol equilibrium that exists for **37**, **39** and **40**

(Scheme 3.5). In principle, the enol form should have its own anodic and cathodic CV peaks, and this counts for the keto form as well. These peaks should closely overlap, as was found for ruthenocenyl β-diketones.[5] The poor resolution for these two sets of redox reactions is consistent with the observed large ΔE values. In the rhodium complexes **41**, **42** and **42**, the β-diketones are ligands, and no enol-keto tautomery is possible. As will be seen below (Table 3.10), ΔE values for the ferrocenyl group in the rhodium complexes are between 69 and 74 mV, lending support for the argument of peak broadening due to two closely overlapping redox processes for the ferrocenyl group in the free ligand. A similar deviation was observed when ferrocenyl carboxylic acid derivatives were studied in ethanol as solvent.[7]

For **37**, **39** and **40** the redox ferrocenyl peak of the β-diketone overlapped with that of the FcH/FcH^+ couple, thus decamethyl ferrocene was used instead as the internal standard. Decamethyl ferrocene was then referenced against FcH/FcH^+ in a separate experiment, and the data of the analyte was manipulated in a spreadsheet to be as if referenced against the FcH/FcH^+ couple.

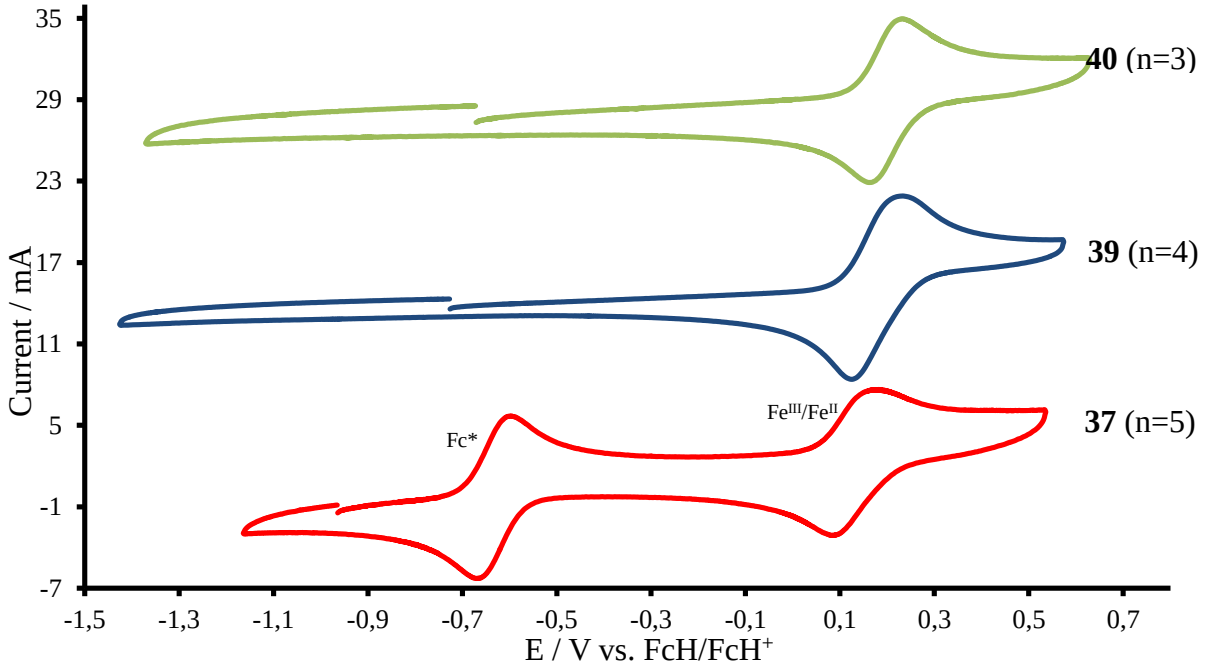

Figure 3.12: Cyclic voltammograms for **37**, **39** and **41** at $\nu = 100$ mVs^{-1} referenced against the FcH/FcH^+ couple at 0 V. [Analyte] = 0.5 mM in DCM with 0.1 M TBAHFP as supporting electrolyte on a glassy carbon working electrode at 25 °C

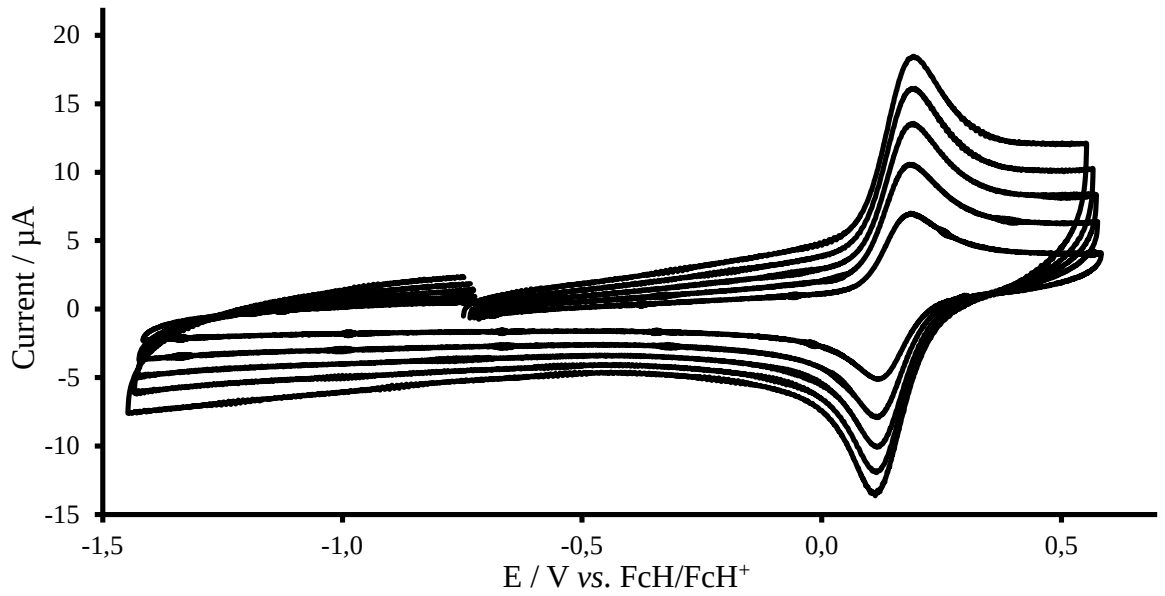

Figure 3.13: Cyclic voltammograms at different scan rates for $FcCOCH_2CO(CH_2)_5OH$ **(37)**. ν = 100 (smallest current voltammogram), 200, 300, 400 and 500 (largest current voltammogram) mV s^{-1} referenced against the FcH/FcH^+ couple at 0 V. **[37]** = 0.5 mM in DCM with 0.1 M TBAHFP as supporting electrolyte on a glassy carbon working electrode at 25 °C

Table 3.10: Cyclic voltammetry data for β-diketones **37**, **39** and **40** at 25°C

$FcCOCH_2CO(CH_2)_5OH$ **(37)**						
scan rate(mVs^{-1})	E_{pa} (mV)	E_{pc} (mV)	$E^{0'}$	ΔE	i_{pa} (µA)	i_{pc}/i_{pa}
100	201	100	151	101	5.33	0.96
200	201	102	151	99	7.43	0.95
300	204	107	155	97	8.95	0.95
400	200	104	152	96	10.67	0.94
500	200	104	152	96	11.81	0.94
$FcCOCH_2CO(CH_2)_4OH$ **(39)**						
100	230	119	174	111	5.98	0.99
200	237	114	176	123	8.11	0.99
300	245	112	179	133	9.89	1.00
400	257	108	183	149	10.88	0.98
500	266	103	184	163	12.11	0.96
$FcCOCH_2CO(CH_2)_3OH$ **(40)**						
100	243	152	197	91	5.66	0.98
200	250	153	201	97	7.78	0.97
300	255	151	203	104	9.42	0.98
400	260	148	204	112	10.78	0.96
500	265	145	205	120	11.96	0.99

From the data could be deduced that the longer the β-diketone sidechain length and thus the further the redox centre is from the –OH group, the easier the Fe^{II} will oxidize to Fe^{III}. Figure

3.14 highlights this trend with a linear relationship between chain length and the formal reduction potential were $E^{0'} = -23n + 266$.

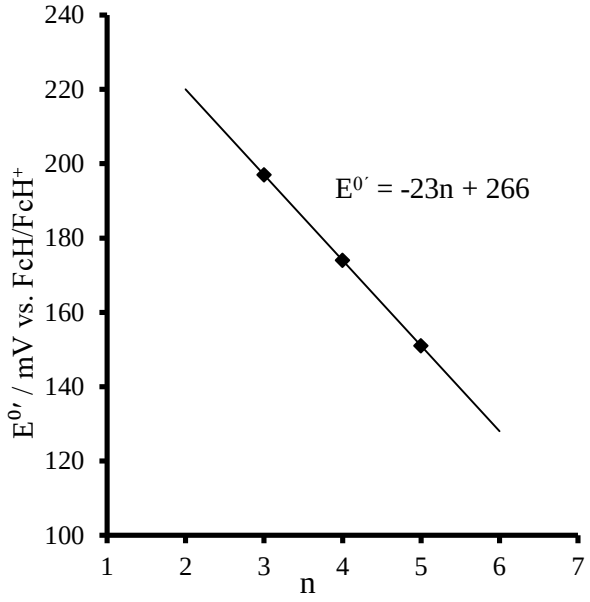

Figure 3.14: Correlation between β-diketone sidechain length and formal reduction potential ($E^{0'}$) of the ferrocenyl group for β-diketones **37** (n = 5), **39** (n = 4) and **40** (n = 3)

Cyclic voltammetry was also performed on the new rhodium complexes **41**, **42** and **43** that were synthesized during this study. $[N(^{n}Bu)_4][B(C_6F_5)_4]$ was used as supporting electrolyte for these compounds to obtain better peak resolution and to increase reversibility.[8] Three redox systems could be observed. The first was assigned to the iron centre of the β-diketonato ligand, the second to the rhodium in 4-coordinated state and the third redox process was assigned to the rhodium interacting with the OH end-group of the chain of the β-diketonato ligand to form a 5-coordinate rhodium centre as postulated in Figure 3.16. Electrochemical data for the Rh-complexes **41**, **42** and **43** is summarized in Table 3.11 and Table 3.12.

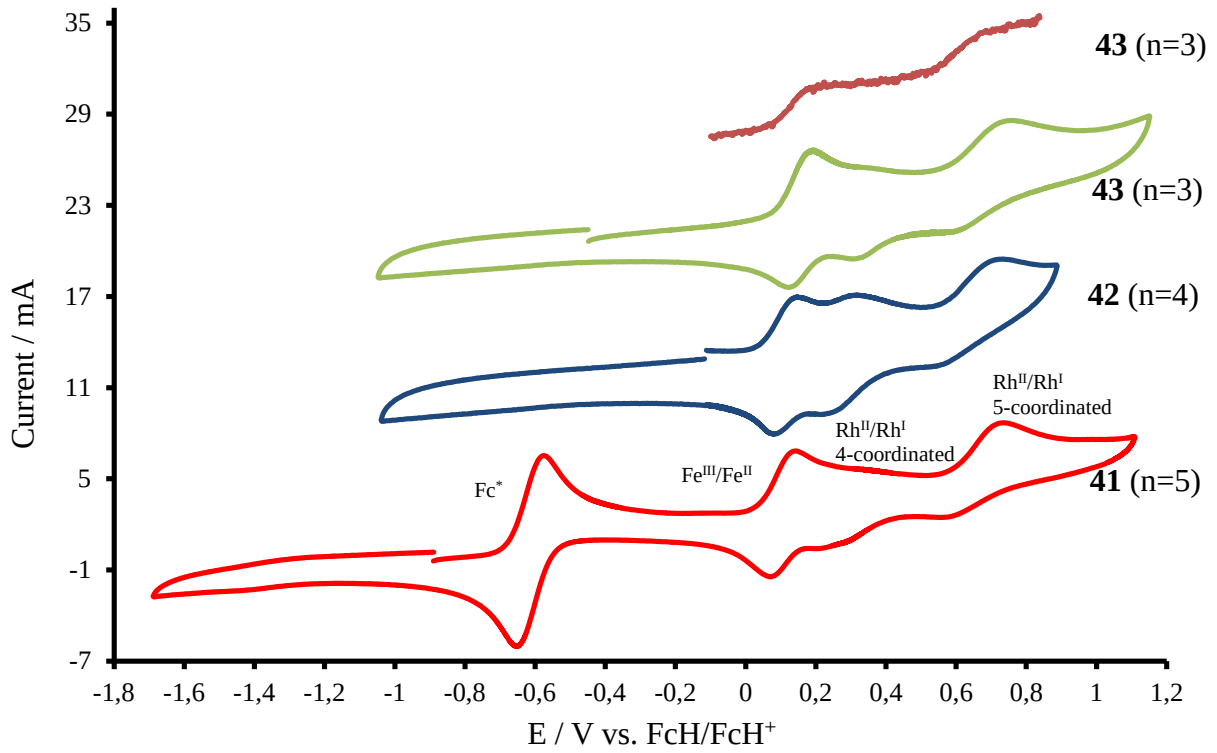

Figure 3.15: Cyclic and linear sweep voltammograms for compounds **41**, **42** and **43** at ν = 100 mV s^{-1} (CV's) and ν = 2 mV s^{-1} (LSV's) referenced against ferrocene as internal standard at 0 V. [Analyte] = 0.5 mM in DCM with $[N(^{n}Bu)_4][B(C_6F_5)_4]$ = 0.1 M as supporting electrolyte on a glassy carbon working electrode at 25 °C

Table 3.11: Cyclic voltammetry data for Rh-complexes **41**, **42** and **43** performed at a scan rate of 100 m V s^{-1}

	E_{pa}(mV)	E_{pc}(mV)	$E^{0'}$	ΔE	i_{pa}(μA)	i_{pc}/i_{pa}
Rh[FcCOCHCO$(CH_2)_5$OH(COD)] **(41)**						
Fe	142	71	107	71	2.45	0.88
Rh 4-coordinate	331	268	300	63	0.73	1.64
Rh 5-coordinate	764	585	675	179	1.71	0.57
Rh[FcCOCHCO$(CH_2)_4$OH(COD)] **(42)**						
Fc	147	73	110	74	2.13	0.94
Rh 4-coordinate	307	235	271	72	0.50	1.44
Rh 5-coordinate	707	563	635	144	1.87	0.57
Rh[FcCOCHCO$(CH_2)_3$OH(COD)] **(43)**						
Fc	163	94	128	69	2.53	0.90
Rh 4-coordinate	334	273	304	61	0.12	4.25
Rh 5-coordinate	710	557	634	153	1.89	0.58

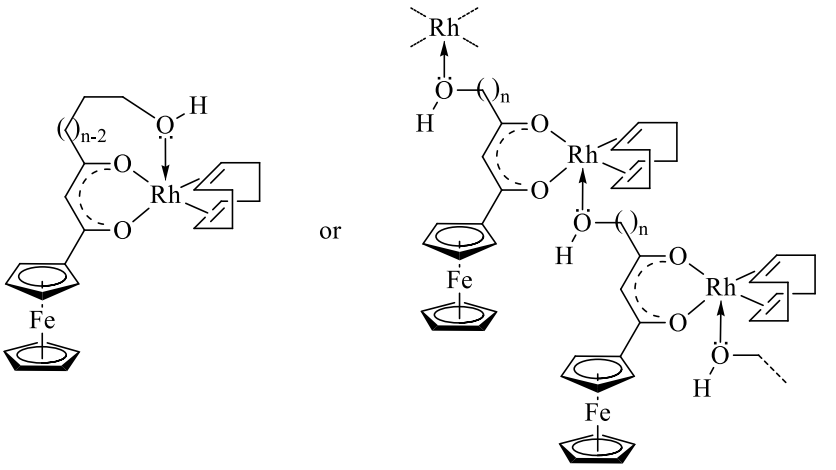

Intramolecular Rh---OH interaction Intermolecular Rh---OH interaction

Figure 3.16: Two possible ways in which complexes **41**, **42** and **43** can exist in a 5-coordinate state in solution

Rhodium is known to form 5-coordinated species, and as the O atom (χ_O = 3.1, χ = electronegativity) bond dative covalently to the Rh atom (χ_{Rh} = 2.2), the oxygen will withdraw electron density, leaving the Rh-redox centre electron poor and thus more difficult to oxidize, consistent with the redox system observed at $E^{0'}$ > 600 mV vs. FcH/FcH^+.

The first Rh^I/Rh^{II} couple at ~ 300 mV vs. FcH/FcH^+ involves an electrochemical reversible one electron transfer process of the 4-coordinated rhodium species by virtue of 61 ≤ ΔE ≤ 72 mV. It also implies a 1-electron transfer process, as a two-electron transfer process must have ΔE = 59/2 = 29.5 mV, whereas a 1-electron transfer process should exhibit ΔE = 59 mV. Current values are small and current ratios (i_{pc}/i_{pa}) are substantially larger than 1. The second Rh^I/Rh^{II} couple at $E^{0'}$ > 600 mV vs. FcH/FcH^+ represents an electrochemically irreversible process for the five-coordinate rhodium species by virtue of 144 ≤ ΔE ≤ 179 mV. Current ratios are substantially smaller than 1, $i_{pc}/i_{pa} \approx 0.57$ at 100 mV s^{-1} scan rate. This is consistent with an equilibrium between the four- and five-coordinate rhodium species that changes with redox state, here Rh^I and Rh^{II}. The existence of an equilibrium between the 4- and 5-coordinate rhodium states is also consistent with the change in current ratios as a function of

scan rate. At faster scan rates, i_{pc}/i_{pa} for the 4-coordinate state increases, while i_{pc}/i_{pa} for the 5-coordinate state decreases. (Table 3.12).

In contrast to the rhodium, the iron redox couple showed good chemical and electrochemical reversibility. Current ratios approached 1 at slow scan rates and $69 \leq \Delta E \leq 74$ mV.

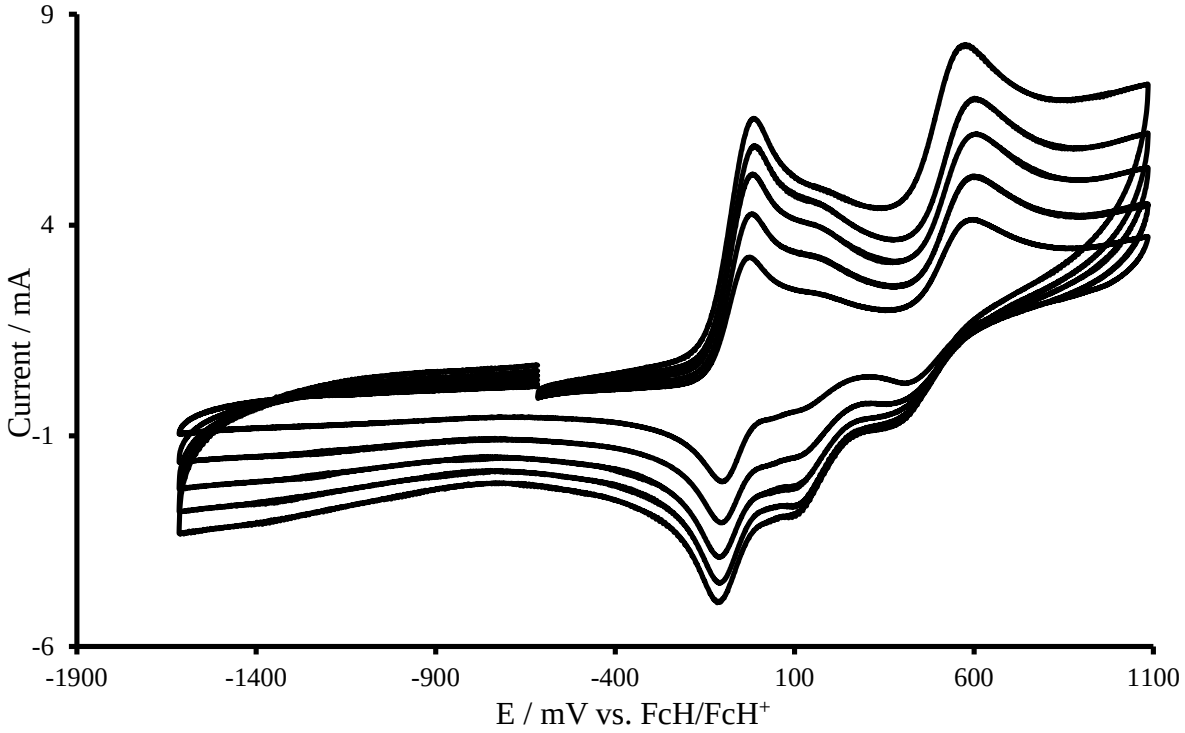

Figure 3.17: Cyclic voltammograms at different scanrates for Rh[FcCOCHCO$(CH_2)_5$OH(COD)] **(41)**. ν = 100 (smallest voltammogram), 200, 300, 400 and 500 (largest voltammogram) mV s^{-1} referenced against the FcH/FcH^+ couple. **[41]** = 0.5 mM in DCM with 0.1 M $[N(^nBu)_4][B(C_6F_5)_4]$ as supporting electrolyte on a glassy carbon working electrode at room temperature.

Table 3.12: Current values and ratios for complex **41** at different scan rates determined from Figure 3.15

Scan rate	100 mV s^{-1}		200 mV s^{-1}		300 mV s^{-1}		400 mV s^{-1}		500 mV s^{-1}	
Coordination	4	5	4	5	4	5	4	5	4	5
i_{pa}	0.73	1.71	1.09	2.03	1.36	2.34	1.72	2.53	1.99	2.91
$i_{pa,\ 4\text{-coordinate}} + i_{pa,5\text{-coordinate}}$	2.44		3.12		3.70		4.25		4.78	
i_{pc}/i_{pa}	1.64	0.57	2.20	0.53	2.31	0.50	2.34	0.50	2.40	0.49
i_{pa} Fc	2.45		3.12		3.79		4.16		4.53	

Further support for the proposed equilibrium between the 4- and 5-coordinate species and a clear indication that these two processes are meaningful related to each other follows from the observation that $i_{pa\ (Rh\ 4\text{-coordinate})} + i_{pa\ (Rh\ 5\text{-coordinate})} \approx i_{pa\ (Fc)}$.

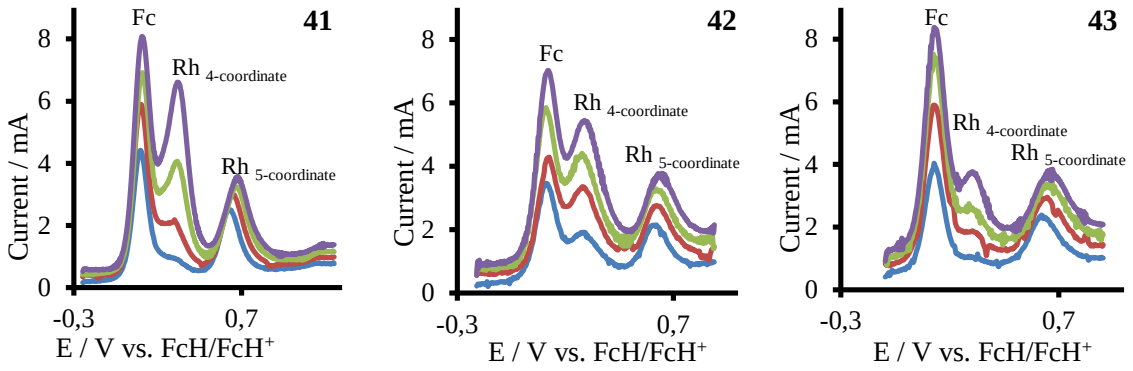

Figure 3.18: Square wave voltammograms of Rh[FcCOCHCO$(CH_2)_n$OH(COD)] complexes **41**, **42** and **43** at 20 (smallest current), 40, 60 and 80 (largest current) Hz referenced against ferrocene as internal standard. [Analyte] = 0.5 mM in DCM with $[N(^nBu)_4][B(C_6F_5)_4]$ = 0.1 M as supporting electrolyte on a glassy carbon working electrode at 25 °C

From the square wave voltammograms of **41**, **42** and **43** (Figure 3.18) it can be observed that the currents of the 4-coordinate rhodium peak increase faster than the currents of the ferrocenyl peak upon increasing the square wave frequencies, while the currents of the 5-coordinate rhodium peak increases slower than the currents of the ferrocenyl peak. This tendency was clearly the strongest with the longest side-chain derivative, **41** (n = 5), and much more subtle with the shortest side-chain derivative, **43** (n = 3).

To understand why in the cyclic, square wave and linear sweep voltammograms, the 4-coordinate rhodium peak is almost absent at slow scan rates (100 mV s^{-1}, 20 Hz and 2 mV s^{-1} respectively), but very prominent at faster scan rates (500 mV s^{-1}, 80 Hz), one may argue as follows:

From the electrochemical results it appears that a 4-coordinate species is dominant. This is the ground state, [Rh(FcCOCHCO$(CH_2)_n$OH)(COD)] because the ferrocenyl group (χ_{Fc} = 1.87) donates electron density into the rhodium core. However, once the ferrocenyl group is oxidized, it becomes strongly electron withdrawing (χ_{Fc^+} = 2.82), comparable to a CF_3 group (χ_{CF_3} = 3.01). This means the ferrocenium species withdraws electron density from the rhodium centre to the point that alcohol-coordination becomes feasible and the Rh^I←:OH bond starts to form slowly. At slow scan rates, by the time the potential is reached where the

4-coordinate Rh^{I} species must be oxidized to Rh^{II} in the intermediate $[Rh^{I}(Fc^{+}COCHCO(CH_2)_nOH)(COD)]$, most of it has already been converted to the 5-coordinate species. Thus the $i_{pa\ (Rh\ 4\text{-}coordinate)}$ current is small, but the anodic current for the 5-coordinate Rh species, that $i_{pa\ (Rh\ 5\text{-}coordinate)}$, is large. At faster scan rates the potential that allows oxidation of the Rh^{I} 4-coordinate species, is reached so quickly that the 5-coordinate Rh^{I} species, because of slow kinetics of formation, have not yet formed in large quantities. Therefor at fast scan rates it was possible to trap the unstable 4-coordinate intermediate $[Rh^{I}(Fc^{+}COCHCO(CH_2)_n\text{-}ÖH)(COD)]$ and see the 4-coordinate Rh^{I} oxidation to liberate $[Rh^{II}(Fc^{+}COCHCO(CH_2)_nOH)(COD)]$by virtue of the large $i_{pa\ (Rh\ 4\text{-}coordinate)}$ value. All the above described results give rise to the electrochemical mechanism described in Scheme 3.6 A.

However, other explanations also exist to account for the two Rh oxidation peaks. It could, for example, be that the free electron pair in the *d*-orbitals of the Rh^{I} interacts with the proton of the OH group to ultimately generate a hydride and free alkoxide. It is clear further research is required, including a computational approach, to clarify the nature of the penta-coordinated Rh centre.

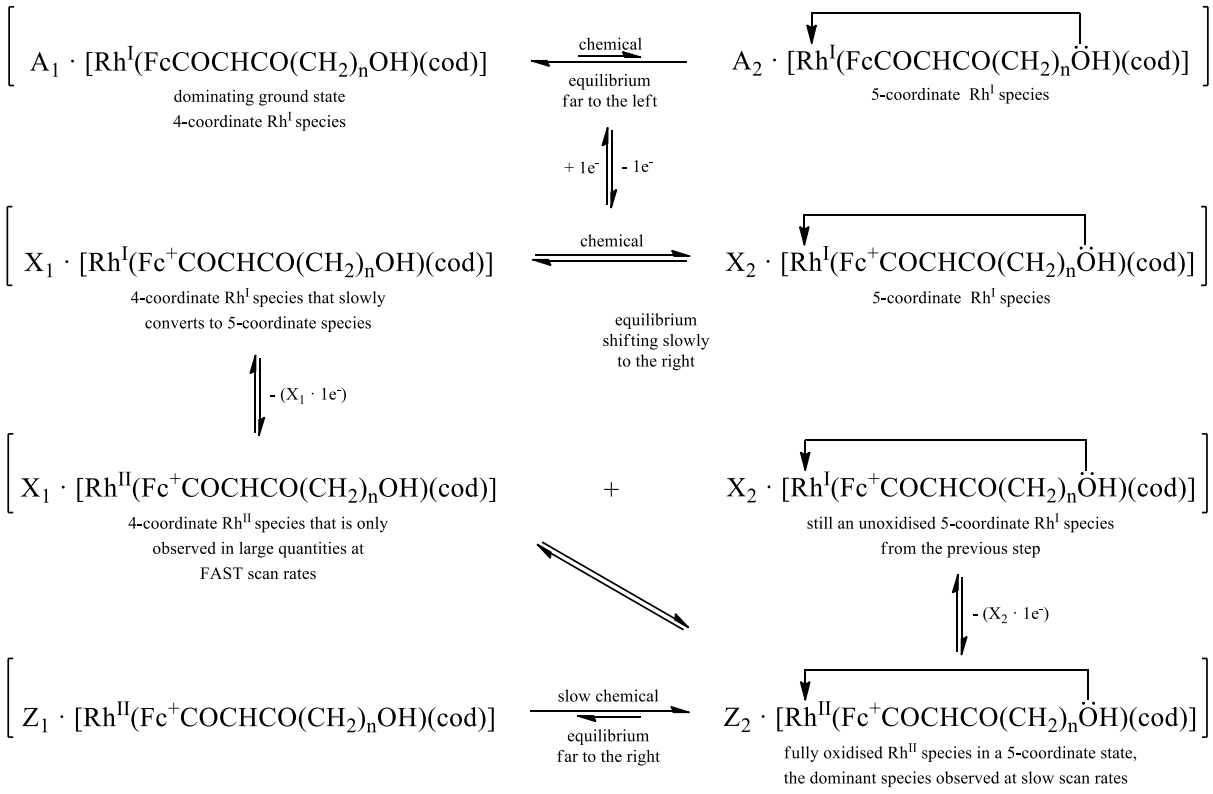

Scheme 3.6 A: Electrochemical mechanism explaining the redox behaviour of [Rh(FcCOCHCO(CH$_2$)$_n$OH)(COD)] complexes **41**, **42** and **43**. A_1, A_2, X_1, X_2, Z_1 and Z_2 are fractions such that $A_1 + A_2 = 1$, $X_1 + X_2 = 1$ and $Z_1 + Z_2 = 1$

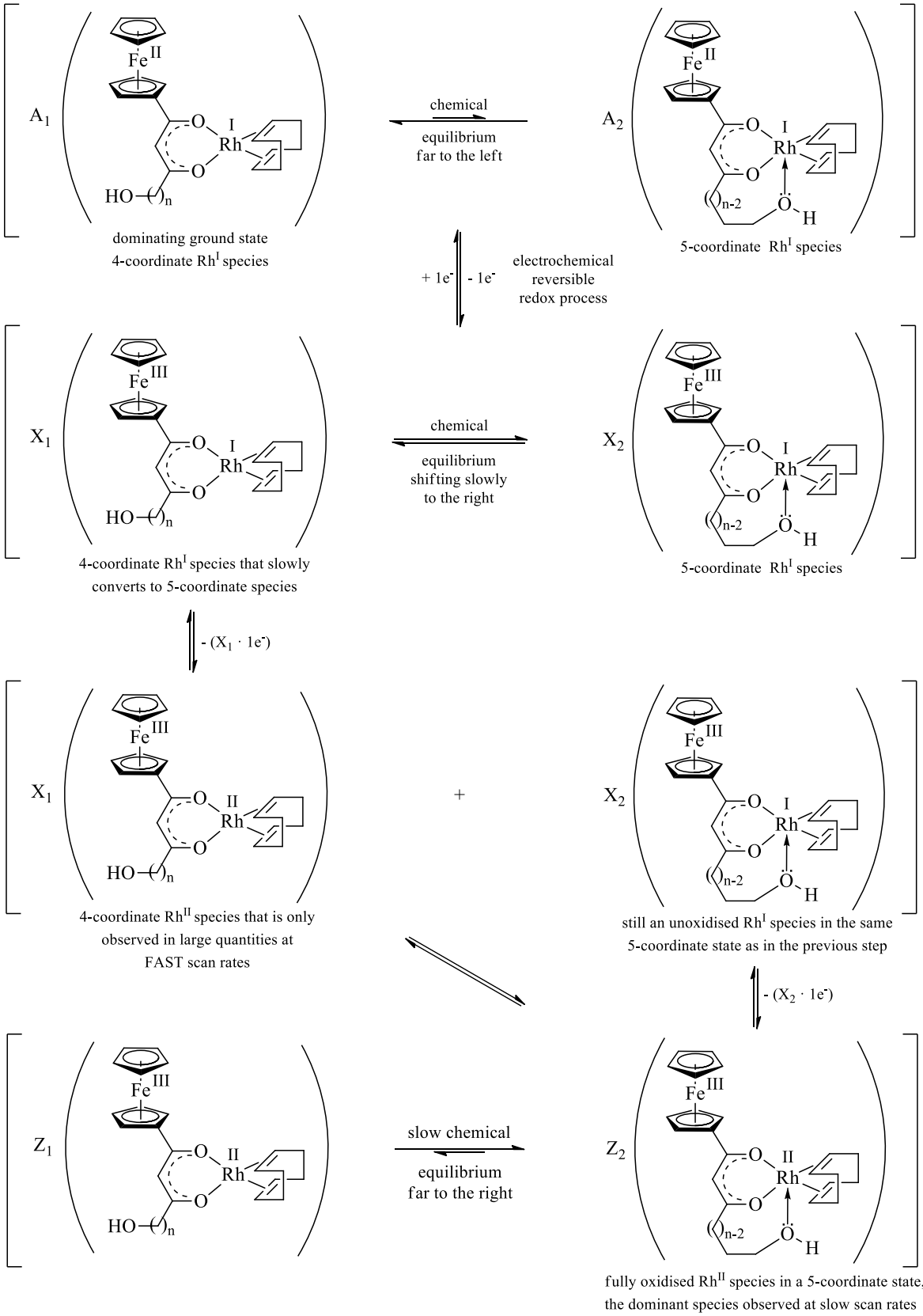

Scheme 3.6 B: Electrochemical scheme showing possible molecular structures of redox species in [Rh(FcCOCHCO(CH$_2$)$_n$OH)(COD)] complexes **41** (n=5), **42** (n=4) and **43** (n=3). Molefractions A_1, A_2, X_1, X_2, Z_1 and Z_2 are such that $A_1 + A_2 = 1$, $X_1 + X_2 = 1$ and $Z_1 + Z_2 = 1$

3.7 Substitution kinetics of [Rh(β-diketonato)(COD)]-complexes with 1,10-phenanthroline

The rate of substitution of the bidentate β-diketonato ligand from [Rh(FcCOCHCO$(CH_2)_n$OH)(COD)] by 1,10-phenanthroline in methanol was investigated during this study. The reaction is showed in Scheme 3.7.

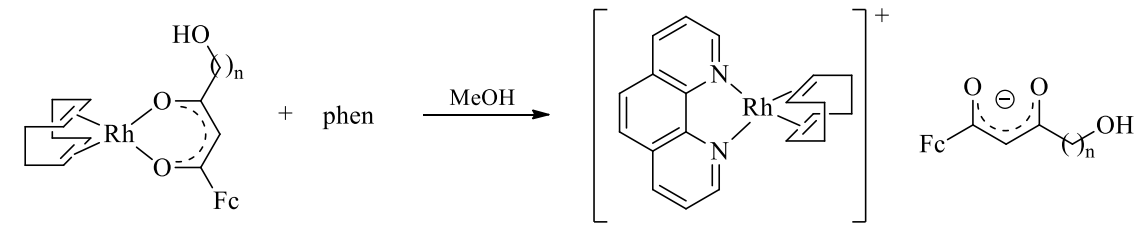

n = 5 (**41**), 4 (**42**), 3 (**43**) (**36**)

Scheme 3.7: Substitution of (FcCOCHCO$(CH_2)_n$OH)$^-$ by 1,10-phenanthroline in square-planar [Rh(FcCOCHCO$(CH_2)_n$OH)(COD)] complexes **41**, **42** and **43** to form the [Rh(phen)(COD)]$^+$ complex **(36)**

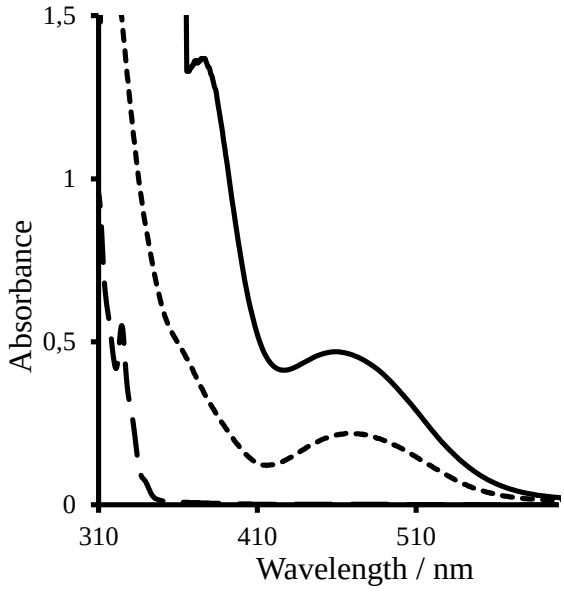

Figure 3.18: Spectra related to the substitution of (FcCOCHCO$(CH_2)_5$OH)$^-$ by 1,10-phenanthroline from [Rh(FcCOCHCO$(CH_2)_5$OH)(COD)], **41**. The solid line represents **41** with **[41]** = 0.6 mol dm^{-3}. The dotted line shows [Rh(phen)(COD)]$^+$ after the complex was reacted with 1,10-phenanthroline and the dashed line represents 1,10 phenanthroline

The extinction coefficients for all three rhodium complexes were determined at 25 °C and are tabulated in Table 3.13. A linear relationship between concentration and absorbance for all

three [Rh(FcCOCHCO(CH$_2$)$_n$OH)(COD)] were observed. Figure 3.19 shows this relationship for **41** with a 5 carbon sidechain length. It is clear the Beer-Lambert law of $A = \varepsilon Cl$ is valid for **41**. It was also found to be valid for **42** and **43**. Two peaks were observed for each of the complexes, but as the one peak (λ_{max} = 342 nm for **41**) exhibited an absorbance exceeding 2 for some of the concentrations used. The other peak (λ_{max} = 470 nm for **41**) was used for all further analysis.

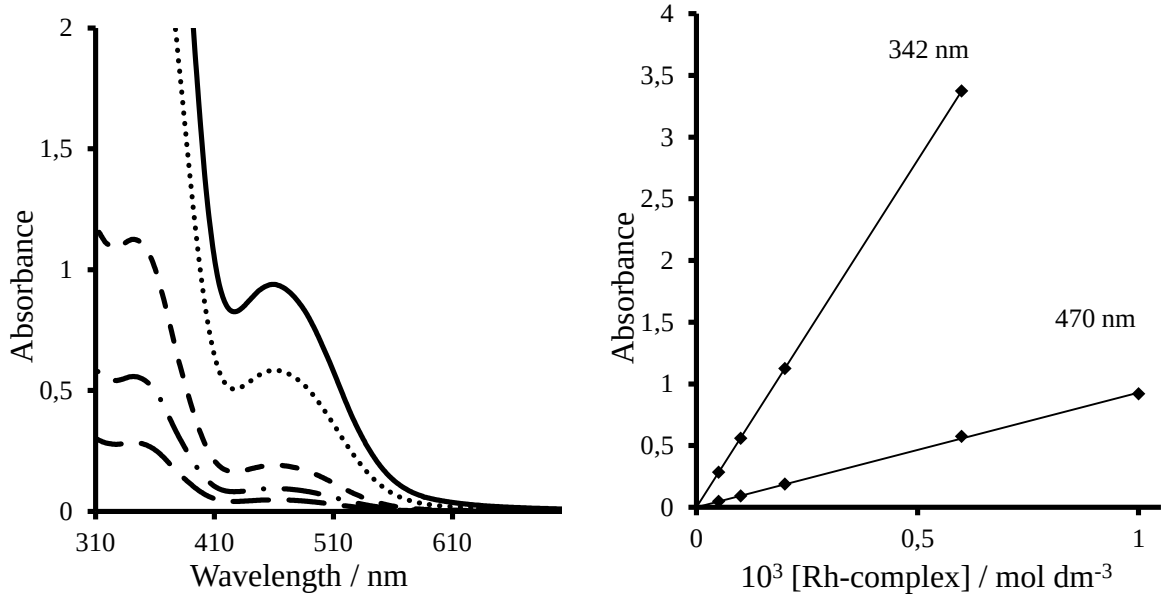

Figure 3.19: UV/vis spectra at different concentrations (left) and Absorbance *vs.* concentration (right) for [Rh(FcCOCHCO(CH$_2$)$_5$OH)(COD)] **(41)** at 25 °C in methanol.

Table 3.13: Molar extinction coefficients (ε) of Rh-complexes **41**, **42** and **43** at 25 °C in methanol

Rh-complex	λ_{max} / nm [ε / dm^3 mol^{-1} cm^{-1}]
41 (n=5)	470 [929]
42 (n=4)	468 [901]
43 (n=3)	467 [889]

[Rh(FcCOCHCO(CH$_2$)$_n$OH)(COD)] was reacted with 1,10-phenanthroline under pseudo-first-order conditions where [phen] was in an excess of 5 – 50 times that of the Rh complex. The disappearance of [Rh(FcCOCHCO(CH$_2$)$_n$OH)(COD)] was monitored by UV/vis at

different temperatures and the observed rate constant k_{obs} was obtained from the stopped-flow software for each temperature using the equation

$$ln\left(\frac{A_0}{A_t}\right) = k_{obs}t$$

eq. 3.5

k_{obs} was found to have a linear relationship with [phen] by plotting k_{obs} *vs.* [phen]. A non-zero y-intercept was found for all three complexes, indicating a solvent pathway is also active in the mechanism of substitution.

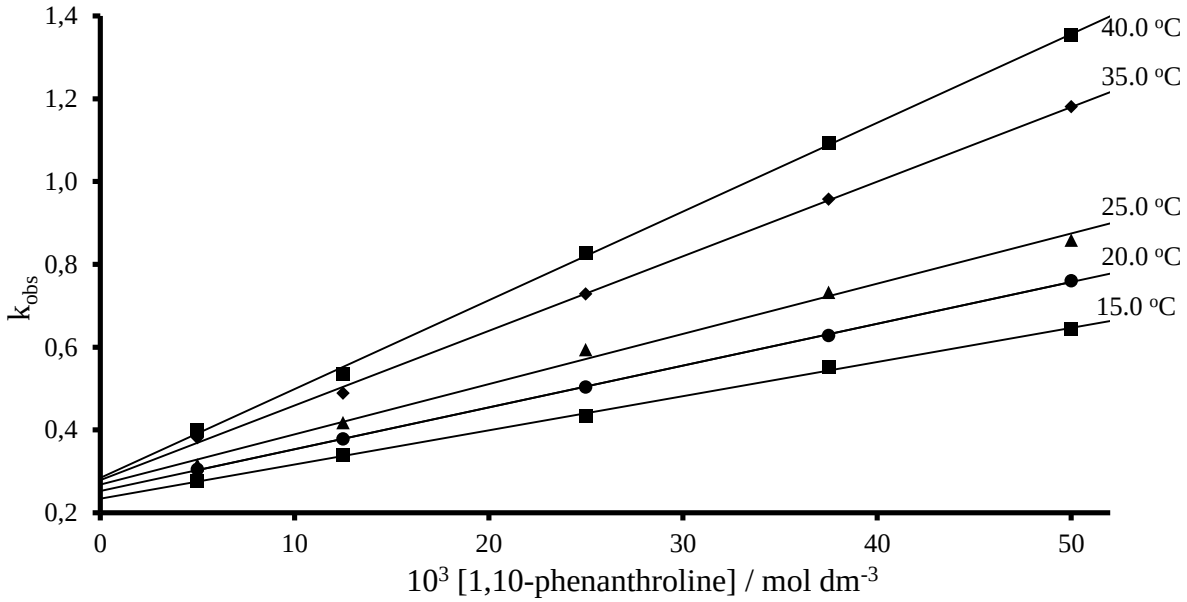

Figure 3.20: k_{obs} *versus* [phen] a) [Rh(FcCOCHCO$(CH_2)_5$OH)(COD)], λ = 470 nm at different temperatures

For this pseudo first order reaction, the rate can be defined as

$$Rate = k_{obs}[Rh - complex]$$

eq. 3.6

As the graphs have non-zero intercepts, is follows that

$$k_{obs} = k_s + k_y[phen]$$

eq. 3.7

Thus the slopes of the graphs in Figure 3.20 represent k_y at the specified temperature and the y-intercept k_s. This is summarized in Table 3.14.

Table 3.14: Activation parameters of the substitution reaction of Rh(β-diketonato)(COD)] complexes with 1,10-phenanthroline in methanol

Complex	T/°C	k_y $dm^3\ mol^{-1}\ s^{-1}$	$\Delta H_y^{\ddagger}$ kJ mol^{-1}	$\Delta S_y^{\ddagger}$ J $mol^{-1}\ K^{-1}$	$\Delta G_y^{\ddagger}$ kJ mol^{-1}	k_s/ s^{-1}	$\Delta H_s^{\ddagger}$ kJ mol^{-1}	$\Delta S_s^{\ddagger}$ J $mol^{-1}\ K^{-1}$	$\Delta G_s^{\ddagger}$ kJ mol^{-1}
41 (n=5)	15.0 20.0 25.0 35.0 40.0	8.25(17) 10.01(7) 12.14(50) 18.0(31) 21.6(32)	26.54(3)	-135.17(70)	66.17(4)	0.235(5) 0.253(2) 0.268(15) 0.278(9) 0.284(10)	2.82(40)	-247(13)	76.5(30)
42 (n=4)	15.0 20.0 25.0 35.0 40.0	99.8(18) 126.8(23) 159.9(6) 248.7(45) 307.0(36)	31.23(12)	-98.31(54)	60.05(13)	0.203(11) 0.221(17) 0.236(9) 0.248(7) 0.267(3)	4.98(53)	-241(31)	76.8(44)
43 (n=3)	15.0 20.0 25.0 35.0 40.0	5922(19) 7328(4) 9006(21) 13343(30) 16095(15)	27.51(9)	-77.27(31)	50.16(10)	0.192(2) 0.213(7) 0.226(14) 0.235(20) 0.248(16)	4.34(46)	-243(27)	76.9(35)

The entropy and enthalpy of activation, $\Delta H^{\ddagger}$ and $\Delta S^{\ddagger}$, can be determined graphically by plotting $ln\frac{k_y}{T}$ against $\frac{1}{T}$. This yields a straight line, and from this, utilizing Equation 3.8, $\Delta H^{\ddagger}$ and $\Delta S^{\ddagger}$ can be found as the slope = $-\frac{\Delta H^{\ddagger}}{R}$ and the y-intercept= $ln\frac{k}{h}+\frac{\Delta S^{\ddagger}}{R}$ respectively.

$$ln\frac{k_y}{T} = ln\frac{k}{h} - \frac{\Delta H^{\ddagger}}{RT} + \frac{\Delta S^{\ddagger}}{R}$$

eq. 3.8

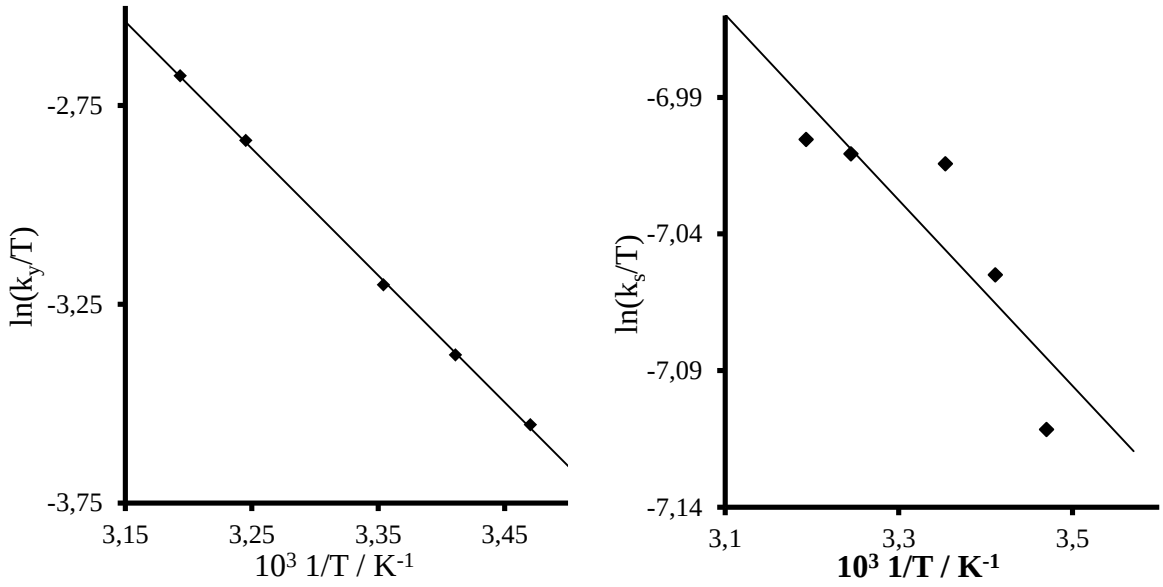

Figure 3.21: The Eyring graph of $ln\frac{k_y}{T}$ against $\frac{1}{T}$ for the substitution reaction of [Rh(FcCOCHCO$(CH_2)_5$OH)(COD)].

The same kinetic treatment can also be applied to the solvent first order constants to yield the activation entropy and enthalpy of the solvent path. This data is summarized in Table 3.14.

All associative substitution mechanisms are associated with large negative $\Delta S^{\ddagger}$ values. [Rh(acac)(COD)] was proven to proceed via an associative mechanism with the aid of a high pressure study. The $\Delta S^{\ddagger}$ value for the acac substitution was found to be -108 J K^{-1} mol^{-1}, this is considered a large negative.[9] Similarly, and by comparison, the large negative $\Delta S^{\ddagger}$ values obtained in this study of the substitution of the β-diketonato ligand from [Rh(FcCOCHCO$(CH_2)_n$OH)(COD)] (**41**, **42** and **43)** by 1,10-phenanthroline, -135.17, -98.31 and -77.27 J mol^{-1} K^{-1} respectively, shows that the reaction occurs *via* an associative mechanism.

The above described results lead to the proposal of the mechanism shown in Scheme 3.8 for the substitution of (FcCOCHCO$(CH_2)_n$OH)$^-$ from [Rh(FcCOCHCO$(CH_2)_n$OH)(COD)] with 1,10-phenanthroline.

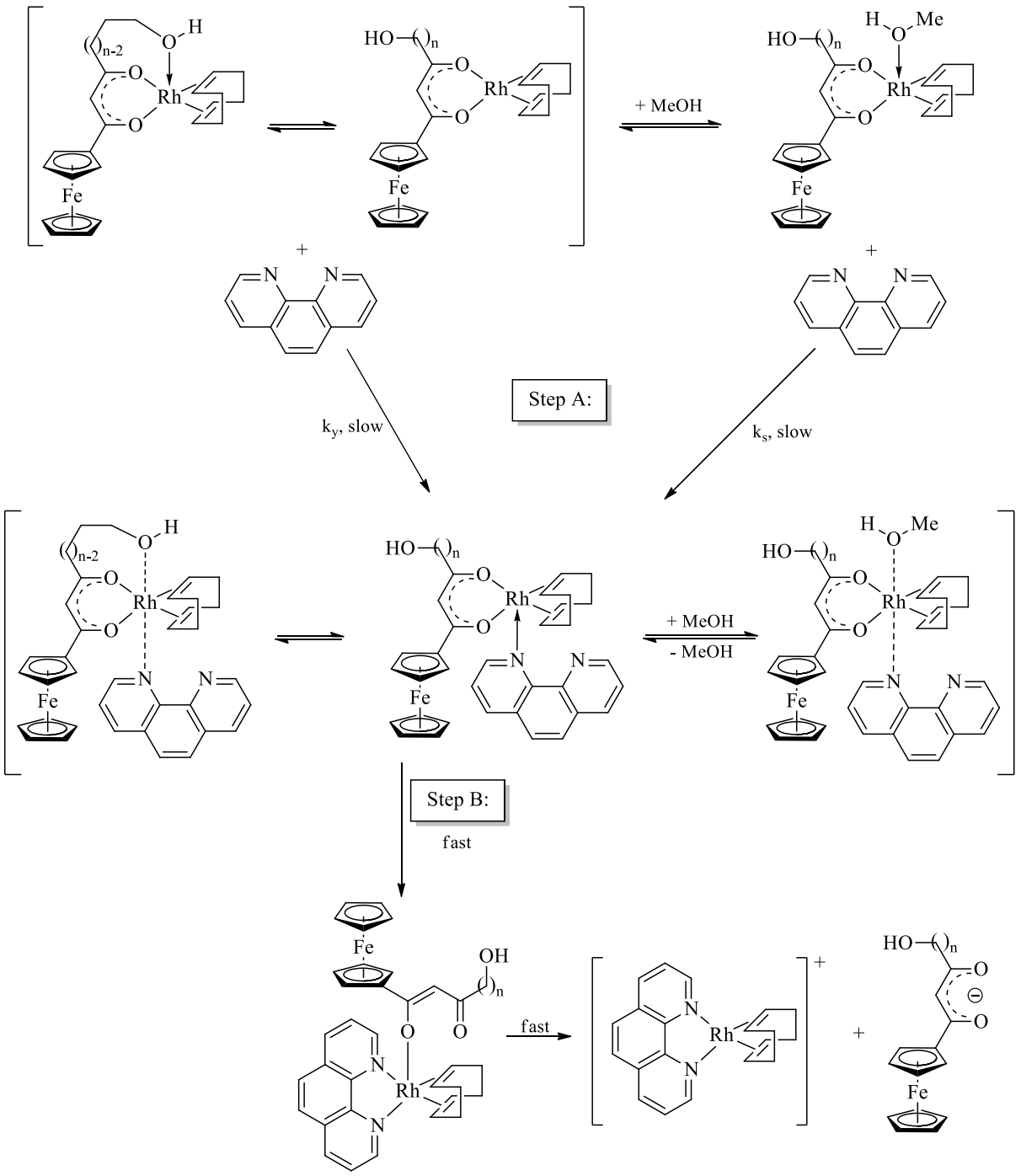

Scheme 3.8: General proposed mechanism for the substitution reaction between [Rh(β-diketonato)(COD)] complexes and 1,10-phenanthroline where n = 5, 4 and 3.[10,11]

Although the above described kinetic results are such that the mechanism suggested in Scheme 3.8 is indistinguishable from one where STEP A is a fast equilibrium and STEP B is the slow, rate determining step, the alternative mechanism is not considered as dominant, simply because electrochemically, evidence of a 5-coordinate rhodium complex is not

possible if Rh-O bond breaking in the Rh-OH interaction is fast. The 5-coordinate species need to exist long enough to allow electrochemical detection. This implies that STEP A must be slow.

3.8 Group electronegativities

Observed group electronegativities can be related to infrared bond stretching frequencies. Calculated group electronegativities can be found for some groups in literature,[12] and by plotting these values against the C=O stretching frequencies of the methyl or ethyl esters of these groups, the apparent group electronegativities of other groups can be extrapolated as shown in Figure 3.22. The observed group electronegativities for $-(CH_2)_nOH$ were found to be χ_R = 2.21 for n = 5, χ_R = 2.34 for n = 4 and χ_R = 2.42 for n = 3.

Table 3.15: Carbonyl stretching frequencies and apparent group electronegativities (Gordy scale)of methyl and ethyl esters[12]

Ester	$\nu_{(C=O)}$ (cm^{-1})	χ_R (Gordy scale)
HCOOMe	1717	2.13
$H_3CCOOMe$	1738	2.34
$(CHCl_2)COOMe$	1755	2.62
$(CCl_3)COOMe$	1768	2.76
ClCOOMe	1780	2.97
FcCOOMe	1700	1.87[1]
$HO(CH_2)_5COOMe$[13]	1725	2.21[a]
$HO(CH_2)_4COOMe$[13]	1735	2.34[a]
$HO(CH_2)_3COOEt$[13]	1741	2.42[a]

[a] Determined through interpolating the linear relationship between $\nu_{(C=O)}$ and χ_R

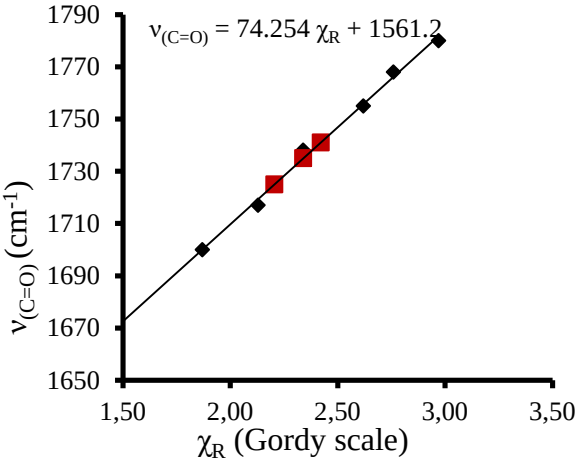

Figure 3.22: The relationship between carbonyl stretching frequencies and apparent group electronegativities (Gordy scale) of methyl and ethyl esters. The interpolated values for $-(CH_2)_nOH$ are shown in red

3.9 Correlations and summary

Table 3.16: Important results relating to $FcCOCH_2CO(CH_2)_nOH$ (**37**, **39** and **40**) and $[Rh(FcCOCHCO(CH_2)_5OH)(COD)]$. (**41**, **42** and **43**) obtained through this study

	37 (n = 5)	**39** (n = 4)	**40** (n = 3)
% enol tautomer in solution	75.1	nd[a]	nd[a]
^1H –methine keto tautomer (ppm)	3.75	3.76	3.79
$(^1H)_2$ –methylene enol tautomer (ppm)	6.65	5.66	5.69
$\nu_{(C=O)}$ (cm^{-1})	1548; 1609	1547; 1604	1542; 1602
λ_{max} nm [ε/dm^{3}mol^{-1}cm^{-1}]	470 [1022]	468 [989]	467 [961]
pK_a'	10.44	8.01	5.97
$E^{0'}$ (mV)	151	174	197
	41 (n=5)	**42** (n=4)	**43** (n=3)
$\nu_{(C=O)}$ (cm^{-1})	1507; 1541	1508; 1540	1510; 1542
λ_{max} nm [ε/dm^{3}mol^{-1}cm^{-1}]	470 [929.]	468 [902]	467 [889]
$E^{0'}$ (mV) Ferrocene	107	110	128
$E^{0'}$ (mV) Rhodium	675	635	634
k_y/ dm^3 mol^{-1} s^{-1} at 25 °C	12.14	159.85	9005.66
$\Delta H_y^{\ddagger}$ kJ mol^{-1}	26.54	31.23	27.51
$\Delta S_y^{\ddagger}$ J mol^{-1} K^{-1}	-135.17	-98.31	-77.27
$\Delta G_y^{\ddagger}$ kJ mol^{-1}	66.17	60.05	50.16

[a] Not determined

With just three compounds, it is difficult to establish reliable trends. It can be noted however that the changes due to the alkyl chain length correlate as expected from literature.[1,14] Two correlations that obey these trends very well were already shown in Figures 3.11 (pK_a' vs. n) and 3.14 ($E^{0'}$ vs. n).

E^0 and pK_a' are both thermodynamic quantities. The relationship between these values can be described as:[15]

$$E^0 = \left(\frac{RT}{nF}\right) ln(K_a)$$

$$E^0 = \left(\frac{RT - 2.303RT}{nF}\right) pK_a$$

$$E^0 = -0.059\, pK_a$$

for a 1-electron process at 25 °C.

By plotting pK_a' against $E^{0'}$, a linear relationship was obtained where slope of -10.265 mV or -0.0103 V was obtained (Figure 3.19). This difference from the theoretical slope of -0.059 V can be ascribed to using the formal reduction potential under the utilized experimental conditions instead of the standard reduction potential which is valid at 25 °C, 1 atm pressure and concentration of 1 mol dm^{-1}.

By comparing the rate of substitution of of the β-diketonato ligand from Rh[FcCOCHCO$(CH_2)_n$OH(COD)] with the pK_a of the free β-diketone, it is evident that the acidic β-diketones accelerate the rate of substitution with phen, but for compounds **41**, **42** and **43** this relationship was non-linear which contrasts literature results.[10] As just three points were used, more data is needed to confirm whether the relationship is truly non-linear.

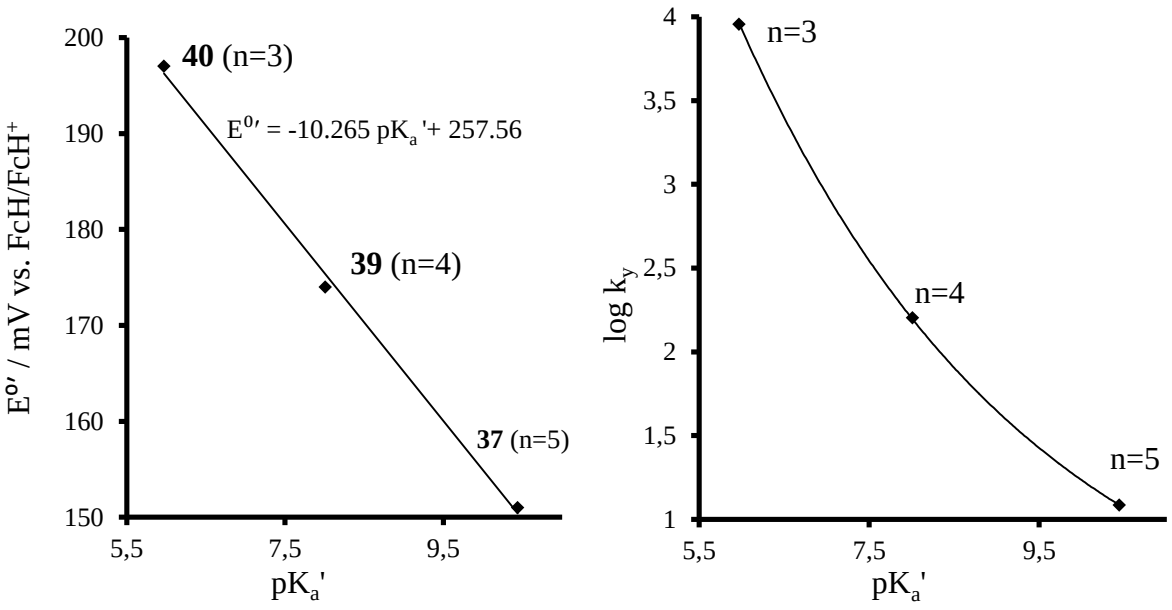

Figure 3.23: Left: Correlation between pK_a' and the formal reduction potentials of the $FcCOCH_2CO(CH_2)_nOH$ β-diketones Right: Correlation between pK_a' and log k_y for the reaction of the different $Rh(FcCOCHCO(CH_2)_nOH)(COD)]$ complexes with 1,10-phenanthroline in methanol at 25 °C.

Correlations with group-electronegativity for compounds **37**, **39** and **40** were also compared to known ferrocene-containing β-diketones.

Apparent group electronegativities for the β-diketone sidechains were determined by interpolation (Figure 3.22). Formal reduction potential increases as the group electronegativity increases. In the case of compounds **37**, **39** and **40**, the formal reduction potentials are much lower than for the other ferrocenyl β-diketones, and the rate of increase is much larger, Figure 3.24, left.

Table 3.17: Apparent group electronegativity (Gordy scale), formal reduction potentials and pK_a' values for some ferrocenyl β-diketones as well as compounds **37**, **39** and **40**

β-diketone	χ_R (Gordy scale)	$E^{0'}$ (mV)	pK_a'
$FcCOCH_2COFc$	1.87	264	13.1
$FcCOCH_2COPh$	2.21	306	10.41
$FcCOCH_2COCH_3$	2.34	313	10.01
$FcCOCH_2COCCl_3$	2.76	370	7.13
$FcCOCH_2COCF_3$	3.01	394	6.56
37 (n=5)	2.21	151	10.44
39 (n=4)	2.34	174	8.01
40 (n=3)	2.42	197	5.97

pK_a' decreases as the group electronegativity increases, thus a more electronegative R group causes the β-diketone to be more acidic. The rate of decrease in pK_a' values for compounds **37**, **39** and **40** is much larger than for the other β-diketones, Figure 3.21, right.

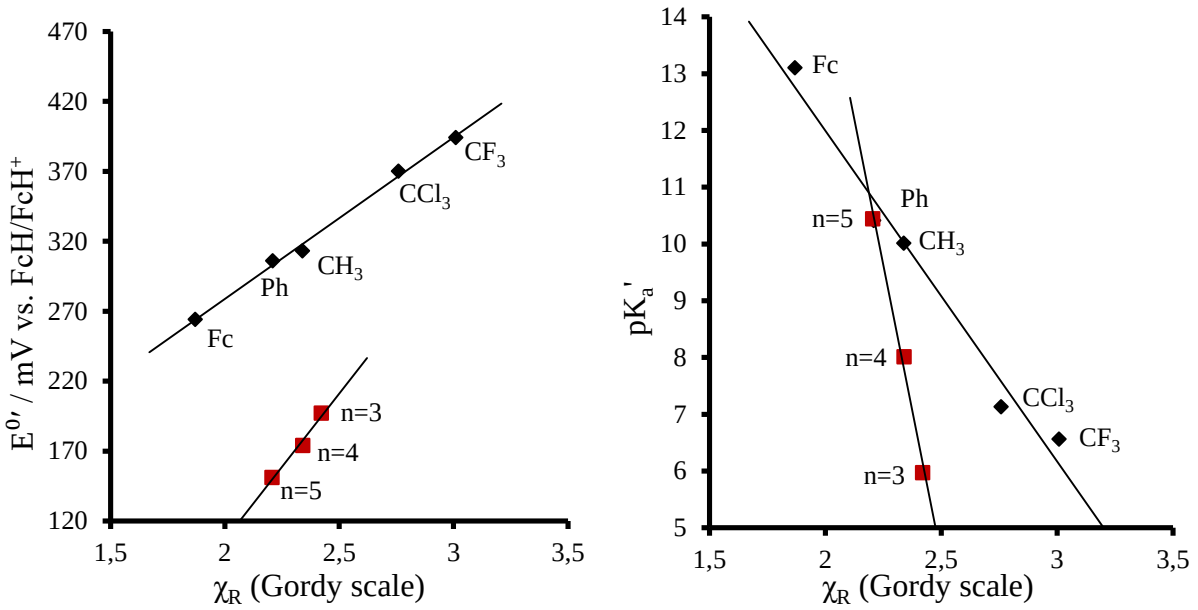

Figure 3.24: Left: Correlation between apparent group electronegativities (Gordy scale) and the formal reduction potentials of the $FcCOCH_2COR$and $FcCOCH_2CO(CH_2)_nOH$ β-diketones . Right: Correlation between pK_a' and apparent group electronegativities (Gordy scale)

All deviations from the properties of $FcCOCH_2COR$ β-diketones (R = Fc, Ph, CH_3, CCl_3 and CF_3) are consistent with the $–(CH_2)OH$ side-chain of **37**, **39** and **40** interacting in some way, possibly through H bonding from the proton to the β-diketonato pseudoaromatic core.

This concludes the discussion of all the experimental results for this study. All goals in Chapter 1 were achieved.

Bibliography

(1) du Plessis, W. C. (Ina); Vosloo, T. G.; Swarts, J. C. *J. Chem. Soc. Dalton Trans.* **1998**, *15*, 2507–2514.

(2) Bertolasi, V.; Ferretti, V.; Gilli, P.; Yao, X.; Li, C.-J. *New J Chem* **2008**, *32* (4), 694–704.

(3) Cotton, F. A.; Wilkinson, G.; Gaus, P. L. *Basic Inorganic Chemistry*, 3rd ed.; Wiley-VCH Verlag GmbH & Co. KGaA, 1995.

(4) Allen, F. H.; Kennard, O.; Watson, D. G.; Brammer, L.; Orpen, A. G.; Taylor, R. *J. Chem. Soc. Perkin Trans. 2* **1987**, No. 12, S1–S19.

(5) Kemp, K. C.; Fourie, E.; Conradie, J.; Swarts, J. C. *Organometallics* **2008**, *27* (3), 353–362.

(6) House, J. E. *Principles of Chemical Kinetics*; Academic Press, 2007.

(7) Swarts, J. C. Unpublished results: Electrochemical study of ferrocenyl carboxylic acids.

(8) Gericke, H. J.; Barnard, N. I.; Erasmus, E.; Swarts, J. C.; Cook, M. J.; Aquino, M. A. S. *Inorganica Chim. Acta* **2010**, *363* (10), 2222–2232.

(9) Leitão, M. L. P.; Pilcher, G.; Meng-Yan, Y.; Brown, J. M.; Conn, A. D. *J. Chem. Thermodyn.* **1990**, *22* (9), 885–891.

(10) Vosloo, T. G.; (Ina) du Plessis, W. C.; Swarts, J. C. *Inorganica Chim. Acta* **2002**, *331* (1), 188–193.

(11) Vosloo, T. G.; Swarts, J. C. *Transit. Met. Chem.* **2002**, *27* (4), 411–415.

(12) Kagarise, R. E. *J. Am. Chem. Soc.* **1955**, *77* (5), 1377–1379.

(13) Mol-Instincts Spectral database http://search.molinstincts.com/spectra (accessed Jan 28, 2016).

(14) du Plessis, W. (Ina); Erasmus, J. J.; Lamprecht, G. J.; Conradie, J.; Cameron, T. S.; Aquino, M. A.; Swarts, J. C. *Can. J. Chem.* **1999**, *77* (3), 378–386.

(15) Hammerich, O.; Lund, H. *Organic Electrochemistry, Fourth Edition*,; CRC Press, 2000.

4 Experimental

4.1 Introduction

In this section the materials, equipment, techniques and experimental procedures used in this study are presented.

4.2 Materials

Reagents (Merck, Aldrich and Fluka) employed for synthesis were used without further purification. Spectroscopic grade solvent was used for all analysis. Organic solvents were dried according to published procedures.[1,2]

Column chromatography was performed on Kieselgel 60 (Merck, grain size 0.040-0.063 mm). Thin layer chromatography was used to follow reactions, to determine the purity of products as well as determine the R_f-values for specific eluents.

4.3 Apparatus

4.3.1 NMR Spectroscopy

^{1}H NMR spectra were measured on a Bruker Advance DPX 300 NMR spectrometer, and ^{13}C NMR spectra were measured on a Bruker 600 NMR spectrometer. All spectra were obtained at 298 K and all chemical shifts are reported relative to TMS ($Si(CH_3)_4$) at 0.00 ppm for ^{1}H

NMR and $CDCl_3$ at 76.98 ppm for ^{13}C NMR. Selected spectra have been provided in the appendix.

4.3.2 Infrared spectroscopy

Infrared spectra were obtained using a Thermo Nicolet i550 FTIR spectrometer using the ATR option.

4.3.3 UV/vis spectroscopy

UV-vis spectra were measured on a Shimadzu UV-1650PC spectrophotometer. pH measurements were performed on a Orion model SA720 with a glass electrode that was calibrated at 4.01, 7.00 and 10.01.

4.3.4 Electrochemistry

An electrochemical study was carried out using a Princeton Applied Research PARSTAT 2273 voltammograph and recorded using PowerSuite (Version 2.58).

4.3.5 Substitution kinetics

Kinetic measurements were performed on a Olis RSM 1000 stopped-flow spectrophotometer.

4.3.6 X-ray crystallography

Data collection was performed with a Bruker D8 Venture kappa geometry diffractometer.

4.4 Synthesis

4.4.1 Acetyl ferrocene

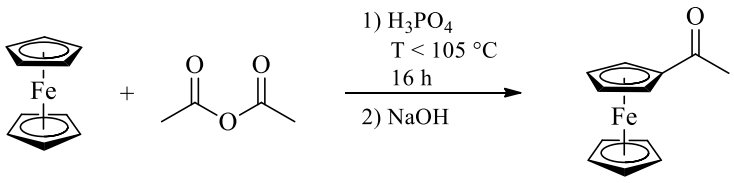

44 **21**

Ferrocene (50.0 g, 0.269 mol) was dissolved in hot (100°C) acetic anhydride (125 ml, 1.32 mol). The mixture was stirred until homogenous, where-after phosphoric acid (85 %, 10 ml) was added. This reaction was exothermic, and care was taken to not exceed 105 °C. The reaction mixture was then placed on ice and left overnight. A cold solution of sodium hydroxide (125 ml, 10 M) was added to neutralize the reaction. Sodium carbonate was added until the solution reached a pH = 10. The resulting precipitate was filtered off and washed with water. The product was recrystallized from hexane to yield orange-brown crystals of acetyl ferrocene (44.87 g, 0.197 mol, 73.2 %). IR ν /cm^{-1} = 1662 (C=O). ^{1}H NMR δ_H (300 MHz, $CDCl_3$)/ppm: 2.36 s (3H; CH_3); 4.16 s (5H; C_5H_5); 4.47 t (2H; C_5H_4); 4.74 t (2H; C_5H_4).

4.4.2 1-Ferrocenyl-8-hydroxyoctane-1,3-dione, 37

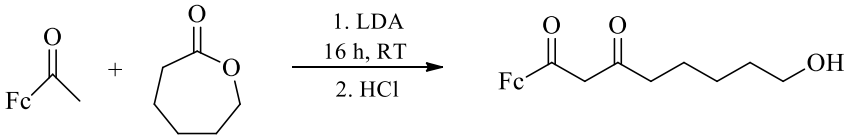

21 **5** **37**

Acetyl ferrocene (4.0 g, 17.54 mmol) was dissolved in dry THF (35 ml) under strict Schlenk conditions (Argon gas). It was then cooled to 0 °C and a lithium diisoproplyamide (LDA) solution (2 M, 10.5 ml, 21 mmol) was added drop wise. The mixture was kept at this temperature for 30 minutes while stirring. ε-Caprolactone (**5**) (1.0 ml, 9.024 mmol) was

added drop wise and the mixture was left to stir overnight at room temperature. Diethyl ether (50 ml) was added and a dark red dispersion was formed. It was then filtered and washed with diethyl ether (4 x 10 ml). The precipitate was then suspended in HCl (1 M, 50 ml) and extracted with diethyl ether, dried with anhydrous $MgSO_4$, and the solvent was removed under reduced pressure. The resulting product was purified using column chromatography (ethyl acetate/hexane 1:1, R_f = 0.28) to yield a spectroscopic pure dark red liquid **37** (1.81 g, 5.289 mmol, 58.6 %). IR ν /cm^{-1} = 1609 and 1548 (C=O). ^{1}H NMR δ_H (300 MHz, $CDCl_3$)/ppm: 2.25 m (2H; keto-CH_2), 2.27 m (2H; enol-CH_2), 2.57 t (2H; keto-CH_2), 3.57 m (2H; keto-CH_2), 3.60 m (2H; enol-CH_2), 3.75 s (2H; keto-CH_2), 4.02 m (2H; keto-CH_2), 4.12 s (5H; enol-C_5H_5), 4.17 s (5H; keto-C_5H_5), 4.43 t (2H; enol-C_5H_4), 4.50 t (2H; keto-C_5H_4), 4.71 t (2H; enol-C_5H_4), 4.72 t (2H; keto-C_5H_4), 5.65 s (1H; enol-CH), 15.85 s (1H, -OH). ^{13}C NMR δ_H (600 MHz, $CDCl_3$)/ppm: 23.01 (keto chain-CH_2); 25.12 (keto chain-CH_2); 25.42 (enol chain-CH_2); 25.87 (enol chain-CH_2); 32.46 (keto and enol chain-CH_2); 37.59 (enol chain-CH_2); 43.34 (keto chain-CH_2); 55.16 (keto CO<u>C</u>H_2CO); 62.69 (keto chain-CH_2); 62.78 (enol chain-CH_2); 68.65 (2C, enol C_5H_4); 69.88 (2C, keto C_5H_4); 70.32 (5C, enol C_5H_5); 70.46 (5C, keto C_5H_5); 72.08 (2C, enol C_5H_4), 73.09 (2C, keto C_5H_4); 96.57 (enol CO<u>C</u>HCO); 189.22 and 192.69 (carbonyl carbons).

4.4.3 1-Ferrocenyl-7-hydroxyheptane-1,3-dione, 39

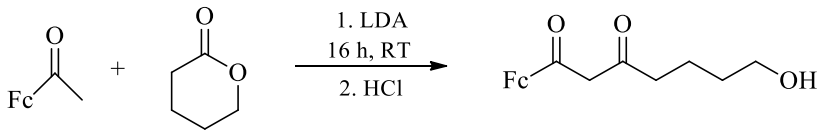

21 **38** **39**

Under Schlenk conditions, acetyl ferrocene (4.0 g, 17.54 mmol) was dissolved in dry THF (35 ml). The solution was cooled to 0 °C and an LDA solution (2 M, 6.43 ml, 12.86 mmol) was added drop wise. The reaction mixture was stirred at this temperature until an orange-

red precipitate formed. δ-Valerolactone (**38**) (1.0 ml, 10.78 mmol) was added drop wise and the mixture was left to stir overnight at room temperature under an argon atmosphere. Diethyl ether (50 ml) was added and a dark red dispersion was formed. It was then filtered and washed with diethyl ether (4 x 10 ml). The precipitate was then suspended in HCl (0.5 M, 50 ml) and extracted with diethyl ether. The ether was washed with water, dried with anhydrous $MgSO_4$, and the solvent was removed under reduced pressure. The resulting product was purified by column chromatography (ethyl acetate/hexane 1:1, R_f = 0.30) to yield pure **39** as a liquid (1.23 g, 3.748 mmol, 40.4 %). IR ν /cm^{-1} = 1604 and 1547 (C=O). ^{1}H NMR δ_H (300 MHz, $CDCl_3$)/ppm: 2.30 t (2H; enol-CH_2), 2.59 m (2H; keto-CH_2), 2.58 t (2H; keto-CH_2), 3.63 m (2H; keto-CH_2), 3.76 m (2H; enol-CH_2), 3.88 s (2H; keto-CH_2), 4.12 s (5H; enol-C_5H_5), 4.17 s (5H; keto-C_5H_5), 4.44 t (2H; enol-C_5H_4), 4.49 t (2H; keto-C_5H_4), 4.68 t (2H; enol-C_5H_4), 4.71 t (2H; keto-C_5H_4), 5.66 s (1H; enol-CH), 15.84 s (1H, -OH). ^{13}C NMR δ_H (600 MHz, $CDCl_3$)/ppm: 24.14 (keto chain-CH_2); 26.23 (enol chain-CH_2); 26.23 (keto chain-CH_2); 28.89 (enol chain-CH_2); 34.60 (enol chain-CH_2); 40.15 (keto chain-CH_2); 54.88 (keto CO<u>C</u>H_2CO); 61.88 (keto chain-CH_2); 62.20 (enol chain-CH_2); 68.60 (2C, enol C_5H_4); 68.60 (2C, keto C_5H_4); 69.75 (5C, keto C_5H_5); 69.85 (5C, enol C_5H_5); 72.12 (2C, enol C_5H_4), 73.05 (2C, keto C_5H_4); 96.55 (enol CO<u>C</u>HCO); 190.11 and 191.91 (carbonyl carbons).

4.4.4 1-Ferrocenyl-6-hydroxyhexane-1,3-dione, 40

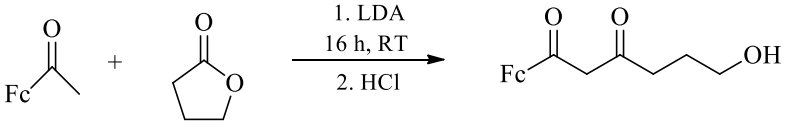

21 **2** **40**

Acetyl ferrocene (1.0 g, 4.385 mmol) was dissolved in dry THF (9 ml) under strict Schlenk conditions. It was then cooled to 0 °C and LDA (2 M, 2.63 ml, 5.260 mmol) was added drop

wise. The mixture was kept at this temperature for 30 minutes while stirring. γ-Butyrolactone (**2**) (0.102 g, 0.102 g, 1.18 mmol) was added drop wise and the mixture was left to stir overnight at room temperature under an argon atmosphere. Diethyl ether (50 ml) was added and a dark red dispersion was formed. It was then filtered and washed with diethyl ether (4 x 5 ml). The precipitate was then suspended in HCl (0.5 M, 50 ml) and extracted with diethyl ether, dried with anhydrous $MgSO_4$, and the solvent was removed under reduced pressure. The resulting product was purified using column chromatography (ethyl acetate/hexane 1:1, R_f = 0.28) and solvent evaporated to yield deep orange crystals (0.13 g, 0.414 mmol, 35.1 %), melting point 58 °C. IR ν /cm^{-1} = 1602 and 1542 (C=O). ^{1}H NMR δ_H (300 MHz, $CDCl_3$)/ppm: 1.87 m (2H; enol-CH_2), 2.39 m (2H; enol-CH_2), 2.69 t (2H; keto-CH_2), 3.61 m (2H; keto-CH_2), 3.67 m (2H; enol-CH_2), 3.88 s (2H; keto-CH_2), 4.12 s (5H; enol-C_5H_5), 4.18 s (5H; keto-C_5H_5), 4.44 t (2H; enol-C_5H_4), 4.51 t (2H; keto-C_5H_4), 4.68 t (2H; enol-C_5H_4), 4.71 t (2H; keto-C_5H_4), 5.68 s (1H; enol-CH), 15.84 s (1H, -OH). ^{13}C NMR δ_H (600 MHz, $CDCl_3$)/ppm: 26.28 (keto chain-CH_2); 28.85 (enol chain-CH_2); 34.57 (enol chain-CH_2); 40.12 (keto chain-CH_2); 54.85 (keto CO$\underline{C}H_2$CO); 61.85 (keto chain-CH_2); 62.17 (enol chain-CH_2); 68.57 (2C, enol C_5H_4); 68.57 (2C, keto C_5H_4); 69.71 (5C, keto C_5H_5); 69.82 (5C, enol C_5H_5); 72.09 (2C, enol C_5H_4), 73.02 (2C, keto C_5H_4); 96.52 (enol CO$\underline{C}$HCO); 190.07 and 191.87 (carbonyl carbons).

4.4.5 Di-μ-chloro-bis[(1,2,5,6-η)1,5-cyclooctadiene]dirhodium(I), 30

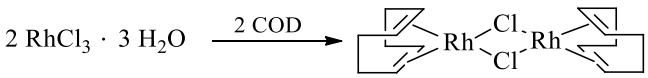

30

Rhodium trichloride (0.5 g, 2.6 mmol) was dissolved in a few drops of water followed by addition of ethanol (10 ml) and dropwise addition of cyclooctadiene (3.25 ml, 27 mmol). The

reaction mixture was refluxed at 78 °C while stirring for 2 hours and cooled in an ice bath to form a yellow precipitate. The precipitate was filtered and washed with cold methanol. This precipitate was left to air-dry, and yielded **30**, $[Rh_2Cl_2(COD)_2]$, (0.20 g, 0.406 mmol, 31.2 %) as a yellow powder. ^1H NMR δ_H (300 MHz, $CDCl_3$)/ppm: 1.3 m (4H; CH_2); 2.08 m (4H; CH_2); 4.42 s (4H; CH).

4.4.6 [RhFcCOCHCO(CH$_2$)$_5$OH(COD)], 41

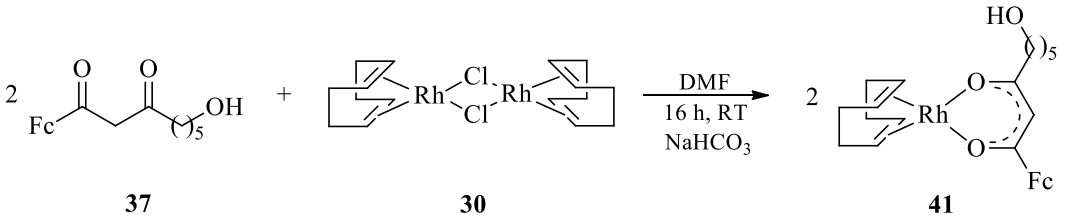

37 **30** **41**

$[RhCl_2(COD)_2]$ (0.36 g, 0.73 mmol) was dissolved in DMF (15 ml). $NaHCO_3$ (0.12 g, 1.46 mmol) was added followed by addition of 1-ferrocenyl-8-hydroxyoctane-1,3-dione, **37**, (0.5 g, 1.46 mmol). The reaction mixture was stirred at room temperature for 16 hours and the product was precipitated with the addition of an excess amount of ice cold water (50 ml) and filtered off. Extraction was done by dissolving precipitate in ether and washing with water. The ether layer was dried over anhydrous $MgSO_4$ and evaporated under reduced pressure. This yielded **41** (0.702 g, 1.27 mmol, 87.0 %). IR ν /cm^{-1} = 1541 and 1507 (C-O). ^1H NMR δ_H (600 MHz, $CDCl_3$)/ppm: 1.50 m (4H; chain-CH_2); 1.77 m (4H; aliphatic protons from C_8H_{12}), 2.15 m (2H; chain-CH_2), 2.39 m (4H; aliphatic protons from C_8H_{12}), 3.38 m (2H; chain-CH_2), 3.56 t (2H; chain-CH_2), 3.97 m (4H; diene protons from C_8H_{12}), 4.03 s (5H; C_5H_5), 4.22 t (2H; C_5H_4), 4.53 t (2H; C_5H_4), 5.50 s (H; C<u>H</u>CO).

4.4.7 [RhFcCOCHCO(CH$_2$)$_4$OH(COD)], 42

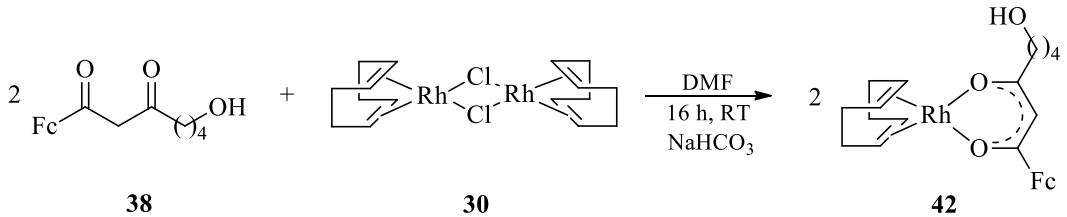

38 **30** **42**

[RhCl$_2$(COD)$_2$] (0.38 g, 0.76 mmol) was dissolved in DMF (15 ml). NaHCO$_3$ (0.13 g, 1.52 mmol) and 1-ferrocenyl-7-hydroxyheptane-1,3-dione, **39**, (0.5 g, 1.52 mmol) were added, and the reaction mixture was stirred at room temperature for 16 hours. Ice cold water (50 ml) was added, and the resulting precipitate was filtered off. The precipitate was dissolved in diethyl ether, and then washed with water. The ether layer was dried over anhydrous MgSO$_4$ and evaporated under reduced pressure. This yielded **43** (0.679 g, 1.26 mmol, 82.9 %). IR ν /cm^{-1} = 1540 and 1508 (C-O). ^{1}H NMR δ_H (600 MHz, CDCl$_3$)/ppm: 1.52-1.58 m (4H; chain-CH$_2$); 1.78 m (4H; ½ aliphatic C$_8$H$_{12}$); 2.17 m (2H; chain-CH$_2$); 2.42 m (4H; ½ aliphatic C$_8$H$_{12}$); 3,59 m (2H; chain-CH$_2$); 3.99 m (4H; diene protons of C$_8$H$_{12}$); 4.05 s (5H; C$_5$H$_5$); 4.25 m (2H; C$_5$H$_4$); 4.55 m (2H; C$_5$H$_4$); 5.525 s (H; C<u>H</u>CO).

4.4.8 [RhFcCOCHCO(CH$_2$)$_3$OH(COD)], 43

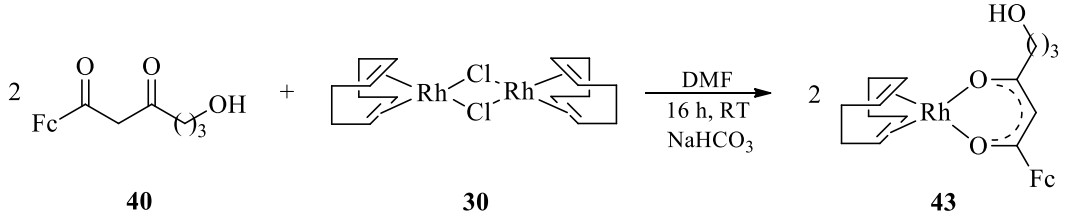

40 **30** **43**

[RhCl$_2$(COD)$_2$] (0.38 g, 0.76 mmol) was dissolved in DMF (15 ml). NaHCO$_3$ (0.13 g, 1.52 mmol) and 1-ferrocenyl-6-hydroxyhexane-1,3-dione (0.5 g, 1.59 mmol) were added, and the reaction mixture was stirred at room temperature for 16 hours. Ice cold water (50 ml) was added, and the resulting precipitate was filtered off. The precipitate was dissolved in diethyl

ether, and then washed with water. The ether layer was dried over anhydrous $MgSO_4$ and evaporated under reduced pressure. This yielded **43** (0.599 g, 1.14 mmol, 71.7 %). IR ν /cm^{-1} = 1542 and 1510 (C-O). ^{1}H NMR δ_H (600 MHz, $CDCl_3$)/ppm: 1.58 m (2H; CH_2); 1.80 m (4H; ½ aliphatic C_8H_{12}); 2.23 m (2H; CH_2); 2.44 m (4H; ½ aliphatic C_8H_{12}); 3,60 m (2H; CH_2); 4.01 m (2H; diene protons of C_8H_{12}); 4.07 m (2H; diene protons of C_8H_{12}); 4.09 s (5H; C_5H_5); 4.27 m (2H; C_5H_4); 4.58 m (2H; C_5H_4); 5.55 s (H; C<u>H</u>CO).

4.5 Isomerization kinetics

The equilibrium ratio of keto-enol tautomers of the free β-diketones was determined for the longest chain β-diketone (**37**) only. The compound was left in solid form until it mainly consisted of the enol isomer. This was then dissolved in deuterated chloroform and the formation of the keto isomer could be studied using ^{1}H NMR until equilibrium was reached. To confirm the results, compound **37** was dissolved in $CDCl_3$, reacted with a 1 M solution of NaOH and extracted back into $CDCl_3$. This yielded a keto-enriched solution and the formation of the enol tautomer could be studied by ^{1}H NMR until equilibrium was reached.

4.6 pK_a' measurements

UV-spectra for the protonated and unprotonated species of β-diketones were measured. The wavelength with the biggest absorbance difference between the spectra was used as the analytical wavelength where the pK_a' measurement was performed. (n=5 **(37)**, 327 nm; n=4 **(39)**, 320 nm and n=3 **(40)**, 317 nm). The analyte was dissolved in a minimum acetonitrile and water was added to a final solution of water/acetonitrile (9:1). The ionic strength of the solution was set on 0.1 mol dm^{-1} with $NaClO_4$ and the solution was made basic with NaOH (0.1 M). The solution was titrated with 0.1 M and 1 M $HClO_4$ at 25 °C and care was taken to

not increase the total volume with more than 5%. pH measurements were taken at regular intervals during the titration.

4.7 Rhodium complex substitution kinetics

UV-spectra for the rhodium complex before and after the reaction with 1,10-phenanthroline were measured. The wavelength with the biggest absorbance difference between the spectra was used as the analytical wavelength where the reaction was followed. [Rh(FcCOCHCO$(CH_2)_4$OH)(COD)] = 0.50 mmol dm^{-3} was used for all three complexes and λ_{exp} was 470 nm for **41**, 468 nm for **42** and 467 nm for **43**. Substitution reactions were performed in methanol under pseudo first-order conditions with 1,10-phenanthroline concentrations in an excess of 5-50 fold that of the Rhodium complexes. These reactions were studied at 5 different temperatures, 15.0 °C, 20.0 °C, 25.0 °C, 35.0 °C and 40.0 °C. The temperature was regulated at ± 0.1 °C with a waterbath.

4.8 Electrochemistry

Cyclic voltammetry (CV), linear sweep voltammetry (LSV) and square wave voltammetry (SWV) was carried out on the three β-diketones as well as the rhodium complexes thereof. A three electrode configuration was used with a silver wire for the reference electrode and a platinum wire as the auxiliary electrode. A glassy carbon working electrode (surface area 3.14 mm^2) was utilized after polishing on a Buhler polishing mat first with 1 micron and then with ¼ micron diamond paste. Spectrochemical grade dichloromethane (Aldrich) was used in a 1 cm^3 cell. Tetrabutylammonium hexafluorophosphate, [NBu_4][PF_6], was used as supporting electrolyte for analysis of the free β-diketones (**37**, **39** and **40**), and tetrabutylammonium tetrakis(pentafluorophenyl)borate, [NBu_4][$B(C_6F_5)_4$], was used as a

supporting electrolyte during analysis of the rhodium complexes (**41**, **42** and **43**). Both were used in a concentration of 0.1 M. The concentration of all analyte solutions was 0.5 mM. Cyclic voltammetry (CV) was carried out at 100, 200, 300, 400 and 500 mV s^{-1}, linear sweep voltammetry (LSV) was performed at 2 mV s^{-1} and square wave voltammetry (SWV) was carried out at 20, 40, 60 and 80 hertz.

4.9 X-ray crystallography

Data for compound **40** was collected at 150 K on a Bruker D8 Venture kappa geometry diffractometer, with duo Iμs sources, a Photon 100 CMOS detector and APEX II control software using Quazar multi-layer optics, monochromated Cu-Kα radiation and by means of a combination of ϕ and ω scans. Data reduction was performed using SAINT+ and the intensities were corrected for absorption using SADABS.[3] The structure was solved by intrinsic phasing using SHELXTS and refined by full-matrix least squares using SHELXTL and SHELXL-2013.[4] In the structure refinement, all hydrogen atoms were added in calculated positions and treated as riding on the atom to which they are attached. All nonhydrogen atoms were refined with anisotropic displacement parameters. All isotropic displacement parameters for hydrogen atoms were calculated as X × Ueq of the atom to which they are attached, X = 1.5 for the hydroxyl hydrogens and 1.2 for all other hydrogens. Drawings were done utilizing ORTEP.[5]

Bibliography

(1) Vogel, A. I.; Furniss, B. S. *Vogel's textbook of practical organic chemistry*; Longman, 1989.

(2) Williams, D. B. G.; Lawton, M. *J. Org. Chem.* **2010**, *75* (24), 8351–8354.

(3) *APEX2 (including SAINT and SADABS)*; Bruker AXS Inc.: Madison, WI, 2012.

(4) Sheldrick, G. M. *Acta Crystallogr. A* **2008**, *64* (1), 112–122.

(5) Farrugia, L. J. *J. Appl. Crystallogr.* **1997**, *30* (5), 565–565.

5 Summary and Future Prospective

5.1 Summary

Claisen condensation of suitable lactones with acetyl ferrocene in the presence of lithium diisopropylamide yielded three new ferrocene-containing β-diketones of the type $FcCOCH_2CO(CH_2)_nOH$, 1-ferrocenyl-8-hydroxyoctane-1,3-dione (n=5), 1-ferrocenyl-7-hydroxyheptane-1,3-dione (n=4) and 1-ferrocenyl-6-hydroxyhexane-1,3-dione (n=3) (Figure 5.1).

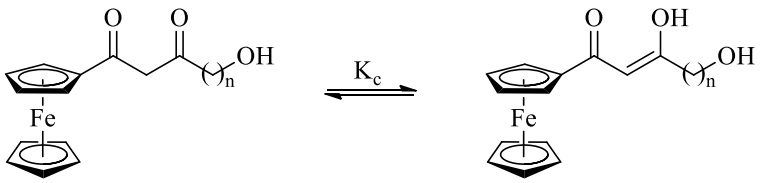

n = 5(**37**), 4(**39**), 3(**40**)

Figure 5.1: Structure of β-diketones synthesized. n = 5 **(37)**, n = 4 **(39)** and n = 3 **(40)**.

The rhodium complexes $[Rh(FcCOCHCO(CH_2)_nOH)(cod)]$,where n = 5, 4 and 3 and cod the bidentate ligand 1,5-cyclooctadiene, were prepared from the corresponding β-diketones.

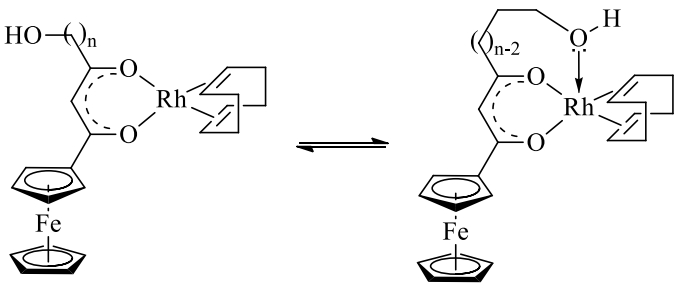

n = 5(**41**), 4(**42**), 3(**43**)

Figure 5.2: Structure of the [Rh(β-diketone)(COD)] complexes with n = 5 **(41)**, n = 4 **(42)** and n = 3 **(43)**.

The single crystal X-ray structure of **40** (monoclinic, P 2_1 space group, Z = 8) was solved. In the solid state it exists exclusively in the enol form with enolization directed away from the ferrocene group as shown in Figure 5.1. Eight, an unusually large number, independent molecules were found per unit cell. The terminal alcohol functionality as well as the CH_2 group to which it is bound was found to be disordered to occupy two possible positions.

In $CDCl_3$ solutions, **37**, **39** and **40** existed as a mixture of keto- and enol tautomers with K_c = 3.02 for **37**. Keto-enol conversion is slow; a half-life for the conversion was measured as $t_{1/2} \approx 4000$ s.

pK_a' values for the β-diketones were determined as 10.44 for $FcCOCH_2CO(CH_2)_5OH$, 8.01 for $FcCOCH_2CO(CH_2)_4OH$ and 5.97 for $FcCOCH_2CO(CH_2)_3OH$. pK_a' values were determined in 10% acetonitrile in water with ionic strength of 0.1 $moldm^{-1}$ ($NaClO_4$) at 25 °C.

Formal reduction potentials, $E^{0'}$ of the ferrocenyl groups were determined as 151 mV for $FcCOCH_2CO(CH_2)_5OH$, 174 mV for $FcCOCH_2CO(CH_2)_4OH$ and 197 mV for $FcCOCH_2CO(CH_2)_3OH$. For the rhodium complexes, $E^{0'}$ was found to be 107 mV for [Rh($FcCOCHCO(CH_2)_5OH$)(COD)] (**41**), 110 mV for [Rh($FcCOCHCO(CH_2)_4OH$)(COD)] (**42**) and 128 mV for [Rh($FcCOCHCO(CH_2)_3OH$)(COD)] (**43**) for the ferrocenyl group. Two redox couples were observed for the rhodium centre; a Rh^I/Rh^{II} couple for the 4-coordinate rhodium species with $E^{0'}$ at 300 mV for **41**, 271 mV for **42** and 304 mV for **43**, as well as evidence of a Rh^I/Rh^{II} couple corresponding to the postulated 5-coordinate rhodium complex (Figure 5.2) were the rhodium interacts with the OH endgroup on the β-diketonato sidechain found at $E^{0'}$ = 675 mV **41**, 635 mV for **42** and 634 mV **43**. The ferrocene couple displayed chemical and electrochemical reversibility, while the 4-coordinate rhodium centre exhibited an irreversible redox couple. The 5-coordinate rhodium couple was found to be

electrochemically reversible. The 4- and 5-coordinate rhodium centres are in equilibrium with each other, with $i_{pa,\ Rh\ 5\text{-}coordinate} + i_{pa,\ Rh\ 4\text{-}coordinate} \approx i_{pa,\ Fc}$.

Substitution of the bidentate β-diketonato ligands from the rhodium complexes by 1,10-phenanthroline was also studied with the aid of stopped flow UV spectroscopy. The effect of the chainlength of the β-diketonato ligands on the rate of substitution could then be compare to the pK_a' values of the free β-diketones as well as the formal reduction potentials of the rhodium complexes. The activation parameters of the substitution reaction were found to be: k_y = 12.14 $dm^3\ mol^{-1}\ s^{-1}$; $\Delta H^{\ddagger}$ = 26.54 kJ mol^{-1}; $\Delta S^{\ddagger}$ = -135.17 J $mol^{-1}\ K^{-1}$ when n = 5 (**41**), k_y = 159.85 $dm^3\ mol^{-1}\ s^{-1}$; $\Delta H^{\ddagger}$ = 31.23 kJ mol^{-1}; $\Delta S^{\ddagger}$ = -98.31 J $mol^{-1}\ K^{-1}$ when n = 4 (**42**) and k_y = 9005.66 $dm^3\ mol^{-1}\ s^{-1}$; $\Delta H^{\ddagger}$ = 27.51 J mol^{-1}; $\Delta S^{\ddagger}$ = -77.27 J $mol^{-1}\ K^{-1}$ when n = 3 **(43)**. All three complexes showed significant solvent interaction. The large negative $\Delta S^{\ddagger}$ values indicate an associative mechanism.

5.2 Future perspective

This study can be extended to include other metallocenes such as ruthenocene or osmocene instead of ferrocene.

The cytotoxic properties in terms of potential anti-cancer application of the β-diketones can be studied as similar compounds were found to have good antineoplastic activity.[1]

Lactams (cyclic amides) could be used instead of lactones in the synthesis of the β-diketones, thus possibly leading to amine end-groups instead of the presently obtained hydroxyl groups.

Other rhodium complexes such as $[Rh(FcCOCHCO(CH_2)_nOH)(CO)_2]$ and $[Rh(FcCOCHCO(CH_2)_nOH)(CO)(PPh_3)]$ can be synthesizedfrom **41**, **42** and **43** as precursors. These carbonyl complexes can be subjected to several studies, including kinetics of CO

substitution with PPh_3, and the rate of oxidative addition of MeI to $[Rh(FcCOCHCO(CH_2)_nOH)(CO)(PPh_3)]$ to liberate complexes with a Rh^{III} centre, $[Rh(FcCOCHCO(CH_2)_nOH)(CO)(PPh_3)(Me)(I)] \rightleftharpoons [Rh(FcCOCHCO(CH_2)_nOH)(PPh_3)(MeCO)(I)]$. This particular oxidative addition reaction is the rate determining step in the Monsanto process of converting methanol to acetic acid.[2] These new rhodium (III) redox active complexes may also be subjected to an electrochemical study. Interesting relationships between rate constants, redox potentials of all active redox groups and catalytic activity may be drawn.

A computational study can also be performed to determine possible isomers of the β-diketones in solution. Computational chemistry can also be utilized to determine possible reasons for the high solvent pathway contribution to substitution reaction mechanism.

Bibliography

(1) Swarts, J. C.; Vosloo, T. G.; Cronje, S. J.; Plessis, W. C. (Ina) D.; Rensburg, C. E. J. V.; Kreft, E.; Lier, J. E. V. *Anticancer Res.* **2008**, *28* (5A), 2781–2784.

(2) Forster, D. In *Advances in Organometallic Chemistry*; West, F. G. A. S. and R., Ed.; Catalysis and Organic Syntheses; Academic Press, 1979; Vol. 17, pp 255–267.

Appendix

^{1}H NMR spectra

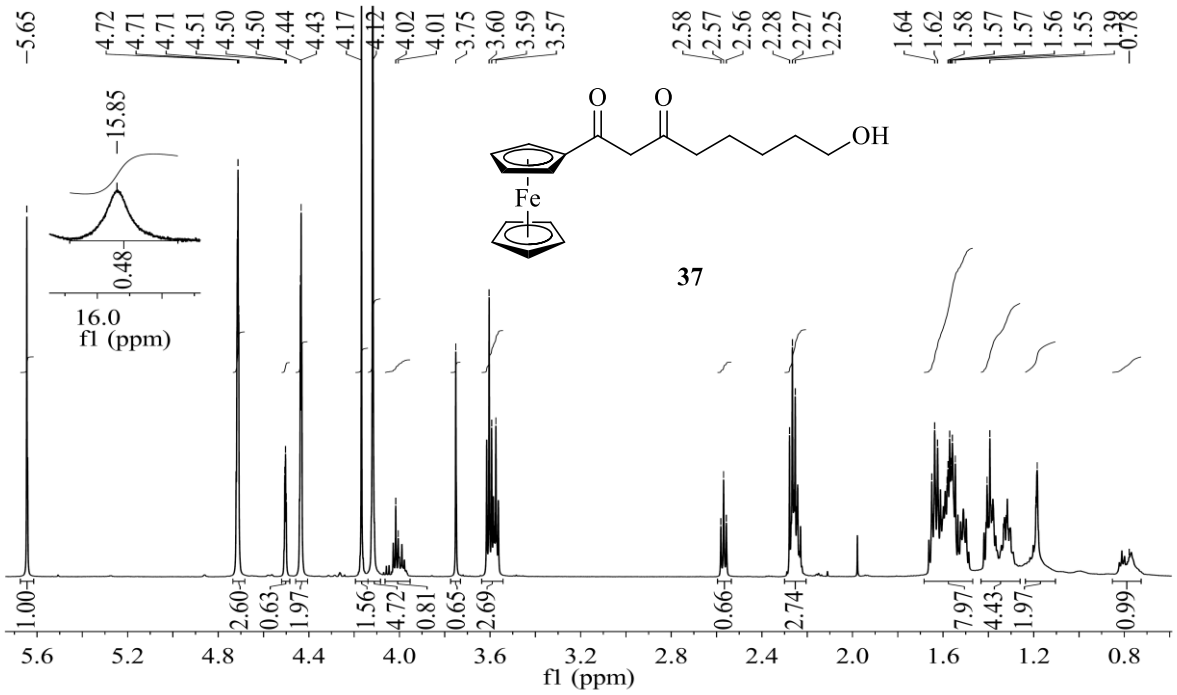

Figure A.1: ^{1}H NMR spectrum of 1-Ferrocenyl-8-hydroxyoctane-1,3-dione (**37**) in $CDCl_3$

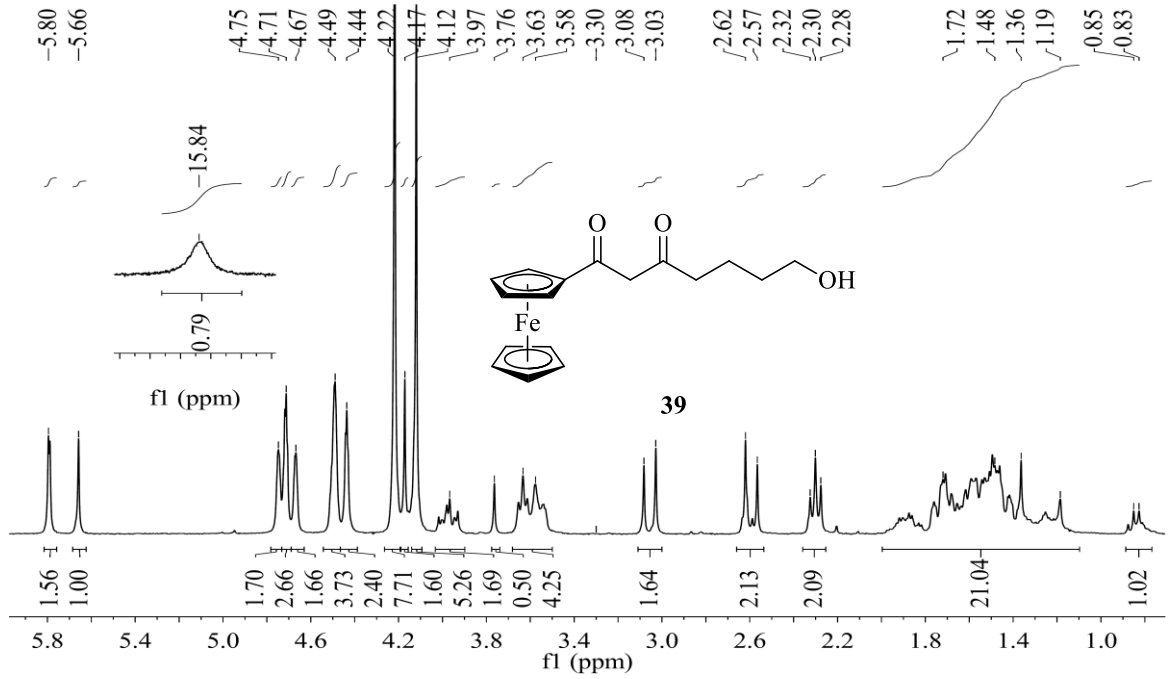

Figure A.2: ^{1}H NMR spectrum of 1-Ferrocenyl-7-hydroxyheptane-1,3-dione (**39**) in $CDCl_3$

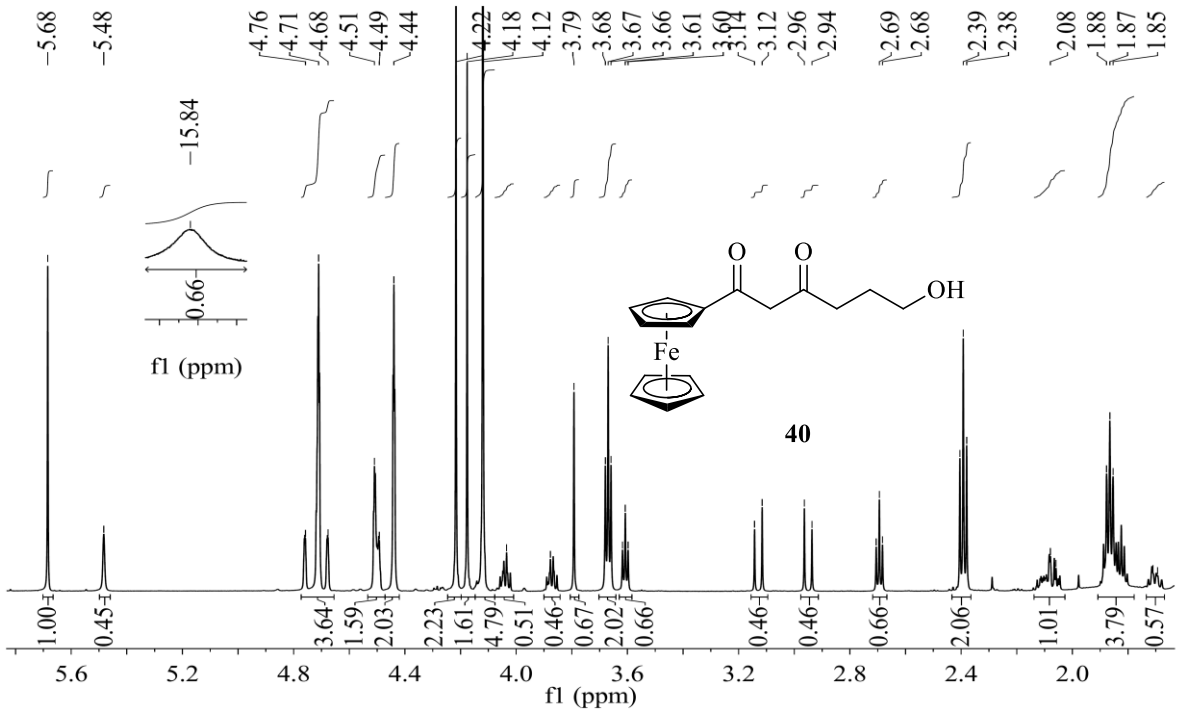

Figure A.3: ^{1}H NMR spectrum of -Ferrocenyl-6-hydroxyhexane-1,3-dione (**40**) in $CDCl_3$

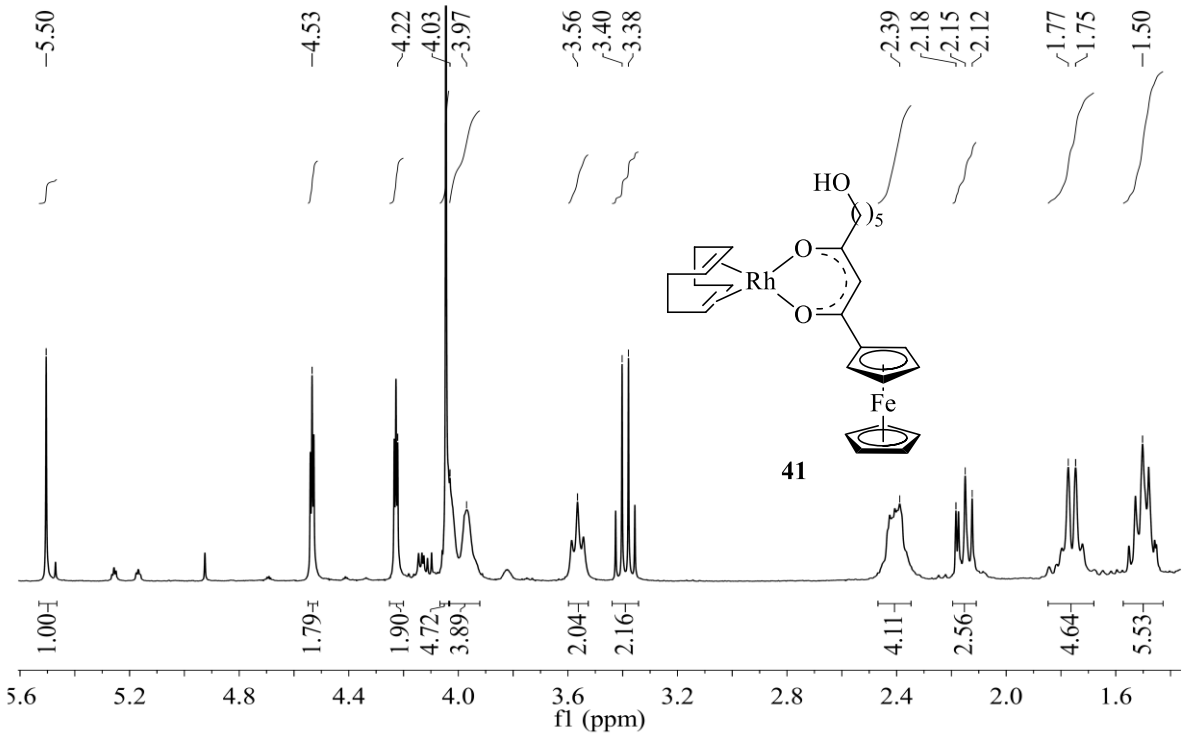

Figure A.4: ^{1}H NMR spectrum of Rh[FcCOCHCO$(CH_2)_5$OH(cod)] (**41**) in $CDCl_3$

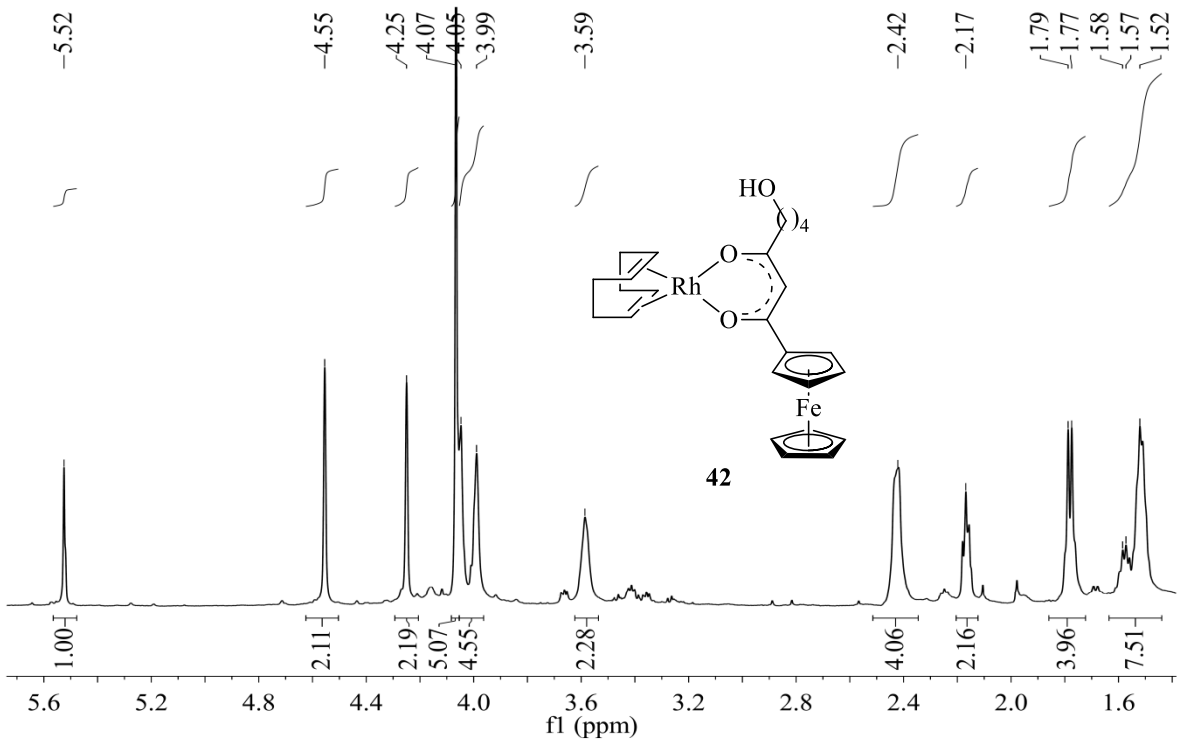

Figure A.5: ^{1}H NMR spectrum of Rh[FcCOCHCO$(CH_2)_4$OH(cod)] (**42**) in $CDCl_3$

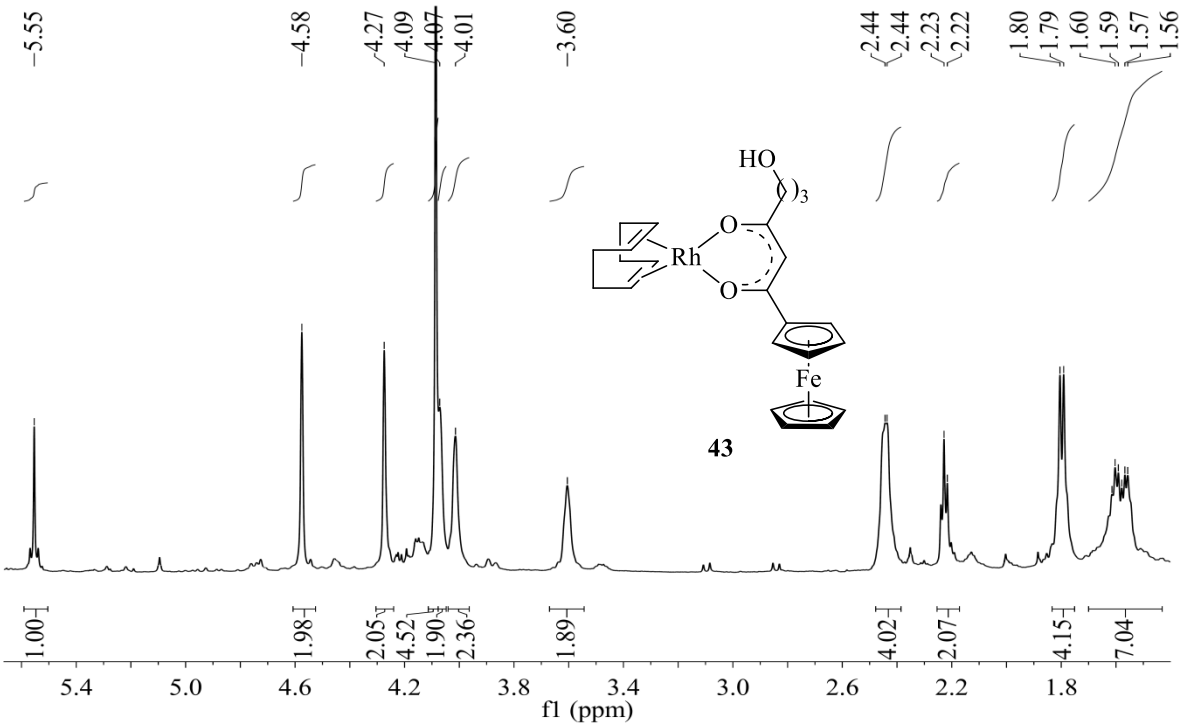

Figure A.6: ^{1}H NMR spectrum of Rh[FcCOCHCO$(CH_2)_3$OH(cod)] (**43**) in $CDCl_3$

^{13}C NMR spectra

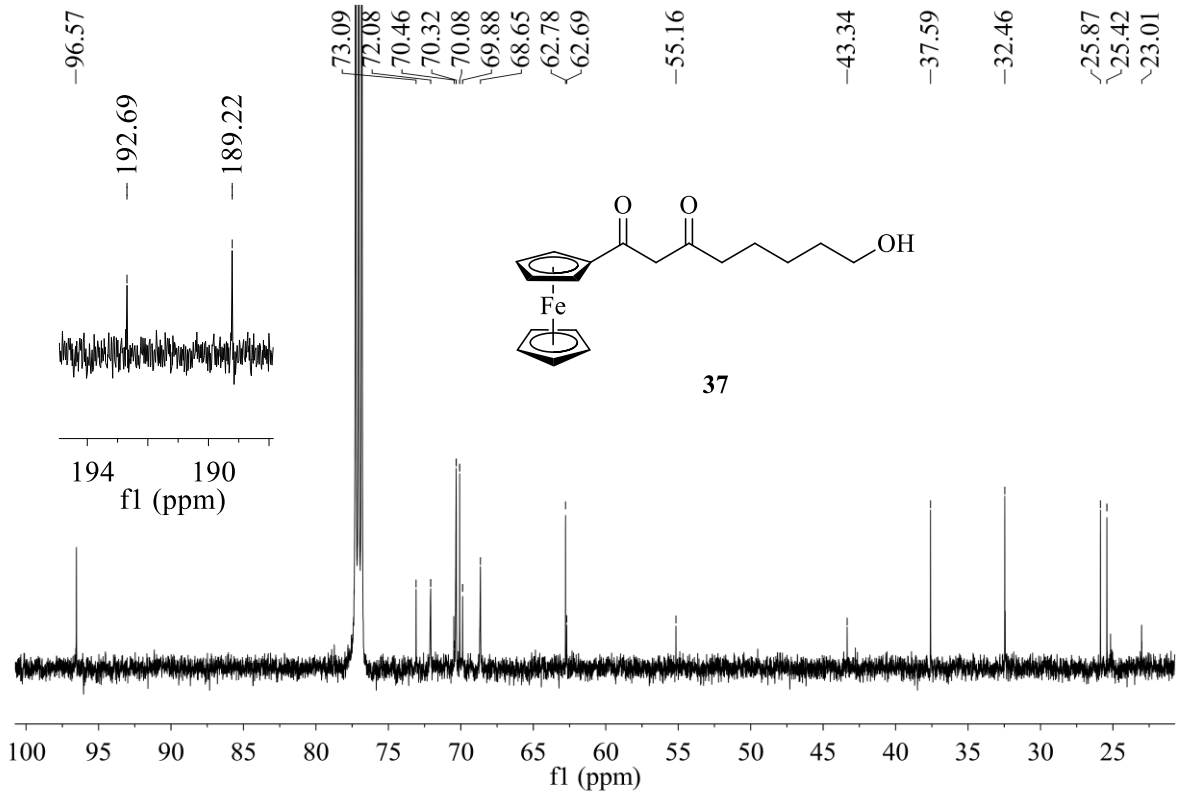

Figure A.7: ^{13}C NMR spectrum of 1-Ferrocenyl-8-hydroxyoctane-1,3-dione (**37**) in $CDCl_3$

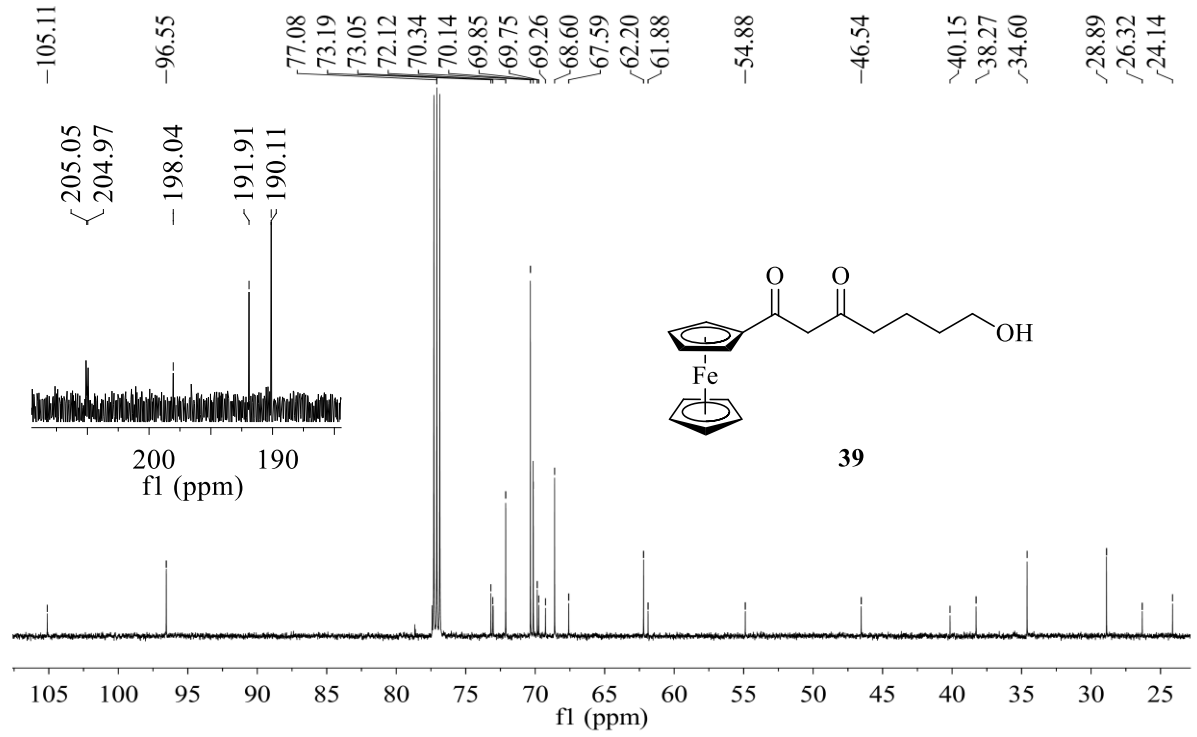

Figure A.8: ^{13}C NMR spectrum of 1-Ferrocenyl-7-hydroxyheptane-1,3-dione (**39**) in $CDCl_3$

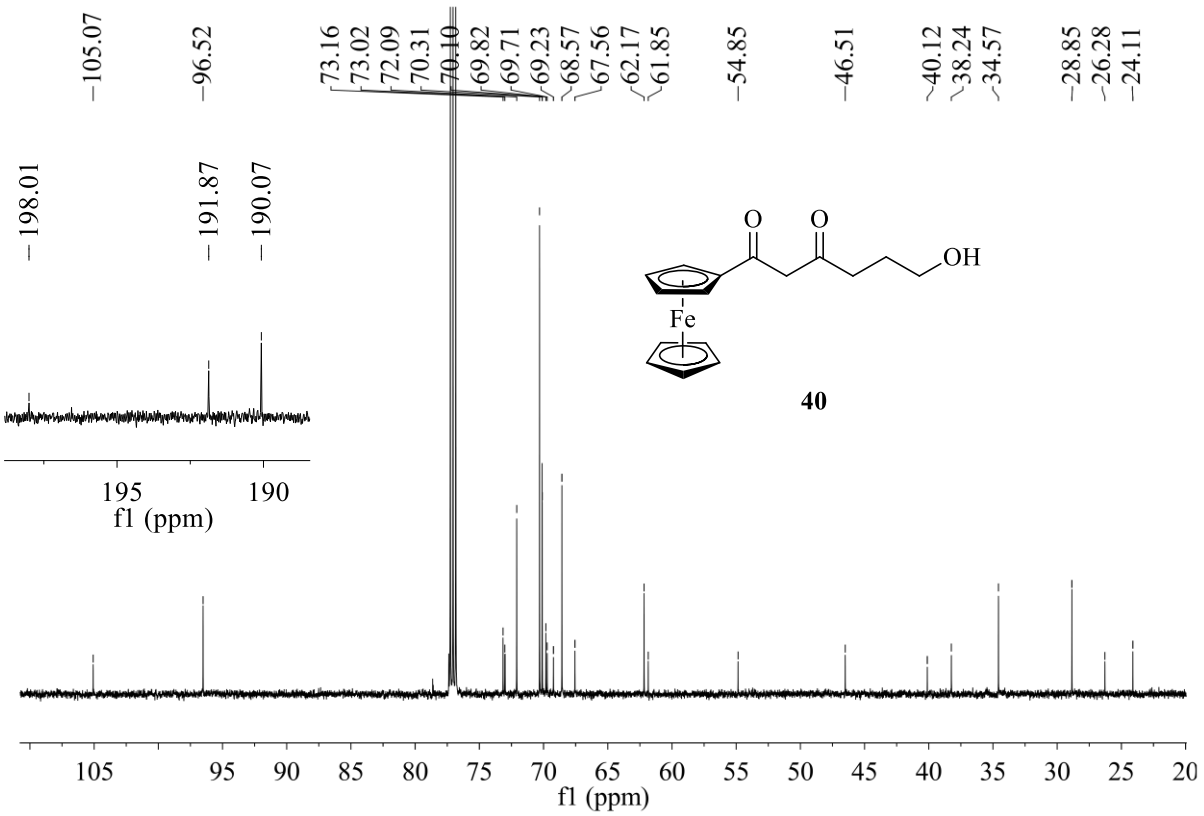

Figure A.9: ^{13}C NMR spectrum of 1-Ferrocenyl-6-hydroxyhexane-1,3-dione (**40**) in $CDCl_3$

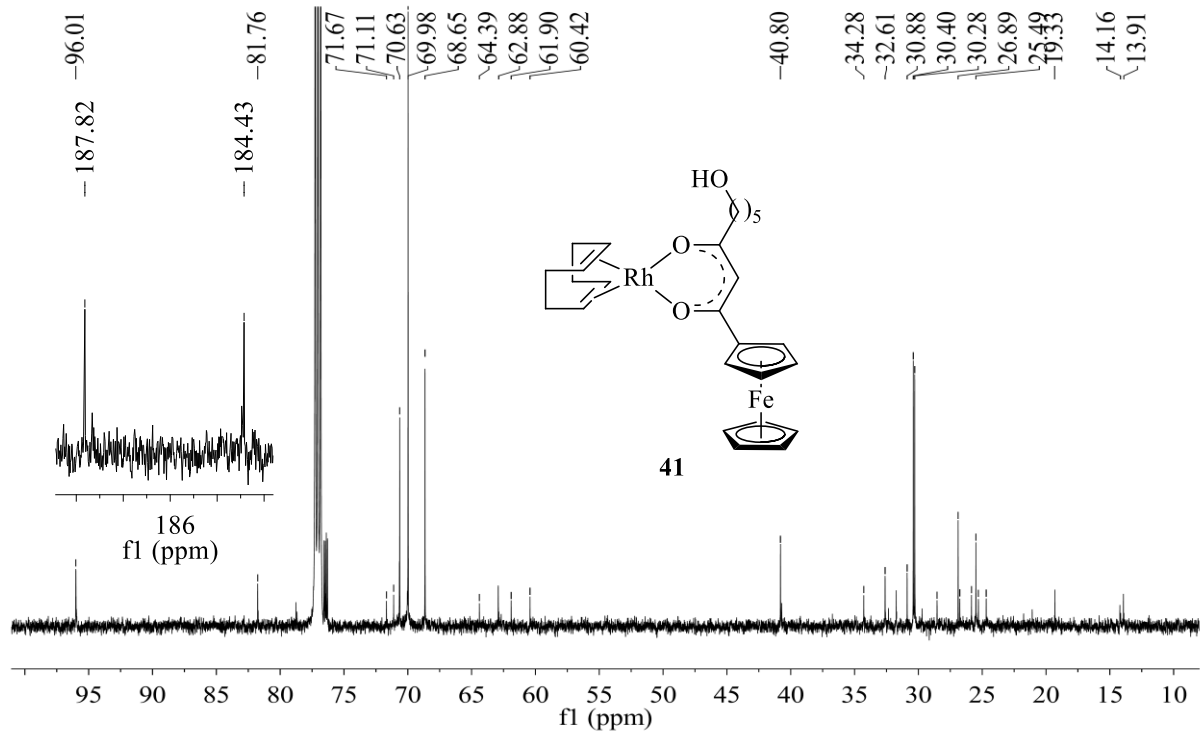

Figure A.10: ^{13}C NMR spectrum of Rh[FcCOCHCO$(CH_2)_5$OH(cod)] (**41**) in $CDCl_3$

HSQC correlation NMR

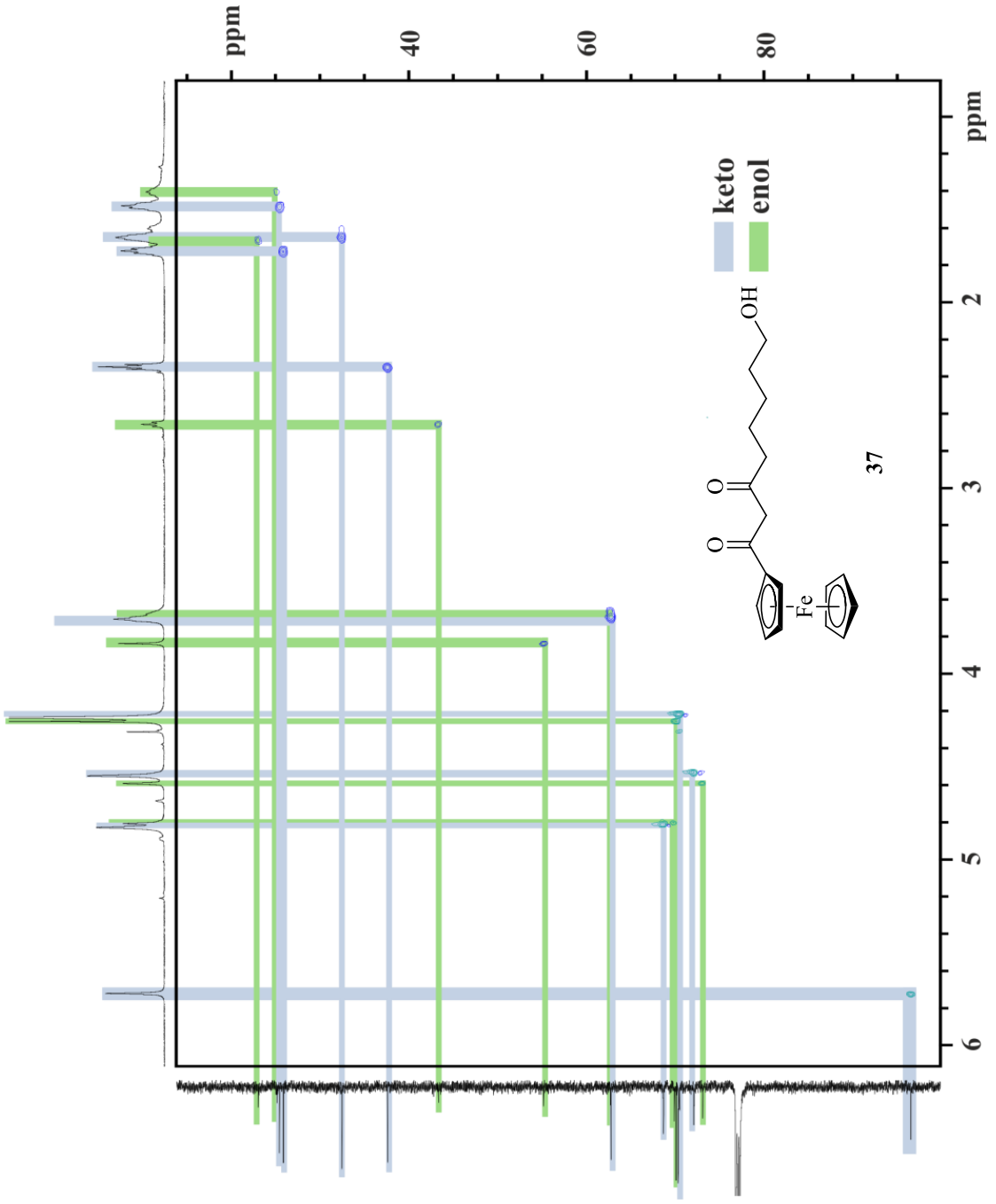

Figure A.13: HSQC correlation NMR spectrum of 1-Ferrocenyl-8-hydroxyoctane-1,3-dione (**37**) in $CDCl_3$

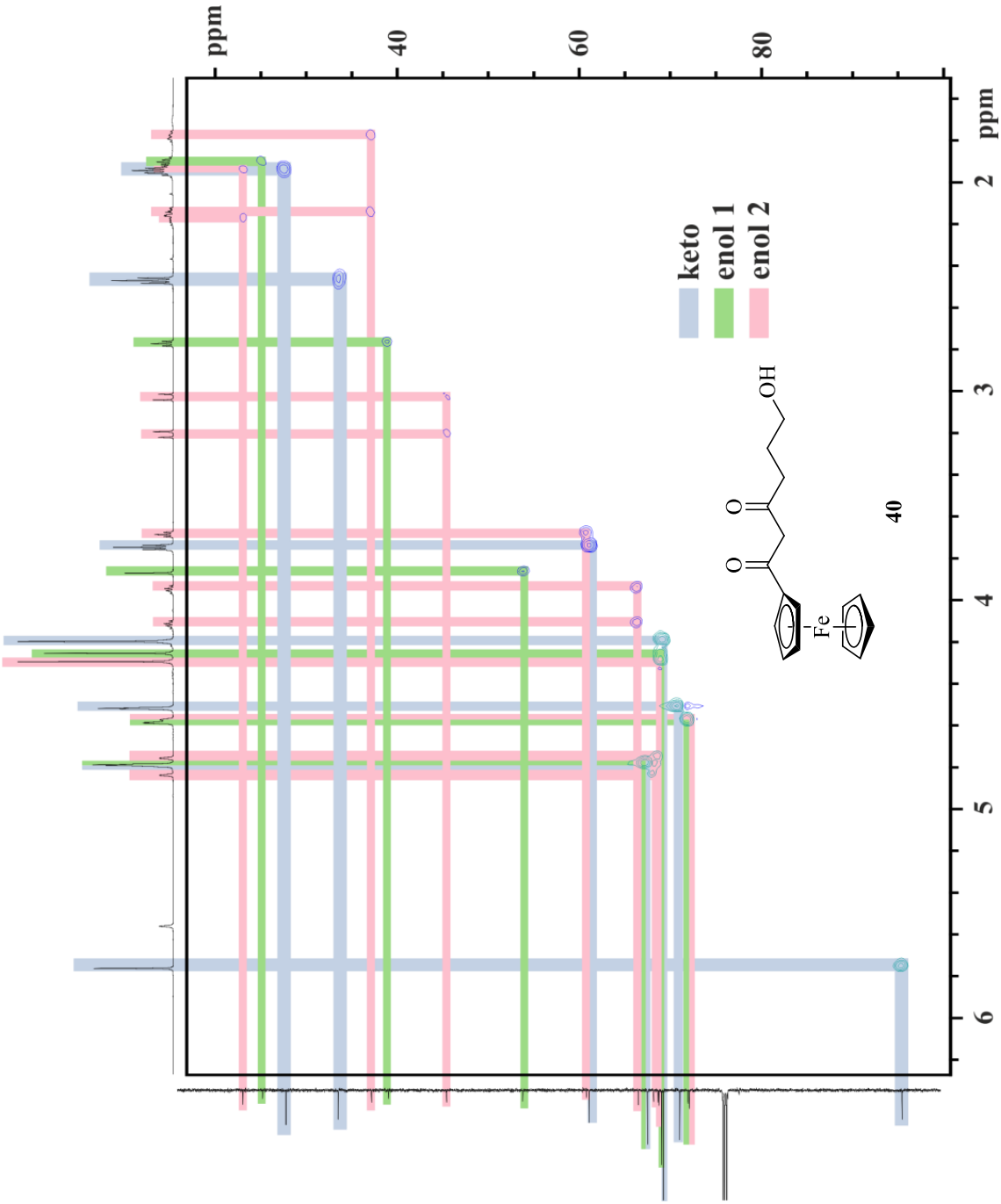

Figure A.14: HSQC correlation NMR spectrum of 1-Ferrocenyl-6-hydroxyhexane-1,3-dione (**40**) in $CDCl_3$

Infrared spectra

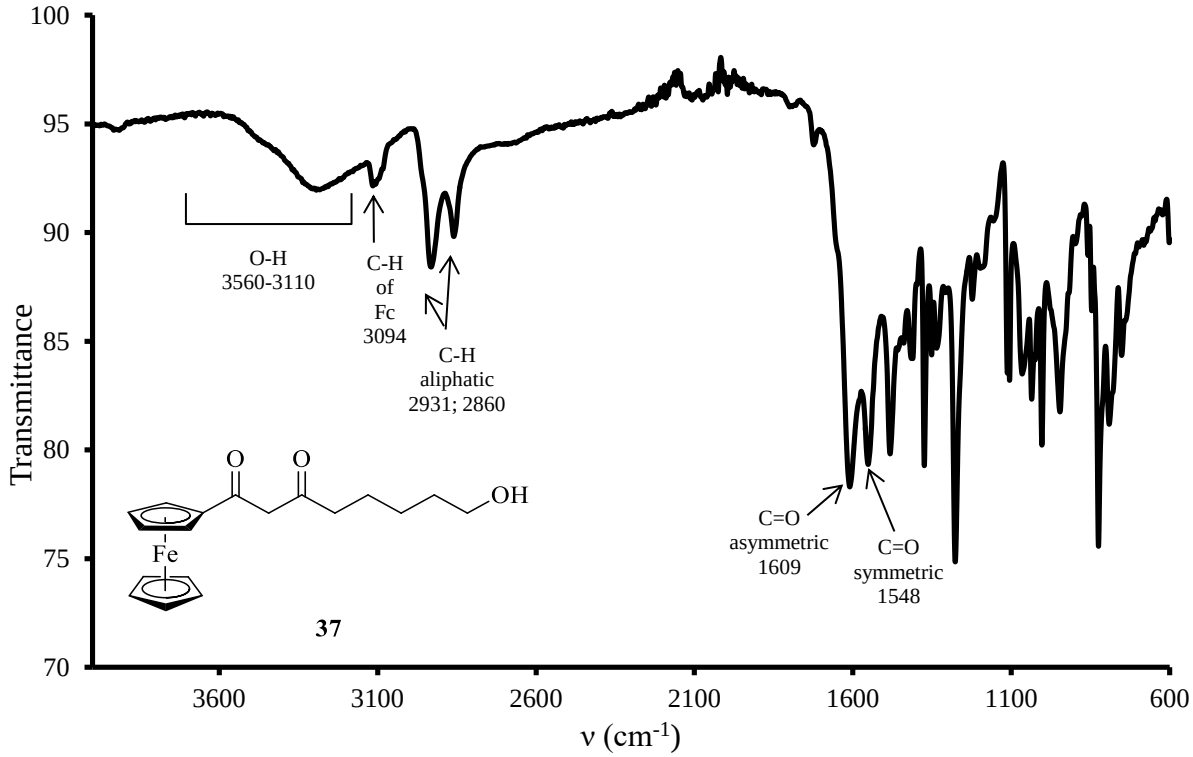

Figure A.15: IR spectrum of 1-Ferrocenyl-8-hydroxyoctane-1,3-dione (**37**)

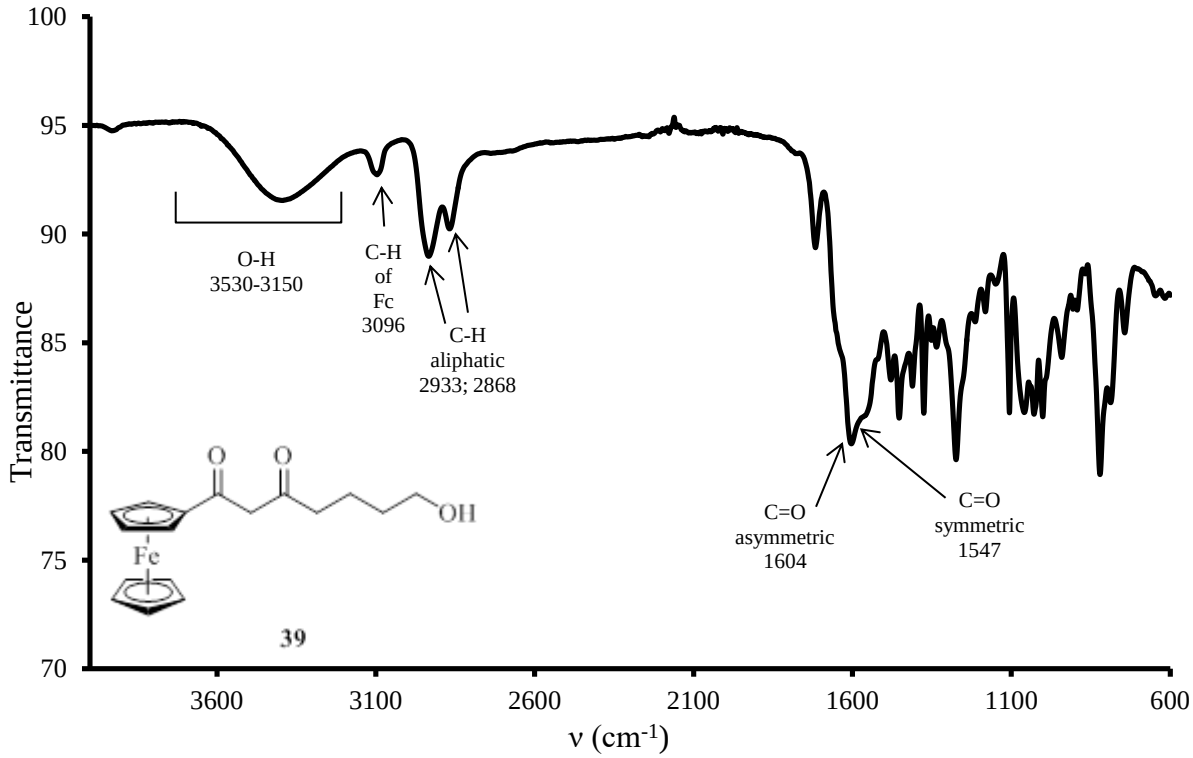

Figure A.16: IR spectrum of 1-Ferrocenyl-7-hydroxyheptane-1,3-dione (**39**)

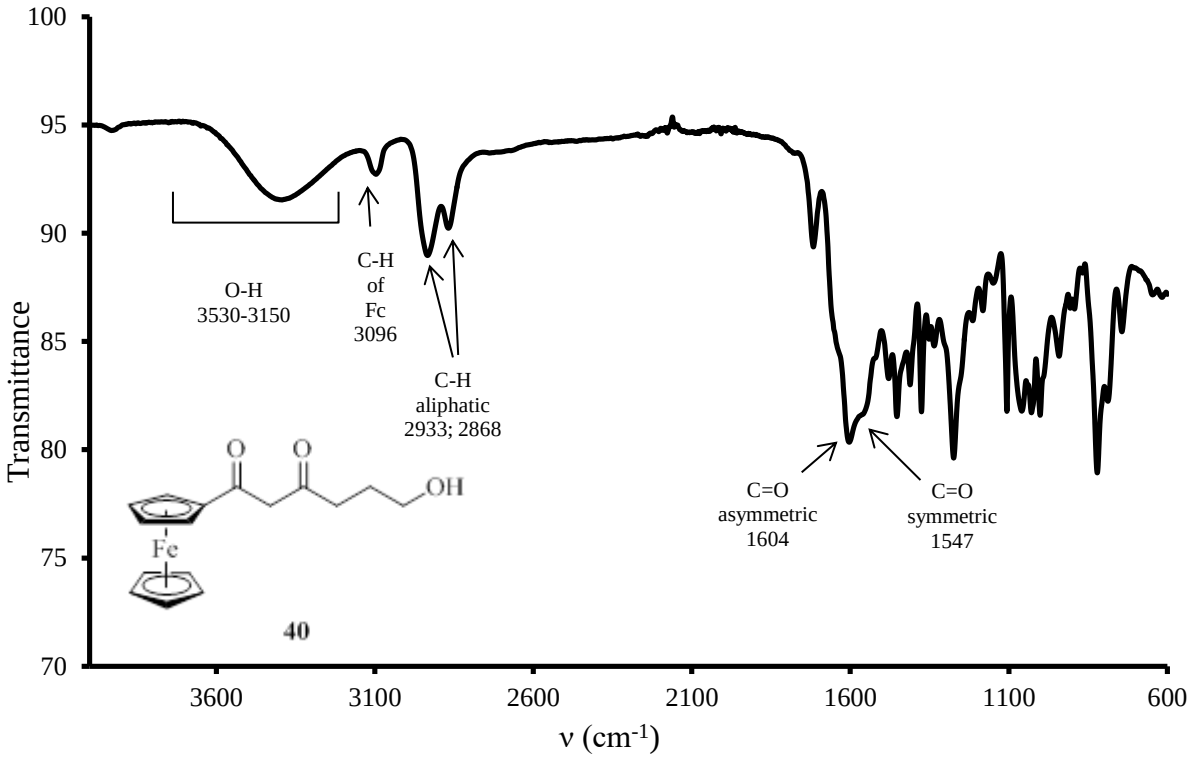

Figure A.17: IR spectrum of 1-Ferrocenyl-6-hydroxyhexane-1,3-dione (**40)**

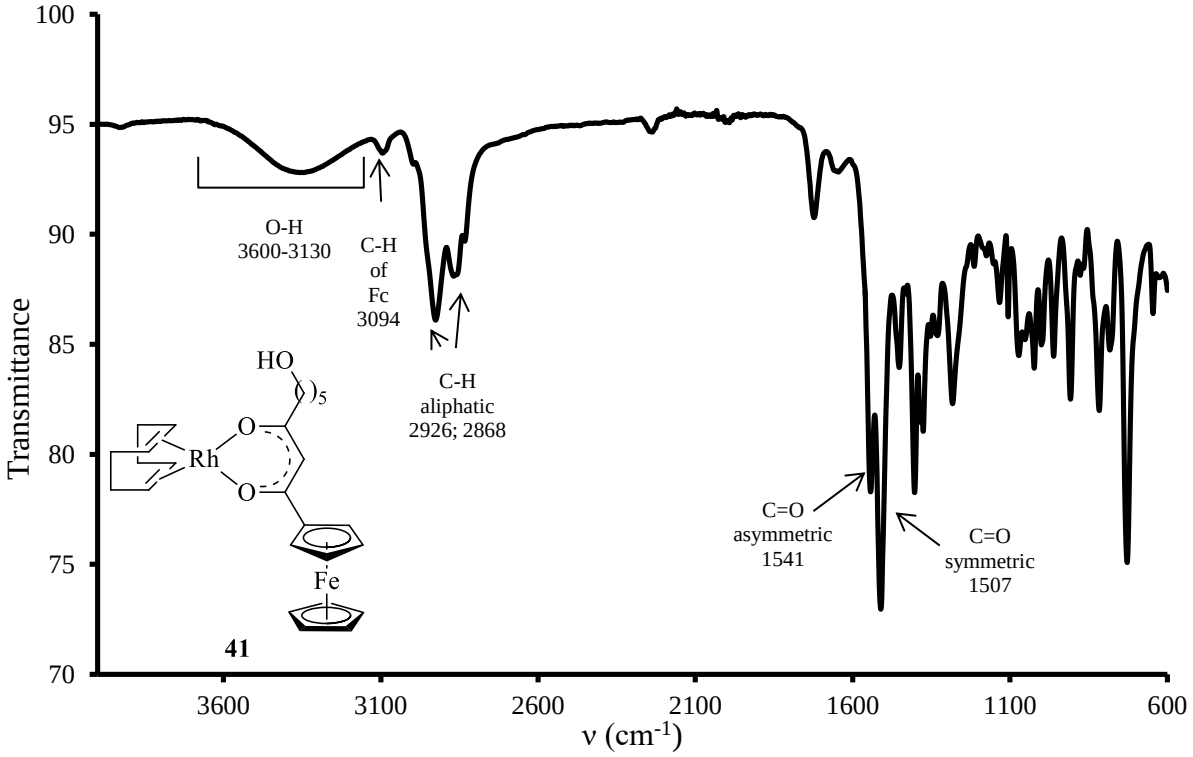

Figure A.18: IR spectrum of Rh[FcCOCHCO$(CH_2)_5$OH(cod)] (**41)**

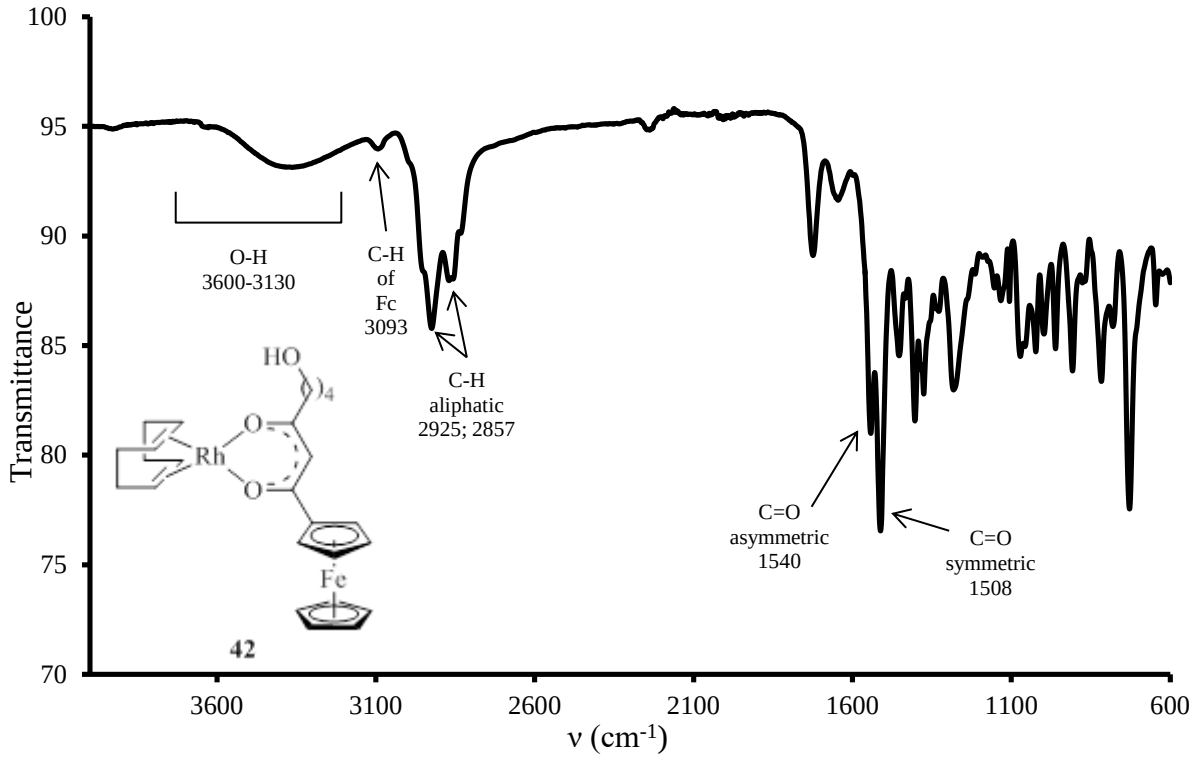

Figure A.19: IR spectrum of Rh[FcCOCHCO$(CH_2)_4$OH(cod)] (**42)**

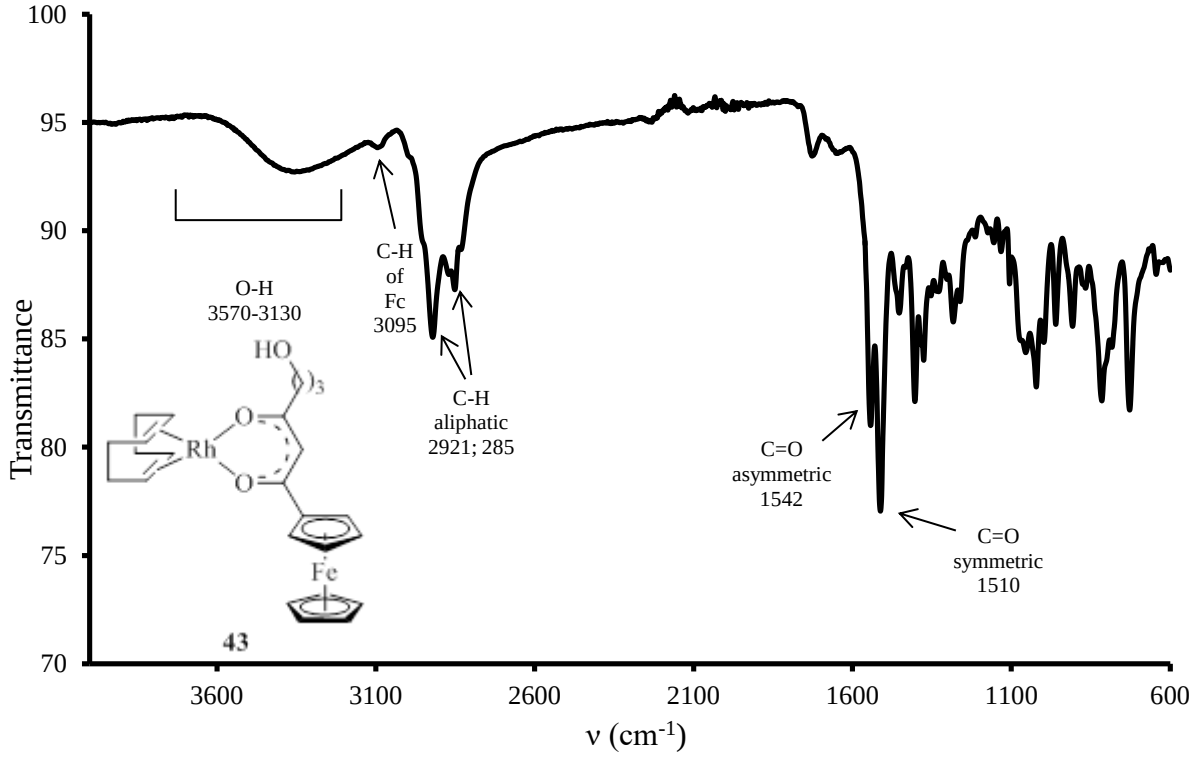

Figure A.20: IR spectrum of Rh[FcCOCHCO$(CH_2)_3$OH(cod)] (**43)**

Crystallographic data

Table A.1. Atomic coordinates (x 10^4) and equivalent isotropic displacement parameters ($Å^2$x 10^3) for $FcCOCH_2CO(CH_2)_3OH$. U(eq) is defined as one third of the trace of the orthogonalized U^{ij} tensor.

	x	y	z	U(eq)
Fe(1)	8979(3)	5337(1)	10217(1)	23(1)
Fe(2)	3488(3)	1651(1)	5896(1)	24(1)
Fe(3)	11500(3)	5325(1)	15067(1)	21(1)
Fe(4)	-3959(3)	1633(1)	914(1)	24(1)
Fe(5)	-13630(3)	4658(1)	2628(1)	21(1)
Fe(6)	21418(3)	8371(1)	13414(1)	22(1)
Fe(7)	13571(3)	4669(1)	7687(1)	24(1)
Fe(8)	1159(3)	3341(1)	1623(1)	24(1)
O(1)	11616(16)	5485(2)	8705(4)	32(2)
O(2)	10701(16)	5860(2)	7904(5)	35(2)
O(3A)	6780(60)	6459(7)	6640(20)	50(6)
O(3B)	5580(50)	6445(5)	6703(15)	50(6)
O(4)	-714(16)	2252(2)	5443(4)	33(2)
O(5)	172(18)	2654(2)	4710(5)	37(2)
O(6A)	8220(40)	3083(4)	3979(12)	71(8)
O(6B)	5650(50)	3338(5)	3885(12)	61(9)
O(7)	7305(15)	5532(2)	13634(4)	28(2)
O(8)	8510(17)	5905(2)	12828(5)	37(2)
O(9A)	13410(70)	6483(4)	11734(13)	68(8)
O(9B)	14660(160)	6471(14)	11900(30)	43(17)
O(10)	199(17)	2231(2)	461(5)	35(2)
O(11)	-902(16)	2635(2)	-271(4)	35(2)
O(12A)	-6770(50)	3326(5)	-1048(12)	75(8)
O(12B)	-8940(50)	3086(4)	-946(10)	48(7)
O(13)	-17912(15)	4456(2)	1179(4)	33(2)
O(14)	-16822(17)	4091(2)	358(5)	37(2)
O(15A)	-11000(200)	3527(7)	-700(20)	55(15)
O(15B)	-12130(130)	3518(5)	-786(17)	34(9)
O(16)	25525(15)	7769(2)	12954(4)	31(2)
O(17)	24483(18)	7362(2)	12238(5)	38(2)
O(18A)	18700(40)	6673(5)	11442(11)	55(7)
O(18B)	16410(30)	6912(4)	11547(11)	46(6)
O(19)	16300(16)	4578(2)	6120(4)	32(2)
O(20)	15547(18)	4179(2)	5339(5)	41(2)
O(21A)	11160(30)	3523(3)	4217(7)	29(3)
O(21B)	9820(60)	3545(6)	4255(15)	29(3)
O(22)	5412(16)	2736(2)	2076(5)	34(2)
O(23)	4471(19)	2330(2)	2800(5)	40(2)
O(24A)	-3480(50)	1892(5)	3503(12)	60(8)
O(24B)	-870(50)	1643(5)	3621(13)	83(9)
C(1)	10430(20)	5739(3)	10296(6)	33(3)
C(2)	8180(20)	5733(3)	10577(6)	31(3)
C(3)	8260(20)	5524(3)	11067(5)	26(2)
C(4)	10520(20)	5402(3)	11097(6)	29(3)
C(5)	11860(30)	5535(3)	10618(6)	37(3)
C(6)	6430(20)	5233(2)	9552(5)	23(2)
C(7)	6560(20)	5016(2)	10031(5)	28(2)
C(8)	8850(20)	4895(2)	10049(6)	26(3)
C(9)	10180(20)	5043(2)	9593(6)	24(2)
C(10)	8660(20)	5254(2)	9281(5)	22(2)
C(11)	9490(20)	5461(3)	8804(6)	24(3)
C(12)	7760(20)	5637(3)	8482(6)	27(3)
C(13)	8490(20)	5831(3)	8018(6)	27(3)

C(14)	6850(20)	6010(3)	7638(6)	33(3)
C(15)	6970(30)	5967(3)	6932(6)	41(3)
C(16A)	5370(30)	6163(4)	6556(7)	53(4)
C(16B)	5370(30)	6163(4)	6556(7)	53(4)
C(17)	3790(20)	1622(3)	4932(6)	31(3)
C(18)	6000(20)	1592(3)	5232(6)	29(3)
C(19)	5840(30)	1347(3)	5648(6)	35(3)
C(20)	3550(30)	1231(3)	5592(7)	38(3)
C(21)	2310(20)	1402(3)	5146(6)	34(3)
C(22)	4420(20)	2008(3)	6391(6)	27(2)
C(23)	4400(20)	1769(3)	6816(6)	28(3)
C(24)	2100(20)	1654(3)	6786(5)	28(2)
C(25)	670(20)	1817(3)	6350(6)	25(2)
C(26)	2140(20)	2041(2)	6109(6)	25(2)
C(27)	1440(20)	2250(3)	5628(6)	22(2)
C(28)	3090(20)	2447(3)	5378(6)	29(3)
C(29)	2330(30)	2648(3)	4930(6)	32(3)
C(30)	3980(30)	2866(3)	4672(6)	42(3)
C(31)	4260(30)	2833(3)	3971(7)	52(4)
C(32A)	5910(30)	3047(4)	3687(8)	53(4)
C(32B)	5910(30)	3047(4)	3687(8)	53(4)
C(33)	11800(20)	5762(3)	15177(6)	30(3)
C(34)	14040(20)	5628(3)	15227(6)	30(3)
C(35)	13960(20)	5429(3)	15738(6)	30(3)
C(36)	11770(20)	5442(3)	16003(6)	28(3)
C(37)	10400(30)	5647(3)	15651(6)	33(3)
C(38)	12350(20)	5115(2)	14257(5)	27(2)
C(39)	12240(20)	4912(2)	14776(5)	24(2)
C(40)	9940(20)	4922(2)	15009(6)	29(3)
C(41)	8610(20)	5130(3)	14658(6)	23(2)
C(42)	10070(20)	5247(2)	14188(5)	24(2)
C(43)	9470(20)	5477(3)	13743(6)	20(2)
C(44)	11240(20)	5636(3)	13444(5)	24(2)
C(45)	10700(20)	5851(3)	12988(6)	26(3)
C(46)	12420(20)	6029(3)	12674(6)	35(3)
C(47)	12310(30)	6015(4)	11974(7)	62(5)
C(48A)	14070(30)	6194(3)	11641(8)	46(4)
C(48B)	14070(30)	6194(3)	11641(8)	46(4)
C(49)	-4420(20)	1612(3)	-46(6)	30(3)
C(50)	-6600(20)	1586(3)	235(6)	32(3)
C(51)	-6400(30)	1334(3)	644(6)	34(3)
C(52)	-4110(30)	1218(3)	584(6)	33(3)
C(53)	-2910(30)	1387(3)	160(6)	34(3)
C(54)	-4720(20)	1989(3)	1430(6)	28(3)
C(55)	-4510(30)	1748(3)	1838(6)	31(3)
C(56)	-2300(20)	1624(3)	1800(5)	32(3)
C(57)	-1010(20)	1793(3)	1360(6)	29(2)
C(58)	-2520(20)	2021(2)	1139(5)	24(2)
C(59)	-1930(20)	2229(2)	643(6)	26(2)
C(60)	-3610(20)	2431(3)	398(6)	30(3)
C(61)	-2980(20)	2630(3)	-48(6)	33(3)
C(62)	-4680(30)	2849(3)	-307(7)	34(3)
C(63)	-5120(30)	2828(4)	-1007(8)	58(5)
C(64A)	-6920(30)	3035(4)	-1277(7)	55(4)
C(64B)	-6920(30)	3035(4)	-1277(7)	55(4)
C(65)	-13330(20)	4222(3)	2763(7)	35(3)
C(66)	-14740(30)	4341(3)	3222(7)	38(3)
C(67)	-13410(20)	4550(3)	3571(6)	32(3)
C(68)	-11120(20)	4554(3)	3311(6)	32(3)
C(69)	-11120(20)	4350(2)	2806(6)	26(2)

C(70)	-12750(20)	4851(2)	1810(5)	22(2)
C(71)	-12770(20)	5062(2)	2311(6)	29(3)
C(72)	-15050(20)	5061(3)	2541(6)	29(3)
C(73)	-16460(20)	4858(3)	2204(6)	25(2)
C(74)	-15030(20)	4730(3)	1732(5)	21(2)
C(75)	-15780(20)	4498(3)	1296(6)	22(2)
C(76)	-14000(20)	4330(2)	989(6)	26(3)
C(77)	-14620(20)	4138(3)	541(6)	24(3)
C(78)	-12900(20)	3947(3)	204(6)	28(3)
C(79)	-13000(30)	3994(3)	-518(7)	47(4)
C(80A)	-11250(30)	3810(3)	-852(7)	40(3)
C(80B)	-11250(30)	3810(3)	-852(7)	40(3)
C(81)	18770(20)	8420(3)	12745(6)	30(3)
C(82)	18890(20)	8665(3)	13133(6)	26(3)
C(83)	21170(20)	8788(3)	13099(6)	30(3)
C(84)	22440(20)	8612(3)	12668(6)	32(3)
C(85)	20980(20)	8389(3)	12443(6)	33(3)
C(86)	24360(20)	8205(3)	13864(5)	23(2)
C(87)	23100(20)	8373(3)	14300(5)	28(2)
C(88)	20810(20)	8254(3)	14332(6)	30(3)
C(89)	20670(20)	8011(3)	13922(6)	28(3)
C(90)	22860(20)	7981(3)	13635(5)	25(2)
C(91)	23400(20)	7767(3)	13138(6)	23(2)
C(92)	21770(20)	7573(3)	12903(6)	32(3)
C(93)	22320(30)	7374(3)	12448(6)	33(3)
C(94)	20690(30)	7151(3)	12182(7)	49(4)
C(95)	20260(30)	7173(4)	11496(8)	62(5)
C(96A)	18490(30)	6967(4)	11221(8)	51(4)
C(96B)	18490(30)	6967(4)	11221(8)	51(4)
C(97)	14920(30)	4268(3)	7779(7)	46(3)
C(98)	12740(30)	4271(3)	8040(6)	35(3)
C(99)	12810(30)	4479(3)	8534(6)	37(3)
C(100)	15100(30)	4601(3)	8563(6)	42(3)
C(101)	16390(30)	4468(4)	8089(8)	49(4)
C(102)	11110(20)	4777(3)	7010(6)	28(2)
C(103)	11190(20)	4991(3)	7501(6)	31(3)
C(104)	13490(30)	5107(3)	7540(6)	37(3)
C(105)	14800(20)	4970(3)	7086(6)	28(3)
C(106)	13390(20)	4769(2)	6751(5)	23(2)
C(107)	14170(20)	4564(3)	6273(6)	29(3)
C(108)	12660(20)	4358(2)	5974(6)	22(2)
C(109)	13350(20)	4178(3)	5519(6)	26(3)
C(110)	11790(20)	3963(3)	5176(6)	30(3)
C(111)	11680(30)	4022(3)	4463(6)	41(4)
C(12A)	10010(30)	3815(3)	4119(7)	43(4)
C(12B)	10010(30)	3815(3)	4119(7)	43(4)
C(113)	-1350(30)	3404(3)	2280(6)	34(3)
C(114)	870(20)	3368(3)	2587(6)	29(3)
C(115)	2370(30)	3588(3)	2372(7)	38(3)
C(116)	1000(30)	3759(3)	1932(7)	40(3)
C(117)	-1230(30)	3640(3)	1871(6)	37(3)
C(118)	230(30)	2980(3)	1120(6)	30(3)
C(119)	320(20)	3224(3)	703(6)	30(3)
C(120)	2550(20)	3341(3)	743(6)	30(3)
C(121)	3950(20)	3175(3)	1168(6)	29(2)
C(122)	2480(20)	2947(2)	1408(6)	27(2)
C(123)	3240(20)	2738(3)	1899(6)	27(3)
C(124)	1630(20)	2544(3)	2139(6)	32(3)
C(125)	2310(30)	2340(3)	2583(6)	37(3)
C(126)	710(30)	2123(3)	2851(7)	39(3)

C(127)	370(30)	2152(4)	3543(9)	58(5)
C(28A)	-1280(30)	1937(4)	3814(8)	57(4)
C(28B)	-1280(30)	1937(4)	3814(8)	57(4)

Table A.2: Bond lengths [Å] for $FcCOCH_2CO(CH_2)_3OH$

Fe(1)-C(10)	2.021(12)		C(33)-C(37)	1.412(19)
Fe(1)-C(9)	2.038(12)		C(33)-C(34)	1.432(18)
Fe(1)-C(2)	2.046(12)		C(33)-H(33)	0.9500
Fe(1)-C(1)	2.046(12)		C(34)-C(35)	1.422(17)
Fe(1)-C(5)	2.051(13)		C(34)-H(34)	0.9500
Fe(1)-C(3)	2.052(12)		C(35)-C(36)	1.402(19)
Fe(1)-C(6)	2.055(12)		C(35)-H(35)	0.9500
Fe(1)-C(4)	2.056(13)		C(36)-C(37)	1.428(19)
Fe(1)-C(7)	2.067(13)		C(36)-H(36)	0.9500
Fe(1)-C(8)	2.083(12)		C(37)-H(37)	0.9500
Fe(2)-C(22)	2.023(12)		C(38)-C(42)	1.449(18)
Fe(2)-C(26)	2.029(12)		C(38)-C(39)	1.450(16)
Fe(2)-C(19)	2.033(14)		C(38)-H(38)	0.9500
Fe(2)-C(20)	2.052(13)		C(39)-C(40)	1.428(18)
Fe(2)-C(17)	2.057(12)		C(39)-H(39)	0.9500
Fe(2)-C(21)	2.058(12)		C(40)-C(41)	1.425(17)
Fe(2)-C(25)	2.061(12)		C(40)-H(40)	0.9500
Fe(2)-C(18)	2.066(13)		C(41)-C(42)	1.431(17)
Fe(2)-C(24)	2.072(12)		C(41)-H(41)	0.9500
Fe(2)-C(23)	2.073(12)		C(42)-C(43)	1.458(16)
Fe(3)-C(35)	2.030(12)		C(43)-C(44)	1.422(17)
Fe(3)-C(42)	2.040(12)		C(44)-C(45)	1.413(18)
Fe(3)-C(38)	2.045(12)		C(44)-H(44)	0.9500
Fe(3)-C(34)	2.045(13)		C(45)-C(46)	1.469(19)
Fe(3)-C(33)	2.048(12)		C(46)-C(47)	1.48(2)
Fe(3)-C(37)	2.052(13)		C(46)-H(46A)	0.9900
Fe(3)-C(36)	2.055(12)		C(46)-H(46B)	0.9900
Fe(3)-C(41)	2.059(12)		C(47)-C(48A)	1.50(2)
Fe(3)-C(39)	2.061(12)		C(47)-H(47A)	0.9900
Fe(3)-C(40)	2.078(12)		C(47)-H(47B)	0.9900
Fe(4)-C(58)	2.030(12)		C(48A)-H(48A)	0.9900
Fe(4)-C(54)	2.036(13)		C(48A)-H(48B)	0.9900
Fe(4)-C(51)	2.042(13)		C(49)-C(50)	1.408(19)
Fe(4)-C(49)	2.042(13)		C(49)-C(53)	1.416(18)
Fe(4)-C(52)	2.048(13)		C(49)-H(49)	0.9500
Fe(4)-C(57)	2.048(13)		C(50)-C(51)	1.457(19)
Fe(4)-C(55)	2.062(14)		C(50)-H(50)	0.9500
Fe(4)-C(50)	2.064(13)		C(51)-C(52)	1.44(2)
Fe(4)-C(53)	2.069(12)		C(51)-H(51)	0.9500
Fe(4)-C(56)	2.074(12)		C(52)-C(53)	1.393(19)
Fe(5)-C(70)	2.029(11)		C(52)-H(52)	0.9500
Fe(5)-C(72)	2.043(12)		C(53)-H(53)	0.9500
Fe(5)-C(73)	2.050(11)		C(54)-C(55)	1.416(19)
Fe(5)-C(65)	2.050(13)		C(54)-C(58)	1.434(18)
Fe(5)-C(66)	2.052(13)		C(54)-H(54)	0.9500
Fe(5)-C(71)	2.055(12)		C(55)-C(56)	1.398(19)
Fe(5)-C(67)	2.058(13)		C(55)-H(55)	0.9500
Fe(5)-C(69)	2.059(11)		C(56)-C(57)	1.441(18)
Fe(5)-C(74)	2.059(11)		C(56)-H(56)	0.9500
Fe(5)-C(68)	2.066(12)		C(57)-C(58)	1.434(16)
Fe(6)-C(84)	2.036(12)		C(57)-H(57)	0.9500
Fe(6)-C(90)	2.038(12)		C(58)-C(59)	1.475(16)
Fe(6)-C(89)	2.042(12)		C(59)-C(60)	1.430(17)

Fe(6)-C(83)	2.051(13)		C(60)-C(61)	1.381(18)
Fe(6)-C(81)	2.057(13)		C(60)-H(60)	0.9500
Fe(6)-C(88)	2.059(12)		C(61)-C(62)	1.501(18)
Fe(6)-C(86)	2.061(12)		C(62)-C(63)	1.50(2)
Fe(6)-C(85)	2.063(12)		C(62)-H(62A)	0.9900
Fe(6)-C(82)	2.064(13)		C(62)-H(62B)	0.9900
Fe(6)-C(87)	2.079(12)		C(63)-C(64A)	1.51(2)
Fe(7)-C(97)	2.021(14)		C(63)-H(63A)	0.9900
Fe(7)-C(101)	2.031(14)		C(63)-H(63B)	0.9900
Fe(7)-C(105)	2.032(13)		C(64A)-H(64A)	0.9900
Fe(7)-C(106)	2.034(12)		C(64A)-H(64B)	0.9900
Fe(7)-C(102)	2.041(13)		C(65)-C(66)	1.40(2)
Fe(7)-C(100)	2.049(13)		C(65)-C(69)	1.401(19)
Fe(7)-C(104)	2.056(13)		C(65)-H(65)	0.9500
Fe(7)-C(103)	2.056(12)		C(66)-C(67)	1.42(2)
Fe(7)-C(98)	2.057(13)		C(66)-H(66)	0.9500
Fe(7)-C(99)	2.059(13)		C(67)-C(68)	1.45(2)
Fe(8)-C(117)	2.036(13)		C(67)-H(67)	0.9500
Fe(8)-C(122)	2.037(12)		C(68)-C(69)	1.430(17)
Fe(8)-C(116)	2.048(13)		C(68)-H(68)	0.9500
Fe(8)-C(118)	2.048(13)		C(69)-H(69)	0.9500
Fe(8)-C(121)	2.051(12)		C(70)-C(74)	1.427(17)
Fe(8)-C(120)	2.054(12)		C(70)-C(71)	1.443(16)
Fe(8)-C(115)	2.057(13)		C(70)-H(70)	0.9500
Fe(8)-C(114)	2.058(13)		C(71)-C(72)	1.416(19)
Fe(8)-C(113)	2.059(13)		C(71)-H(71)	0.9500
Fe(8)-C(119)	2.062(13)		C(72)-C(73)	1.416(18)
O(1)-C(11)	1.254(16)		C(72)-H(72)	0.9500
O(2)-C(13)	1.310(16)		C(73)-C(74)	1.443(17)
O(2)-H(2)	0.8400		C(73)-H(73)	0.9500
O(3A)-C(16A)	1.60(4)		C(74)-C(75)	1.473(17)
O(3A)-H(3A)	0.8400		C(75)-C(76)	1.457(17)
O(3B)-H(3B)	0.8400		C(76)-C(77)	1.340(18)
O(4)-C(27)	1.289(15)		C(76)-H(76)	0.9500
O(5)-C(29)	1.311(17)		C(77)-C(78)	1.526(17)
O(5)-H(5)	0.8400		C(78)-C(79)	1.541(18)
O(6A)-C(32A)	1.46(3)		C(78)-H(78A)	0.9900
O(6A)-H(6A)	0.8400		C(78)-H(78B)	0.9900
O(6B)-H(6B)	0.8400		C(79)-C(80A)	1.51(2)
O(7)-C(43)	1.285(15)		C(79)-H(79A)	0.9900
O(8)-C(45)	1.316(16)		C(79)-H(79B)	0.9900
O(8)-H(8)	0.8400		C(80A)-H(80A)	0.9900
O(9A)-C(48A)	1.41(3)		C(80A)-H(80B)	0.9900
O(9A)-H(9A)	0.8400		C(81)-C(82)	1.402(18)
O(9B)-H(9B)	0.8400		C(81)-C(85)	1.45(2)
O(10)-C(59)	1.296(15)		C(81)-H(81)	0.9500
O(11)-C(61)	1.300(16)		C(82)-C(83)	1.433(19)
O(11)-H(11)	0.8400		C(82)-H(82)	0.9500
O(12A)-C(64A)	1.44(3)		C(83)-C(84)	1.442(18)
O(12A)-H(12A)	0.8400		C(83)-H(83)	0.9500
O(12B)-H(12B)	0.8403		C(84)-C(85)	1.40(2)
O(13)-C(75)	1.257(15)		C(84)-H(84)	0.9500
O(14)-C(77)	1.328(15)		C(85)-H(85)	0.9500
O(14)-H(14)	0.8400		C(86)-C(87)	1.425(17)
O(15A)-C(80A)	1.36(4)		C(86)-C(90)	1.427(17)
O(15A)-H(15A)	0.8410		C(86)-H(86)	0.9500
O(15B)-H(15B)	0.8400		C(87)-C(88)	1.429(18)
O(16)-C(91)	1.297(15)		C(87)-H(87)	0.9500
O(17)-C(93)	1.337(17)		C(88)-C(89)	1.423(17)
O(17)-H(17)	0.8400		C(88)-H(88)	0.9500

O(18A)-C(96A)	1.45(3)		C(89)-C(90)	1.425(18)
O(18A)-H(18A)	0.8400		C(89)-H(89)	0.9500
O(18B)-H(18B)	0.8418		C(90)-C(91)	1.486(17)
O(19)-C(107)	1.279(16)		C(91)-C(92)	1.381(18)
O(20)-C(109)	1.332(16)		C(92)-C(93)	1.379(18)
O(20)-H(20)	0.8400		C(92)-H(92)	0.9500
O(21A)-C(12A)	1.52(2)		C(93)-C(94)	1.495(19)
O(21A)-H(21A)	0.8400		C(94)-C(95)	1.47(2)
O(21B)-H(21B)	0.8400		C(94)-H(94A)	0.9900
O(22)-C(123)	1.294(15)		C(94)-H(94B)	0.9900
O(23)-C(125)	1.313(18)		C(95)-C(96A)	1.50(2)
O(23)-H(23)	0.8400		C(95)-H(95A)	0.9900
O(24A)-C(28A)	1.42(3)		C(95)-H(95B)	0.9900
O(24A)-H(24A)	0.8413		C(96A)-H(96A)	0.9900
O(24B)-H(24B)	0.8400		C(96A)-H(96B)	0.9900
C(1)-C(5)	1.41(2)		C(97)-C(98)	1.39(2)
C(1)-C(2)	1.439(19)		C(97)-C(101)	1.40(2)
C(1)-H(1)	0.9500		C(97)-H(97)	0.9500
C(2)-C(3)	1.420(17)		C(98)-C(99)	1.423(18)
C(2)-H(2B)	0.9500		C(98)-H(98)	0.9500
C(3)-C(4)	1.418(18)		C(99)-C(100)	1.43(2)
C(3)-H(3)	0.9500		C(99)-H(99)	0.9500
C(4)-C(5)	1.434(19)		C(100)-C(101)	1.41(2)
C(4)-H(4)	0.9500		C(100)-H(100)	0.9500
C(5)-H(5B)	0.9500		C(101)-H(101)	0.9500
C(6)-C(10)	1.428(17)		C(102)-C(103)	1.438(17)
C(6)-C(7)	1.427(16)		C(102)-C(106)	1.441(18)
C(6)-H(6)	0.9500		C(102)-H(102)	0.9500
C(7)-C(8)	1.431(18)		C(103)-C(104)	1.43(2)
C(7)-H(7)	0.9500		C(103)-H(103)	0.9500
C(8)-C(9)	1.427(17)		C(104)-C(105)	1.40(2)
C(8)-H(8B)	0.9500		C(104)-H(104)	0.9500
C(9)-C(10)	1.456(16)		C(105)-C(106)	1.411(16)
C(9)-H(9)	0.9500		C(105)-H(105)	0.9500
C(10)-C(11)	1.484(17)		C(106)-C(107)	1.472(18)
C(11)-C(12)	1.441(17)		C(107)-C(108)	1.422(18)
C(12)-C(13)	1.407(18)		C(108)-C(109)	1.347(17)
C(12)-H(12)	0.9500		C(108)-H(108)	0.9500
C(13)-C(14)	1.474(18)		C(109)-C(110)	1.508(17)
C(14)-C(15)	1.510(18)		C(110)-C(111)	1.534(17)
C(14)-H(14A)	0.9900		C(110)-H(11A)	0.9900
C(14)-H(14B)	0.9900		C(110)-H(11B)	0.9900
C(15)-C(16A)	1.501(19)		C(111)-C(12A)	1.521(19)
C(15)-H(15C)	0.9900		C(111)-H(11E)	0.9900
C(15)-H(15D)	0.9900		C(111)-H(11F)	0.9900
C(16A)-H(16A)	0.9900		C(12A)-H(12C)	0.9900
C(16A)-H(16B)	0.9900		C(12A)-H(12D)	0.9900
C(17)-C(18)	1.404(19)		C(113)-C(117)	1.401(19)
C(17)-C(21)	1.418(18)		C(113)-C(114)	1.420(19)
C(17)-H(17B)	0.9500		C(113)-H(113)	0.9500
C(18)-C(19)	1.440(18)		C(114)-C(115)	1.424(19)
C(18)-H(18)	0.9500		C(114)-H(114)	0.9500
C(19)-C(20)	1.42(2)		C(115)-C(116)	1.43(2)
C(19)-H(19)	0.9500		C(115)-H(115)	0.9500
C(20)-C(21)	1.41(2)		C(116)-C(117)	1.40(2)
C(20)-H(20B)	0.9500		C(116)-H(116)	0.9500
C(21)-H(21)	0.9500		C(117)-H(117)	0.9500
C(22)-C(23)	1.427(18)		C(118)-C(122)	1.417(19)
C(22)-C(26)	1.431(18)		C(118)-C(119)	1.438(19)
C(22)-H(22)	0.9500		C(118)-H(118)	0.9500

C(23)-C(24)	1.424(18)		C(119)-C(120)	1.395(19)
C(23)-H(23B)	0.9500		C(119)-H(119)	0.9500
C(24)-C(25)	1.427(17)		C(120)-C(121)	1.415(18)
C(24)-H(24)	0.9500		C(120)-H(120)	0.9500
C(25)-C(26)	1.444(16)		C(121)-C(122)	1.456(17)
C(25)-H(25)	0.9500		C(121)-H(121)	0.9500
C(26)-C(27)	1.450(17)		C(122)-C(123)	1.475(17)
C(27)-C(28)	1.427(17)		C(123)-C(124)	1.399(17)
C(28)-C(29)	1.388(18)		C(124)-C(125)	1.378(19)
C(28)-H(28)	0.9500		C(124)-H(124)	0.9500
C(29)-C(30)	1.505(19)		C(125)-C(126)	1.49(2)
C(30)-C(31)	1.51(2)		C(126)-C(127)	1.49(2)
C(30)-H(30A)	0.9900		C(126)-H(12G)	0.9900
C(30)-H(30B)	0.9900		C(126)-H(12H)	0.9900
C(31)-C(32A)	1.51(2)		C(127)-C(28A)	1.50(2)
C(31)-H(31A)	0.9900		C(127)-H(12J)	0.9900
C(31)-H(31B)	0.9900		C(127)-H(12K)	0.9900
C(32A)-H(32A)	0.9900		C(28A)-H(12L)	0.9900
C(32A)-H(32B)	0.9900		C(28A)-H(12M)	0.9900

Table A.3: Bond angles [°] for $FcCOCH_2CO(CH_2)_3OH$

C(10)-Fe(1)-C(9)	42.0(5)		C(29)-C(30)-H(30B)	109.2
C(10)-Fe(1)-C(2)	121.5(5)		H(30A)-C(30)-H(30B)	107.9
C(9)-Fe(1)-C(2)	158.2(5)		C(30)-C(31)-C(32A)	114.4(13)
C(10)-Fe(1)-C(1)	106.1(5)		C(30)-C(31)-H(31A)	108.6
C(9)-Fe(1)-C(1)	121.2(5)		C(32A)-C(31)-H(31A)	108.6
C(2)-Fe(1)-C(1)	41.2(5)		C(30)-C(31)-H(31B)	108.7
C(10)-Fe(1)-C(5)	122.3(5)		C(32A)-C(31)-H(31B)	108.7
C(9)-Fe(1)-C(5)	106.3(5)		H(31A)-C(31)-H(31B)	107.6
C(2)-Fe(1)-C(5)	68.5(6)		O(6A)-C(32A)-C(31)	118.9(15)
C(1)-Fe(1)-C(5)	40.4(6)		O(6A)-C(32A)-H(32A)	107.6
C(10)-Fe(1)-C(3)	157.9(5)		C(31)-C(32A)-H(32A)	107.6
C(9)-Fe(1)-C(3)	159.2(5)		O(6A)-C(32A)-H(32B)	107.6
C(2)-Fe(1)-C(3)	40.6(5)		C(31)-C(32A)-H(32B)	107.6
C(1)-Fe(1)-C(3)	68.7(5)		H(32A)-C(32A)-H(32B)	107.0
C(5)-Fe(1)-C(3)	68.5(5)		C(37)-C(33)-C(34)	108.5(12)
C(10)-Fe(1)-C(6)	41.0(5)		C(37)-C(33)-Fe(3)	70.0(7)
C(9)-Fe(1)-C(6)	69.4(5)		C(34)-C(33)-Fe(3)	69.4(7)
C(2)-Fe(1)-C(6)	107.6(5)		C(37)-C(33)-H(33)	125.8
C(1)-Fe(1)-C(6)	123.3(5)		C(34)-C(33)-H(33)	125.8
C(5)-Fe(1)-C(6)	159.3(5)		Fe(3)-C(33)-H(33)	126.4
C(3)-Fe(1)-C(6)	122.6(5)		C(35)-C(34)-C(33)	106.7(11)
C(10)-Fe(1)-C(4)	159.6(5)		C(35)-C(34)-Fe(3)	69.0(7)
C(9)-Fe(1)-C(4)	122.7(5)		C(33)-C(34)-Fe(3)	69.6(7)
C(2)-Fe(1)-C(4)	68.1(5)		C(35)-C(34)-H(34)	126.6
C(1)-Fe(1)-C(4)	68.4(6)		C(33)-C(34)-H(34)	126.6
C(5)-Fe(1)-C(4)	40.9(5)		Fe(3)-C(34)-H(34)	126.3
C(3)-Fe(1)-C(4)	40.4(5)		C(36)-C(35)-C(34)	109.1(12)
C(6)-Fe(1)-C(4)	158.4(5)		C(36)-C(35)-Fe(3)	70.9(7)
C(10)-Fe(1)-C(7)	68.8(5)		C(34)-C(35)-Fe(3)	70.2(7)
C(9)-Fe(1)-C(7)	68.5(5)		C(36)-C(35)-H(35)	125.4
C(2)-Fe(1)-C(7)	124.0(6)		C(34)-C(35)-H(35)	125.4
C(1)-Fe(1)-C(7)	160.3(6)		Fe(3)-C(35)-H(35)	125.1
C(5)-Fe(1)-C(7)	158.4(6)		C(35)-C(36)-C(37)	107.9(12)
C(3)-Fe(1)-C(7)	108.5(5)		C(35)-C(36)-Fe(3)	68.9(7)
C(6)-Fe(1)-C(7)	40.5(4)		C(37)-C(36)-Fe(3)	69.5(7)
C(4)-Fe(1)-C(7)	123.0(5)		C(35)-C(36)-H(36)	126.0
C(10)-Fe(1)-C(8)	69.1(5)		C(37)-C(36)-H(36)	126.0

C(9)-Fe(1)-C(8)	40.5(5)		Fe(3)-C(36)-H(36)	127.0
C(2)-Fe(1)-C(8)	160.1(5)		C(33)-C(37)-C(36)	107.8(12)
C(1)-Fe(1)-C(8)	157.4(6)		C(33)-C(37)-Fe(3)	69.7(7)
C(5)-Fe(1)-C(8)	122.3(6)		C(36)-C(37)-Fe(3)	69.8(7)
C(3)-Fe(1)-C(8)	124.0(5)		C(33)-C(37)-H(37)	126.1
C(6)-Fe(1)-C(8)	68.3(5)		C(36)-C(37)-H(37)	126.1
C(4)-Fe(1)-C(8)	108.1(5)		Fe(3)-C(37)-H(37)	126.0
C(7)-Fe(1)-C(8)	40.3(5)		C(42)-C(38)-C(39)	106.8(11)
C(22)-Fe(2)-C(26)	41.4(5)		C(42)-C(38)-Fe(3)	69.1(7)
C(22)-Fe(2)-C(19)	122.3(6)		C(39)-C(38)-Fe(3)	69.9(6)
C(26)-Fe(2)-C(19)	159.9(6)		C(42)-C(38)-H(38)	126.6
C(22)-Fe(2)-C(20)	158.8(6)		C(39)-C(38)-H(38)	126.6
C(26)-Fe(2)-C(20)	158.3(6)		Fe(3)-C(38)-H(38)	125.9
C(19)-Fe(2)-C(20)	40.8(6)		C(40)-C(39)-C(38)	107.8(11)
C(22)-Fe(2)-C(17)	122.4(5)		C(40)-C(39)-Fe(3)	70.4(7)
C(26)-Fe(2)-C(17)	108.9(5)		C(38)-C(39)-Fe(3)	68.7(6)
C(19)-Fe(2)-C(17)	67.7(5)		C(40)-C(39)-H(39)	126.1
C(20)-Fe(2)-C(17)	68.0(5)		C(38)-C(39)-H(39)	126.1
C(22)-Fe(2)-C(21)	158.9(5)		Fe(3)-C(39)-H(39)	126.3
C(26)-Fe(2)-C(21)	123.6(5)		C(39)-C(40)-C(41)	109.2(11)
C(19)-Fe(2)-C(21)	67.5(6)		C(39)-C(40)-Fe(3)	69.2(7)
C(20)-Fe(2)-C(21)	40.1(6)		C(41)-C(40)-Fe(3)	69.1(7)
C(17)-Fe(2)-C(21)	40.3(5)		C(39)-C(40)-H(40)	125.4
C(22)-Fe(2)-C(25)	69.5(5)		C(41)-C(40)-H(40)	125.4
C(26)-Fe(2)-C(25)	41.3(5)		Fe(3)-C(40)-H(40)	127.9
C(19)-Fe(2)-C(25)	156.9(5)		C(40)-C(41)-C(42)	107.5(11)
C(20)-Fe(2)-C(25)	121.7(6)		C(40)-C(41)-Fe(3)	70.6(7)
C(17)-Fe(2)-C(25)	125.6(5)		C(42)-C(41)-Fe(3)	68.9(7)
C(21)-Fe(2)-C(25)	109.0(5)		C(40)-C(41)-H(41)	126.2
C(22)-Fe(2)-C(18)	106.4(5)		C(42)-C(41)-H(41)	126.2
C(26)-Fe(2)-C(18)	123.4(5)		Fe(3)-C(41)-H(41)	125.9
C(19)-Fe(2)-C(18)	41.1(5)		C(41)-C(42)-C(38)	108.7(10)
C(20)-Fe(2)-C(18)	68.9(5)		C(41)-C(42)-C(43)	126.6(12)
C(17)-Fe(2)-C(18)	39.8(5)		C(38)-C(42)-C(43)	124.5(11)
C(21)-Fe(2)-C(18)	67.8(5)		C(41)-C(42)-Fe(3)	70.3(7)
C(25)-Fe(2)-C(18)	160.9(5)		C(38)-C(42)-Fe(3)	69.4(6)
C(22)-Fe(2)-C(24)	68.0(5)		C(43)-C(42)-Fe(3)	122.5(8)
C(26)-Fe(2)-C(24)	68.2(5)		O(7)-C(43)-C(44)	121.3(11)
C(19)-Fe(2)-C(24)	121.4(5)		O(7)-C(43)-C(42)	117.8(11)
C(20)-Fe(2)-C(24)	107.7(5)		C(44)-C(43)-C(42)	120.8(11)
C(17)-Fe(2)-C(24)	162.0(5)		C(45)-C(44)-C(43)	121.8(12)
C(21)-Fe(2)-C(24)	125.3(5)		C(45)-C(44)-H(44)	119.1
C(25)-Fe(2)-C(24)	40.4(5)		C(43)-C(44)-H(44)	119.1
C(18)-Fe(2)-C(24)	156.9(5)		O(8)-C(45)-C(44)	119.6(12)
C(22)-Fe(2)-C(23)	40.8(5)		O(8)-C(45)-C(46)	115.6(11)
C(26)-Fe(2)-C(23)	68.9(5)		C(44)-C(45)-C(46)	124.8(12)
C(19)-Fe(2)-C(23)	106.1(5)		C(45)-C(46)-C(47)	114.9(12)
C(20)-Fe(2)-C(23)	122.6(6)		C(45)-C(46)-H(46A)	108.5
C(17)-Fe(2)-C(23)	157.1(5)		C(47)-C(46)-H(46A)	108.5
C(21)-Fe(2)-C(23)	159.8(5)		C(45)-C(46)-H(46B)	108.5
C(25)-Fe(2)-C(23)	68.8(5)		C(47)-C(46)-H(46B)	108.6
C(18)-Fe(2)-C(23)	121.0(5)		H(46A)-C(46)-H(46B)	107.5
C(24)-Fe(2)-C(23)	40.2(5)		C(46)-C(47)-C(48A)	116.0(13)
C(35)-Fe(3)-C(42)	158.5(5)		C(46)-C(47)-H(47A)	108.3
C(35)-Fe(3)-C(38)	121.3(6)		C(48A)-C(47)-H(47A)	108.3
C(42)-Fe(3)-C(38)	41.6(5)		C(46)-C(47)-H(47B)	108.3
C(35)-Fe(3)-C(34)	40.9(5)		C(48A)-C(47)-H(47B)	108.3
C(42)-Fe(3)-C(34)	122.4(5)		H(47A)-C(47)-H(47B)	107.4
C(38)-Fe(3)-C(34)	106.1(5)		O(9A)-C(48A)-C(47)	105.7(17)
C(35)-Fe(3)-C(33)	68.3(5)		O(9A)-C(48A)-H(48A)	110.5

C(42)-Fe(3)-C(33)	108.0(5)		C(47)-C(48A)-H(48A)	110.6
C(38)-Fe(3)-C(33)	123.1(5)		O(9A)-C(48A)-H(48B)	110.7
C(34)-Fe(3)-C(33)	41.0(5)		C(47)-C(48A)-H(48B)	110.6
C(35)-Fe(3)-C(37)	68.2(5)		H(48A)-C(48A)-H(48B)	108.7
C(42)-Fe(3)-C(37)	123.7(5)		C(50)-C(49)-C(53)	110.7(12)
C(38)-Fe(3)-C(37)	159.8(5)		C(50)-C(49)-Fe(4)	70.8(7)
C(34)-Fe(3)-C(37)	68.6(6)		C(53)-C(49)-Fe(4)	70.9(7)
C(33)-Fe(3)-C(37)	40.3(5)		C(50)-C(49)-H(49)	124.6
C(35)-Fe(3)-C(36)	40.1(5)		C(53)-C(49)-H(49)	124.6
C(42)-Fe(3)-C(36)	160.1(5)		Fe(4)-C(49)-H(49)	125.3
C(38)-Fe(3)-C(36)	157.2(5)		C(49)-C(50)-C(51)	105.6(12)
C(34)-Fe(3)-C(36)	68.3(5)		C(49)-C(50)-Fe(4)	69.1(8)
C(33)-Fe(3)-C(36)	68.0(5)		C(51)-C(50)-Fe(4)	68.4(7)
C(37)-Fe(3)-C(36)	40.7(5)		C(49)-C(50)-H(50)	127.2
C(35)-Fe(3)-C(41)	159.0(5)		C(51)-C(50)-H(50)	127.2
C(42)-Fe(3)-C(41)	40.9(5)		Fe(4)-C(50)-H(50)	126.8
C(38)-Fe(3)-C(41)	69.5(5)		C(52)-C(51)-C(50)	107.4(12)
C(34)-Fe(3)-C(41)	159.0(5)		C(52)-C(51)-Fe(4)	69.7(8)
C(33)-Fe(3)-C(41)	123.1(5)		C(50)-C(51)-Fe(4)	70.0(7)
C(37)-Fe(3)-C(41)	108.1(6)		C(52)-C(51)-H(51)	126.3
C(36)-Fe(3)-C(41)	123.6(5)		C(50)-C(51)-H(51)	126.3
C(35)-Fe(3)-C(39)	106.5(5)		Fe(4)-C(51)-H(51)	125.6
C(42)-Fe(3)-C(39)	69.1(5)		C(53)-C(52)-C(51)	108.9(12)
C(38)-Fe(3)-C(39)	41.3(5)		C(53)-C(52)-Fe(4)	71.0(7)
C(34)-Fe(3)-C(39)	122.3(5)		C(51)-C(52)-Fe(4)	69.2(7)
C(33)-Fe(3)-C(39)	159.7(5)		C(53)-C(52)-H(52)	125.5
C(37)-Fe(3)-C(39)	158.0(5)		C(51)-C(52)-H(52)	125.5
C(36)-Fe(3)-C(39)	121.6(5)		Fe(4)-C(52)-H(52)	125.8
C(41)-Fe(3)-C(39)	68.7(5)		C(52)-C(53)-C(49)	107.4(12)
C(35)-Fe(3)-C(40)	123.1(5)		C(52)-C(53)-Fe(4)	69.4(7)
C(42)-Fe(3)-C(40)	68.0(5)		C(49)-C(53)-Fe(4)	68.8(7)
C(38)-Fe(3)-C(40)	68.6(5)		C(52)-C(53)-H(53)	126.3
C(34)-Fe(3)-C(40)	158.9(5)		C(49)-C(53)-H(53)	126.3
C(33)-Fe(3)-C(40)	158.9(6)		Fe(4)-C(53)-H(53)	127.0
C(37)-Fe(3)-C(40)	123.3(6)		C(55)-C(54)-C(58)	106.5(12)
C(36)-Fe(3)-C(40)	108.2(5)		C(55)-C(54)-Fe(4)	70.8(8)
C(41)-Fe(3)-C(40)	40.3(5)		C(58)-C(54)-Fe(4)	69.1(7)
C(39)-Fe(3)-C(40)	40.4(5)		C(55)-C(54)-H(54)	126.7
C(58)-Fe(4)-C(54)	41.3(5)		C(58)-C(54)-H(54)	126.7
C(58)-Fe(4)-C(51)	159.8(5)		Fe(4)-C(54)-H(54)	125.0
C(54)-Fe(4)-C(51)	122.8(6)		C(56)-C(55)-C(54)	110.3(12)
C(58)-Fe(4)-C(49)	108.3(5)		C(56)-C(55)-Fe(4)	70.7(8)
C(54)-Fe(4)-C(49)	123.3(5)		C(54)-C(55)-Fe(4)	68.8(8)
C(51)-Fe(4)-C(49)	67.9(6)		C(56)-C(55)-H(55)	124.8
C(58)-Fe(4)-C(52)	157.6(5)		C(54)-C(55)-H(55)	124.8
C(54)-Fe(4)-C(52)	159.8(6)		Fe(4)-C(55)-H(55)	127.2
C(51)-Fe(4)-C(52)	41.1(6)		C(55)-C(56)-C(57)	107.6(11)
C(49)-Fe(4)-C(52)	67.2(5)		C(55)-C(56)-Fe(4)	69.8(7)
C(58)-Fe(4)-C(57)	41.2(5)		C(57)-C(56)-Fe(4)	68.6(7)
C(54)-Fe(4)-C(57)	69.5(5)		C(55)-C(56)-H(56)	126.2
C(51)-Fe(4)-C(57)	157.6(5)		C(57)-C(56)-H(56)	126.2
C(49)-Fe(4)-C(57)	123.5(5)		Fe(4)-C(56)-H(56)	127.1
C(52)-Fe(4)-C(57)	121.4(5)		C(58)-C(57)-C(56)	107.0(11)
C(58)-Fe(4)-C(55)	67.9(5)		C(58)-C(57)-Fe(4)	68.7(7)
C(54)-Fe(4)-C(55)	40.4(5)		C(56)-C(57)-Fe(4)	70.5(7)
C(51)-Fe(4)-C(55)	108.3(6)		C(58)-C(57)-H(57)	126.5
C(49)-Fe(4)-C(55)	159.5(6)		C(56)-C(57)-H(57)	126.5
C(52)-Fe(4)-C(55)	124.1(5)		Fe(4)-C(57)-H(57)	125.8
C(57)-Fe(4)-C(55)	67.8(5)		C(54)-C(58)-C(57)	108.5(11)
C(58)-Fe(4)-C(50)	122.7(5)		C(54)-C(58)-C(59)	126.9(11)

C(54)-Fe(4)-C(50)	107.0(6)		C(57)-C(58)-C(59)	124.4(11)
C(51)-Fe(4)-C(50)	41.6(5)		C(54)-C(58)-Fe(4)	69.6(7)
C(49)-Fe(4)-C(50)	40.1(5)		C(57)-C(58)-Fe(4)	70.1(7)
C(52)-Fe(4)-C(50)	69.1(6)		C(59)-C(58)-Fe(4)	121.2(8)
C(57)-Fe(4)-C(50)	159.1(5)		O(10)-C(59)-C(60)	121.5(11)
C(55)-Fe(4)-C(50)	123.6(6)		O(10)-C(59)-C(58)	117.3(11)
C(58)-Fe(4)-C(53)	122.7(5)		C(60)-C(59)-C(58)	121.2(11)
C(54)-Fe(4)-C(53)	159.1(5)		C(61)-C(60)-C(59)	119.7(12)
C(51)-Fe(4)-C(53)	68.1(6)		C(61)-C(60)-H(60)	120.2
C(49)-Fe(4)-C(53)	40.3(5)		C(59)-C(60)-H(60)	120.2
C(52)-Fe(4)-C(53)	39.6(5)		O(11)-C(61)-C(60)	121.8(12)
C(57)-Fe(4)-C(53)	107.2(6)		O(11)-C(61)-C(62)	116.9(12)
C(55)-Fe(4)-C(53)	159.0(5)		C(60)-C(61)-C(62)	121.2(12)
C(50)-Fe(4)-C(53)	68.4(6)		C(63)-C(62)-C(61)	113.5(12)
C(58)-Fe(4)-C(56)	68.5(5)		C(63)-C(62)-H(62A)	108.9
C(54)-Fe(4)-C(56)	68.4(5)		C(61)-C(62)-H(62A)	108.9
C(51)-Fe(4)-C(56)	122.0(5)		C(63)-C(62)-H(62B)	108.9
C(49)-Fe(4)-C(56)	159.8(6)		C(61)-C(62)-H(62B)	108.9
C(52)-Fe(4)-C(56)	107.7(5)		H(62A)-C(62)-H(62B)	107.7
C(57)-Fe(4)-C(56)	40.9(5)		C(62)-C(63)-C(64A)	114.9(13)
C(55)-Fe(4)-C(56)	39.5(5)		C(62)-C(63)-H(63A)	108.5
C(50)-Fe(4)-C(56)	158.5(6)		C(64A)-C(63)-H(63A)	108.5
C(53)-Fe(4)-C(56)	123.4(5)		C(62)-C(63)-H(63B)	108.5
C(70)-Fe(5)-C(72)	68.3(5)		C(64A)-C(63)-H(63B)	108.6
C(70)-Fe(5)-C(73)	69.2(5)		H(63A)-C(63)-H(63B)	107.5
C(72)-Fe(5)-C(73)	40.5(5)		O(12A)-C(64A)-C(63)	116.0(17)
C(70)-Fe(5)-C(65)	122.2(5)		O(12A)-C(64A)-H(64A)	108.3
C(72)-Fe(5)-C(65)	161.0(6)		C(63)-C(64A)-H(64A)	108.3
C(73)-Fe(5)-C(65)	124.6(5)		O(12A)-C(64A)-H(64B)	108.3
C(70)-Fe(5)-C(66)	158.6(6)		C(63)-C(64A)-H(64B)	108.3
C(72)-Fe(5)-C(66)	125.4(6)		H(64A)-C(64A)-H(64B)	107.4
C(73)-Fe(5)-C(66)	109.5(6)		C(66)-C(65)-C(69)	109.6(13)
C(65)-Fe(5)-C(66)	39.8(6)		C(66)-C(65)-Fe(5)	70.2(8)
C(70)-Fe(5)-C(71)	41.4(5)		C(69)-C(65)-Fe(5)	70.4(7)
C(72)-Fe(5)-C(71)	40.4(5)		C(66)-C(65)-H(65)	125.2
C(73)-Fe(5)-C(71)	69.0(5)		C(69)-C(65)-H(65)	125.2
C(65)-Fe(5)-C(71)	157.6(6)		Fe(5)-C(65)-H(65)	125.8
C(66)-Fe(5)-C(71)	159.6(6)		C(65)-C(66)-C(67)	108.4(13)
C(70)-Fe(5)-C(67)	158.0(6)		C(65)-C(66)-Fe(5)	70.0(7)
C(72)-Fe(5)-C(67)	108.8(5)		C(67)-C(66)-Fe(5)	70.0(7)
C(73)-Fe(5)-C(67)	123.8(5)		C(65)-C(66)-H(66)	125.8
C(65)-Fe(5)-C(67)	67.7(6)		C(67)-C(66)-H(66)	125.8
C(66)-Fe(5)-C(67)	40.5(6)		Fe(5)-C(66)-H(66)	125.8
C(71)-Fe(5)-C(67)	122.2(5)		C(66)-C(67)-C(68)	107.0(12)
C(70)-Fe(5)-C(69)	105.6(5)		C(66)-C(67)-Fe(5)	69.5(7)
C(72)-Fe(5)-C(69)	158.1(5)		C(68)-C(67)-Fe(5)	69.8(7)
C(73)-Fe(5)-C(69)	159.1(5)		C(66)-C(67)-H(67)	126.5
C(65)-Fe(5)-C(69)	39.9(5)		C(68)-C(67)-H(67)	126.5
C(66)-Fe(5)-C(69)	67.6(5)		Fe(5)-C(67)-H(67)	125.8
C(71)-Fe(5)-C(69)	121.2(5)		C(69)-C(68)-C(67)	107.2(12)
C(67)-Fe(5)-C(69)	68.5(5)		C(69)-C(68)-Fe(5)	69.4(7)
C(70)-Fe(5)-C(74)	40.9(5)		C(67)-C(68)-Fe(5)	69.1(7)
C(72)-Fe(5)-C(74)	68.1(5)		C(69)-C(68)-H(68)	126.4
C(73)-Fe(5)-C(74)	41.1(5)		C(67)-C(68)-H(68)	126.4
C(65)-Fe(5)-C(74)	108.4(5)		Fe(5)-C(68)-H(68)	126.6
C(66)-Fe(5)-C(74)	124.1(6)		C(65)-C(69)-C(68)	107.8(12)
C(71)-Fe(5)-C(74)	69.1(5)		C(65)-C(69)-Fe(5)	69.7(7)
C(67)-Fe(5)-C(74)	160.2(5)		C(68)-C(69)-Fe(5)	70.0(7)
C(69)-Fe(5)-C(74)	121.9(5)		C(65)-C(69)-H(69)	126.1
C(70)-Fe(5)-C(68)	120.8(5)		C(68)-C(69)-H(69)	126.1

C(72)-Fe(5)-C(68)	123.0(5)		Fe(5)-C(69)-H(69)	125.8
C(73)-Fe(5)-C(68)	159.5(5)		C(74)-C(70)-C(71)	108.8(11)
C(65)-Fe(5)-C(68)	67.5(5)		C(74)-C(70)-Fe(5)	70.7(6)
C(66)-Fe(5)-C(68)	68.1(6)		C(71)-C(70)-Fe(5)	70.3(6)
C(71)-Fe(5)-C(68)	105.7(5)		C(74)-C(70)-H(70)	125.6
C(67)-Fe(5)-C(68)	41.1(5)		C(71)-C(70)-H(70)	125.6
C(69)-Fe(5)-C(68)	40.6(5)		Fe(5)-C(70)-H(70)	125.0
C(74)-Fe(5)-C(68)	157.3(5)		C(72)-C(71)-C(70)	106.3(11)
C(84)-Fe(6)-C(90)	122.6(5)		C(72)-C(71)-Fe(5)	69.3(7)
C(84)-Fe(6)-C(89)	158.3(5)		C(70)-C(71)-Fe(5)	68.4(6)
C(90)-Fe(6)-C(89)	40.9(5)		C(72)-C(71)-H(71)	126.9
C(84)-Fe(6)-C(83)	41.3(5)		C(70)-C(71)-H(71)	126.9
C(90)-Fe(6)-C(83)	159.4(5)		Fe(5)-C(71)-H(71)	127.0
C(89)-Fe(6)-C(83)	158.5(5)		C(73)-C(72)-C(71)	110.4(11)
C(84)-Fe(6)-C(81)	68.3(6)		C(73)-C(72)-Fe(5)	70.0(7)
C(90)-Fe(6)-C(81)	122.8(5)		C(71)-C(72)-Fe(5)	70.2(7)
C(89)-Fe(6)-C(81)	106.8(6)		C(73)-C(72)-H(72)	124.8
C(83)-Fe(6)-C(81)	68.3(5)		C(71)-C(72)-H(72)	124.8
C(84)-Fe(6)-C(88)	159.9(5)		Fe(5)-C(72)-H(72)	126.6
C(90)-Fe(6)-C(88)	68.3(5)		C(72)-C(73)-C(74)	107.0(11)
C(89)-Fe(6)-C(88)	40.6(5)		C(72)-C(73)-Fe(5)	69.5(7)
C(83)-Fe(6)-C(88)	123.0(5)		C(74)-C(73)-Fe(5)	69.8(6)
C(81)-Fe(6)-C(88)	122.2(6)		C(72)-C(73)-H(73)	126.5
C(84)-Fe(6)-C(86)	108.0(5)		C(74)-C(73)-H(73)	126.5
C(90)-Fe(6)-C(86)	40.7(5)		Fe(5)-C(73)-H(73)	125.8
C(89)-Fe(6)-C(86)	68.7(5)		C(70)-C(74)-C(73)	107.5(10)
C(83)-Fe(6)-C(86)	123.3(5)		C(70)-C(74)-C(75)	127.5(11)
C(81)-Fe(6)-C(86)	159.4(5)		C(73)-C(74)-C(75)	124.8(11)
C(88)-Fe(6)-C(86)	68.3(5)		C(70)-C(74)-Fe(5)	68.4(6)
C(84)-Fe(6)-C(85)	39.9(5)		C(73)-C(74)-Fe(5)	69.1(6)
C(90)-Fe(6)-C(85)	107.4(5)		C(75)-C(74)-Fe(5)	123.8(8)
C(89)-Fe(6)-C(85)	122.5(6)		O(13)-C(75)-C(76)	121.5(12)
C(83)-Fe(6)-C(85)	68.4(5)		O(13)-C(75)-C(74)	120.1(11)
C(81)-Fe(6)-C(85)	41.3(5)		C(76)-C(75)-C(74)	118.3(11)
C(88)-Fe(6)-C(85)	158.7(6)		C(77)-C(76)-C(75)	119.9(12)
C(86)-Fe(6)-C(85)	123.0(5)		C(77)-C(76)-H(76)	120.0
C(84)-Fe(6)-C(82)	68.4(5)		C(75)-C(76)-H(76)	120.0
C(90)-Fe(6)-C(82)	158.3(5)		O(14)-C(77)-C(76)	122.9(12)
C(89)-Fe(6)-C(82)	122.2(5)		O(14)-C(77)-C(78)	113.3(11)
C(83)-Fe(6)-C(82)	40.8(5)		C(76)-C(77)-C(78)	123.8(12)
C(81)-Fe(6)-C(82)	39.8(5)		C(77)-C(78)-C(79)	112.3(11)
C(88)-Fe(6)-C(82)	107.8(5)		C(77)-C(78)-H(78A)	109.1
C(86)-Fe(6)-C(82)	159.6(5)		C(79)-C(78)-H(78A)	109.1
C(85)-Fe(6)-C(82)	68.1(5)		C(77)-C(78)-H(78B)	109.2
C(84)-Fe(6)-C(87)	124.1(6)		C(79)-C(78)-H(78B)	109.2
C(90)-Fe(6)-C(87)	67.9(5)		H(78A)-C(78)-H(78B)	107.9
C(89)-Fe(6)-C(87)	68.2(5)		C(80A)-C(79)-C(78)	112.4(12)
C(83)-Fe(6)-C(87)	108.3(5)		C(80A)-C(79)-H(79A)	109.1
C(81)-Fe(6)-C(87)	158.5(5)		C(78)-C(79)-H(79A)	109.1
C(88)-Fe(6)-C(87)	40.4(5)		C(80A)-C(79)-H(79B)	109.1
C(86)-Fe(6)-C(87)	40.3(5)		C(78)-C(79)-H(79B)	109.1
C(85)-Fe(6)-C(87)	159.2(6)		H(79A)-C(79)-H(79B)	107.8
C(82)-Fe(6)-C(87)	123.8(5)		O(15A)-C(80A)-C(79)	121(4)
C(97)-Fe(7)-C(101)	40.5(7)		O(15A)-C(80A)-H(80A)	107.2
C(97)-Fe(7)-C(105)	123.5(6)		C(79)-C(80A)-H(80A)	107.1
C(101)-Fe(7)-C(105)	106.7(6)		O(15A)-C(80A)-H(80B)	107.3
C(97)-Fe(7)-C(106)	108.1(5)		C(79)-C(80A)-H(80B)	107.2
C(101)-Fe(7)-C(106)	121.7(6)		H(80A)-C(80A)-H(80B)	106.8
C(105)-Fe(7)-C(106)	40.6(5)		C(82)-C(81)-C(85)	108.1(12)
C(97)-Fe(7)-C(102)	123.2(6)		C(82)-C(81)-Fe(6)	70.4(7)

C(101)-Fe(7)-C(102)	158.5(6)		C(85)-C(81)-Fe(6)	69.6(8)
C(105)-Fe(7)-C(102)	69.0(5)		C(82)-C(81)-H(81)	126.0
C(106)-Fe(7)-C(102)	41.4(5)		C(85)-C(81)-H(81)	126.0
C(97)-Fe(7)-C(100)	67.7(6)		Fe(6)-C(81)-H(81)	125.6
C(101)-Fe(7)-C(100)	40.4(6)		C(81)-C(82)-C(83)	108.8(12)
C(105)-Fe(7)-C(100)	121.5(6)		C(81)-C(82)-Fe(6)	69.8(7)
C(106)-Fe(7)-C(100)	157.2(6)		C(83)-C(82)-Fe(6)	69.2(7)
C(102)-Fe(7)-C(100)	159.8(6)		C(81)-C(82)-H(82)	125.6
C(97)-Fe(7)-C(104)	158.5(7)		C(83)-C(82)-H(82)	125.6
C(101)-Fe(7)-C(104)	122.1(7)		Fe(6)-C(82)-H(82)	127.0
C(105)-Fe(7)-C(104)	39.9(6)		C(82)-C(83)-C(84)	106.7(12)
C(106)-Fe(7)-C(104)	68.1(5)		C(82)-C(83)-Fe(6)	70.1(7)
C(102)-Fe(7)-C(104)	68.9(5)		C(84)-C(83)-Fe(6)	68.8(7)
C(100)-Fe(7)-C(104)	107.2(6)		C(82)-C(83)-H(83)	126.7
C(97)-Fe(7)-C(103)	159.7(7)		C(84)-C(83)-H(83)	126.7
C(101)-Fe(7)-C(103)	158.5(7)		Fe(6)-C(83)-H(83)	126.0
C(105)-Fe(7)-C(103)	68.1(6)		C(85)-C(84)-C(83)	109.0(12)
C(106)-Fe(7)-C(103)	68.7(5)		C(85)-C(84)-Fe(6)	71.1(7)
C(102)-Fe(7)-C(103)	41.1(5)		C(83)-C(84)-Fe(6)	69.9(7)
C(100)-Fe(7)-C(103)	123.1(6)		C(85)-C(84)-H(84)	125.5
C(104)-Fe(7)-C(103)	40.7(6)		C(83)-C(84)-H(84)	125.5
C(97)-Fe(7)-C(98)	39.8(6)		Fe(6)-C(84)-H(84)	125.1
C(101)-Fe(7)-C(98)	68.1(6)		C(84)-C(85)-C(81)	107.4(12)
C(105)-Fe(7)-C(98)	159.3(5)		C(84)-C(85)-Fe(6)	69.0(7)
C(106)-Fe(7)-C(98)	123.7(5)		C(81)-C(85)-Fe(6)	69.2(7)
C(102)-Fe(7)-C(98)	108.1(6)		C(84)-C(85)-H(85)	126.3
C(100)-Fe(7)-C(98)	68.3(6)		C(81)-C(85)-H(85)	126.3
C(104)-Fe(7)-C(98)	159.8(6)		Fe(6)-C(85)-H(85)	127.1
C(103)-Fe(7)-C(98)	124.1(6)		C(87)-C(86)-C(90)	107.5(11)
C(97)-Fe(7)-C(99)	67.3(6)		C(87)-C(86)-Fe(6)	70.5(7)
C(101)-Fe(7)-C(99)	68.2(6)		C(90)-C(86)-Fe(6)	68.8(7)
C(105)-Fe(7)-C(99)	158.1(5)		C(87)-C(86)-H(86)	126.3
C(106)-Fe(7)-C(99)	160.3(6)		C(90)-C(86)-H(86)	126.3
C(102)-Fe(7)-C(99)	123.6(6)		Fe(6)-C(86)-H(86)	126.0
C(100)-Fe(7)-C(99)	40.8(6)		C(86)-C(87)-C(88)	108.2(11)
C(104)-Fe(7)-C(99)	123.4(6)		C(86)-C(87)-Fe(6)	69.2(7)
C(103)-Fe(7)-C(99)	108.5(6)		C(88)-C(87)-Fe(6)	69.0(7)
C(98)-Fe(7)-C(99)	40.5(5)		C(86)-C(87)-H(87)	125.9
C(117)-Fe(8)-C(122)	158.3(6)		C(88)-C(87)-H(87)	125.9
C(117)-Fe(8)-C(116)	40.1(6)		Fe(6)-C(87)-H(87)	127.4
C(122)-Fe(8)-C(116)	160.3(6)		C(89)-C(88)-C(87)	108.1(11)
C(117)-Fe(8)-C(118)	121.8(6)		C(89)-C(88)-Fe(6)	69.1(7)
C(122)-Fe(8)-C(118)	40.6(5)		C(87)-C(88)-Fe(6)	70.5(7)
C(116)-Fe(8)-C(118)	158.1(6)		C(89)-C(88)-H(88)	126.0
C(117)-Fe(8)-C(121)	157.7(6)		C(87)-C(88)-H(88)	125.9
C(122)-Fe(8)-C(121)	41.7(5)		Fe(6)-C(88)-H(88)	126.0
C(116)-Fe(8)-C(121)	123.4(6)		C(88)-C(89)-C(90)	107.7(12)
C(118)-Fe(8)-C(121)	69.0(5)		C(88)-C(89)-Fe(6)	70.3(7)
C(117)-Fe(8)-C(120)	121.6(5)		C(90)-C(89)-Fe(6)	69.4(7)
C(122)-Fe(8)-C(120)	68.7(5)		C(88)-C(89)-H(89)	126.2
C(116)-Fe(8)-C(120)	108.2(5)		C(90)-C(89)-H(89)	126.2
C(118)-Fe(8)-C(120)	68.4(5)		Fe(6)-C(89)-H(89)	125.7
C(121)-Fe(8)-C(120)	40.3(5)		C(89)-C(90)-C(86)	108.6(11)
C(117)-Fe(8)-C(115)	68.5(6)		C(89)-C(90)-C(91)	125.2(11)
C(122)-Fe(8)-C(115)	123.6(6)		C(86)-C(90)-C(91)	126.0(11)
C(116)-Fe(8)-C(115)	40.9(6)		C(89)-C(90)-Fe(6)	69.7(7)
C(118)-Fe(8)-C(115)	158.7(6)		C(86)-C(90)-Fe(6)	70.5(7)
C(121)-Fe(8)-C(115)	108.8(6)		C(91)-C(90)-Fe(6)	121.5(8)
C(120)-Fe(8)-C(115)	124.6(5)		O(16)-C(91)-C(92)	122.1(12)
C(117)-Fe(8)-C(114)	67.9(5)		O(16)-C(91)-C(90)	115.6(11)

C(122)-Fe(8)-C(114)	108.5(5)		C(92)-C(91)-C(90)	122.2(11)
C(116)-Fe(8)-C(114)	67.8(6)		C(93)-C(92)-C(91)	121.2(13)
C(118)-Fe(8)-C(114)	122.3(6)		C(93)-C(92)-H(92)	119.4
C(121)-Fe(8)-C(114)	125.4(5)		C(91)-C(92)-H(92)	119.4
C(120)-Fe(8)-C(114)	161.4(5)		O(17)-C(93)-C(92)	120.0(13)
C(115)-Fe(8)-C(114)	40.5(5)		O(17)-C(93)-C(94)	115.2(12)
C(117)-Fe(8)-C(113)	40.0(5)		C(92)-C(93)-C(94)	124.7(14)
C(122)-Fe(8)-C(113)	123.5(5)		C(95)-C(94)-C(93)	114.0(13)
C(116)-Fe(8)-C(113)	67.1(6)		C(95)-C(94)-H(94A)	108.8
C(118)-Fe(8)-C(113)	106.9(6)		C(93)-C(94)-H(94A)	108.8
C(121)-Fe(8)-C(113)	161.4(5)		C(95)-C(94)-H(94B)	108.8
C(120)-Fe(8)-C(113)	156.6(6)		C(93)-C(94)-H(94B)	108.8
C(115)-Fe(8)-C(113)	68.0(6)		H(94A)-C(94)-H(94B)	107.7
C(114)-Fe(8)-C(113)	40.4(5)		C(94)-C(95)-C(96A)	115.4(14)
C(117)-Fe(8)-C(119)	106.6(6)		C(94)-C(95)-H(95A)	108.4
C(122)-Fe(8)-C(119)	68.2(5)		C(96A)-C(95)-H(95A)	108.4
C(116)-Fe(8)-C(119)	122.7(6)		C(94)-C(95)-H(95B)	108.4
C(118)-Fe(8)-C(119)	41.0(5)		C(96A)-C(95)-H(95B)	108.4
C(121)-Fe(8)-C(119)	67.6(5)		H(95A)-C(95)-H(95B)	107.5
C(120)-Fe(8)-C(119)	39.6(5)		O(18A)-C(96A)-C(95)	115.2(16)
C(115)-Fe(8)-C(119)	159.4(6)		O(18A)-C(96A)-H(96A)	108.5
C(114)-Fe(8)-C(119)	158.0(6)		C(95)-C(96A)-H(96A)	108.5
C(113)-Fe(8)-C(119)	121.9(6)		O(18A)-C(96A)-H(96B)	108.5
C(13)-O(2)-H(2)	109.5		C(95)-C(96A)-H(96B)	108.5
C(16A)-O(3A)-H(3A)	109.5		H(96A)-C(96A)-H(96B)	107.5
C(29)-O(5)-H(5)	109.5		C(98)-C(97)-C(101)	110.3(14)
C(32A)-O(6A)-H(6A)	109.5		C(98)-C(97)-Fe(7)	71.5(8)
C(45)-O(8)-H(8)	109.5		C(101)-C(97)-Fe(7)	70.2(9)
C(48A)-O(9A)-H(9A)	109.5		C(98)-C(97)-H(97)	124.9
C(61)-O(11)-H(11)	109.5		C(101)-C(97)-H(97)	124.8
C(64A)-O(12A)-H(12A)	109.5		Fe(7)-C(97)-H(97)	125.1
C(77)-O(14)-H(14)	109.5		C(97)-C(98)-C(99)	107.1(13)
C(80A)-O(15A)-H(15A)	109.5		C(97)-C(98)-Fe(7)	68.7(8)
C(93)-O(17)-H(17)	109.5		C(99)-C(98)-Fe(7)	69.9(8)
C(96A)-O(18A)-H(18A)	109.5		C(97)-C(98)-H(98)	126.5
C(109)-O(20)-H(20)	109.5		C(99)-C(98)-H(98)	126.5
C(12A)-O(21A)-H(21A)	109.5		Fe(7)-C(98)-H(98)	126.5
C(125)-O(23)-H(23)	109.5		C(98)-C(99)-C(100)	107.7(13)
C(28A)-O(24A)-H(24A)	109.6		C(98)-C(99)-Fe(7)	69.7(7)
C(5)-C(1)-C(2)	107.8(12)		C(100)-C(99)-Fe(7)	69.2(7)
C(5)-C(1)-Fe(1)	70.0(7)		C(98)-C(99)-H(99)	126.2
C(2)-C(1)-Fe(1)	69.4(7)		C(100)-C(99)-H(99)	126.2
C(5)-C(1)-H(1)	126.1		Fe(7)-C(99)-H(99)	126.5
C(2)-C(1)-H(1)	126.1		C(101)-C(100)-C(99)	107.5(13)
Fe(1)-C(1)-H(1)	126.1		C(101)-C(100)-Fe(7)	69.1(8)
C(3)-C(2)-C(1)	108.0(12)		C(99)-C(100)-Fe(7)	69.9(7)
C(3)-C(2)-Fe(1)	70.0(7)		C(101)-C(100)-H(100)	126.3
C(1)-C(2)-Fe(1)	69.4(7)		C(99)-C(100)-H(100)	126.3
C(3)-C(2)-H(2B)	126.0		Fe(7)-C(100)-H(100)	126.2
C(1)-C(2)-H(2B)	126.0		C(97)-C(101)-C(100)	107.5(14)
Fe(1)-C(2)-H(2B)	126.2		C(97)-C(101)-Fe(7)	69.4(8)
C(2)-C(3)-C(4)	108.1(12)		C(100)-C(101)-Fe(7)	70.5(8)
C(2)-C(3)-Fe(1)	69.5(7)		C(97)-C(101)-H(101)	126.3
C(4)-C(3)-Fe(1)	69.9(7)		C(100)-C(101)-H(101)	126.3
C(2)-C(3)-H(3)	126.0		Fe(7)-C(101)-H(101)	125.5

C(4)-C(3)-H(3)	126.0		C(103)-C(102)-C(106)	106.6(11)
Fe(1)-C(3)-H(3)	126.2		C(103)-C(102)-Fe(7)	70.0(7)
C(3)-C(4)-C(5)	108.1(12)		C(106)-C(102)-Fe(7)	69.0(7)
C(3)-C(4)-Fe(1)	69.7(7)		C(103)-C(102)-H(102)	126.7
C(5)-C(4)-Fe(1)	69.4(7)		C(106)-C(102)-H(102)	126.7
C(3)-C(4)-H(4)	125.9		Fe(7)-C(102)-H(102)	125.8
C(5)-C(4)-H(4)	125.9		C(104)-C(103)-C(102)	107.9(12)
Fe(1)-C(4)-H(4)	126.6		C(104)-C(103)-Fe(7)	69.7(7)
C(1)-C(5)-C(4)	108.0(13)		C(102)-C(103)-Fe(7)	68.9(7)
C(1)-C(5)-Fe(1)	69.6(7)		C(104)-C(103)-H(103)	126.0
C(4)-C(5)-Fe(1)	69.7(7)		C(102)-C(103)-H(103)	126.0
C(1)-C(5)-H(5B)	126.0		Fe(7)-C(103)-H(103)	127.0
C(4)-C(5)-H(5B)	126.0		C(105)-C(104)-C(103)	108.2(12)
Fe(1)-C(5)-H(5B)	126.2		C(105)-C(104)-Fe(7)	69.1(7)
C(10)-C(6)-C(7)	108.0(11)		C(103)-C(104)-Fe(7)	69.7(7)
C(10)-C(6)-Fe(1)	68.2(7)		C(105)-C(104)-H(104)	125.9
C(7)-C(6)-Fe(1)	70.2(7)		C(103)-C(104)-H(104)	125.9
C(10)-C(6)-H(6)	126.0		Fe(7)-C(104)-H(104)	126.9
C(7)-C(6)-H(6)	126.0		C(104)-C(105)-C(106)	109.3(12)
Fe(1)-C(6)-H(6)	127.1		C(104)-C(105)-Fe(7)	70.9(8)
C(6)-C(7)-C(8)	108.7(11)		C(106)-C(105)-Fe(7)	69.8(7)
C(6)-C(7)-Fe(1)	69.3(7)		C(104)-C(105)-H(105)	125.4
C(8)-C(7)-Fe(1)	70.4(7)		C(106)-C(105)-H(105)	125.3
C(6)-C(7)-H(7)	125.6		Fe(7)-C(105)-H(105)	125.5
C(8)-C(7)-H(7)	125.6		C(105)-C(106)-C(102)	107.9(11)
Fe(1)-C(7)-H(7)	126.2		C(105)-C(106)-C(107)	126.2(12)
C(9)-C(8)-C(7)	107.9(11)		C(102)-C(106)-C(107)	125.5(11)
C(9)-C(8)-Fe(1)	68.0(7)		C(105)-C(106)-Fe(7)	69.6(7)
C(7)-C(8)-Fe(1)	69.2(7)		C(102)-C(106)-Fe(7)	69.5(7)
C(9)-C(8)-H(8B)	126.0		C(107)-C(106)-Fe(7)	120.9(8)
C(7)-C(8)-H(8B)	126.0		O(19)-C(107)-C(108)	119.8(12)
Fe(1)-C(8)-H(8B)	128.3		O(19)-C(107)-C(106)	117.3(12)
C(8)-C(9)-C(10)	107.6(11)		C(108)-C(107)-C(106)	123.0(12)
C(8)-C(9)-Fe(1)	71.4(7)		C(109)-C(108)-C(107)	122.9(12)
C(10)-C(9)-Fe(1)	68.4(7)		C(109)-C(108)-H(108)	118.5
C(8)-C(9)-H(9)	126.2		C(107)-C(108)-H(108)	118.5
C(10)-C(9)-H(9)	126.2		O(20)-C(109)-C(108)	120.5(12)
Fe(1)-C(9)-H(9)	125.6		O(20)-C(109)-C(110)	114.9(11)
C(6)-C(10)-C(9)	107.7(11)		C(108)-C(109)-C(110)	124.6(12)
C(6)-C(10)-C(11)	129.3(11)		C(109)-C(110)-C(111)	111.2(10)
C(9)-C(10)-C(11)	122.9(11)		C(109)-C(110)-H(11A)	109.4
C(6)-C(10)-Fe(1)	70.8(7)		C(111)-C(110)-H(11A)	109.4
C(9)-C(10)-Fe(1)	69.6(7)		C(109)-C(110)-H(11B)	109.4
C(11)-C(10)-Fe(1)	121.5(8)		C(111)-C(110)-H(11B)	109.4
O(1)-C(11)-C(12)	122.2(12)		H(11A)-C(110)-H(11B)	108.0
O(1)-C(11)-C(10)	120.7(11)		C(12A)-C(111)-C(110)	111.4(12)
C(12)-C(11)-C(10)	117.1(12)		C(12A)-C(111)-H(11E)	109.4
C(13)-C(12)-C(11)	118.2(12)		C(110)-C(111)-H(11E)	109.3
C(13)-C(12)-H(12)	120.9		C(12A)-C(111)-H(11F)	109.3
C(11)-C(12)-H(12)	120.9		C(110)-C(111)-H(11F)	109.4
O(2)-C(13)-C(12)	120.6(12)		H(11E)-C(111)-H(11F)	108.0
O(2)-C(13)-C(14)	116.7(11)		O(21A)-C(12A)-C(111)	103.5(12)
C(12)-C(13)-C(14)	122.7(12)		O(21A)-C(12A)-H(12C)	111.1
C(13)-C(14)-C(15)	114.6(11)		C(111)-C(12A)-H(12C)	111.0
C(13)-C(14)-H(14A)	108.6		O(21A)-C(12A)-H(12D)	111.0
C(15)-C(14)-H(14A)	108.6		C(111)-C(12A)-H(12D)	111.1
C(13)-C(14)-H(14B)	108.6		H(12C)-C(12A)-H(12D)	109.0
C(15)-C(14)-H(14B)	108.6		C(117)-C(113)-C(114)	108.4(13)
H(14A)-C(14)-H(14B)	107.6		C(117)-C(113)-Fe(8)	69.1(8)
C(16A)-C(15)-C(14)	113.4(12)		C(114)-C(113)-Fe(8)	69.8(8)

C(16A)-C(15)-H(15C)	108.9		C(117)-C(113)-H(113)	125.8
C(14)-C(15)-H(15C)	108.9		C(114)-C(113)-H(113)	125.8
C(16A)-C(15)-H(15D)	108.9		Fe(8)-C(113)-H(113)	126.9
C(14)-C(15)-H(15D)	108.9		C(113)-C(114)-C(115)	108.1(12)
H(15C)-C(15)-H(15D)	107.7		C(113)-C(114)-Fe(8)	69.9(7)
C(15)-C(16A)-O(3A)	99.7(19)		C(115)-C(114)-Fe(8)	69.7(8)
C(15)-C(16A)-H(16A)	111.9		C(113)-C(114)-H(114)	125.9
O(3A)-C(16A)-H(16A)	111.8		C(115)-C(114)-H(114)	126.0
C(15)-C(16A)-H(16B)	111.8		Fe(8)-C(114)-H(114)	126.1
O(3A)-C(16A)-H(16B)	111.8		C(114)-C(115)-C(116)	106.4(13)
H(16A)-C(16A)-H(16B)	109.6		C(114)-C(115)-Fe(8)	69.8(7)
C(18)-C(17)-C(21)	109.1(12)		C(116)-C(115)-Fe(8)	69.2(8)
C(18)-C(17)-Fe(2)	70.4(7)		C(114)-C(115)-H(115)	126.8
C(21)-C(17)-Fe(2)	69.9(7)		C(116)-C(115)-H(115)	126.8
C(18)-C(17)-H(17B)	125.5		Fe(8)-C(115)-H(115)	125.7
C(21)-C(17)-H(17B)	125.4		C(117)-C(116)-C(115)	108.7(12)
Fe(2)-C(17)-H(17B)	125.8		C(117)-C(116)-Fe(8)	69.5(8)
C(17)-C(18)-C(19)	106.4(12)		C(115)-C(116)-Fe(8)	69.8(7)
C(17)-C(18)-Fe(2)	69.7(7)		C(117)-C(116)-H(116)	125.6
C(19)-C(18)-Fe(2)	68.2(7)		C(115)-C(116)-H(116)	125.6
C(17)-C(18)-H(18)	126.8		Fe(8)-C(116)-H(116)	126.6
C(19)-C(18)-H(18)	126.8		C(116)-C(117)-C(113)	108.3(13)
Fe(2)-C(18)-H(18)	126.7		C(116)-C(117)-Fe(8)	70.4(8)
C(20)-C(19)-C(18)	109.0(12)		C(113)-C(117)-Fe(8)	70.9(8)
C(20)-C(19)-Fe(2)	70.3(8)		C(116)-C(117)-H(117)	125.8
C(18)-C(19)-Fe(2)	70.7(7)		C(113)-C(117)-H(117)	125.8
C(20)-C(19)-H(19)	125.5		Fe(8)-C(117)-H(117)	124.4
C(18)-C(19)-H(19)	125.5		C(122)-C(118)-C(119)	107.3(12)
Fe(2)-C(19)-H(19)	125.1		C(122)-C(118)-Fe(8)	69.3(7)
C(21)-C(20)-C(19)	106.8(12)		C(119)-C(118)-Fe(8)	70.1(8)
C(21)-C(20)-Fe(2)	70.2(7)		C(122)-C(118)-H(118)	126.4
C(19)-C(20)-Fe(2)	68.9(8)		C(119)-C(118)-H(118)	126.4
C(21)-C(20)-H(20B)	126.6		Fe(8)-C(118)-H(118)	125.8
C(19)-C(20)-H(20B)	126.6		C(120)-C(119)-C(118)	108.8(12)
Fe(2)-C(20)-H(20B)	125.8		C(120)-C(119)-Fe(8)	69.9(7)
C(20)-C(21)-C(17)	108.7(13)		C(118)-C(119)-Fe(8)	69.0(7)
C(20)-C(21)-Fe(2)	69.7(8)		C(120)-C(119)-H(119)	125.6
C(17)-C(21)-Fe(2)	69.8(7)		C(118)-C(119)-H(119)	125.6
C(20)-C(21)-H(21)	125.6		Fe(8)-C(119)-H(119)	127.2
C(17)-C(21)-H(21)	125.6		C(119)-C(120)-C(121)	109.1(12)
Fe(2)-C(21)-H(21)	126.5		C(119)-C(120)-Fe(8)	70.5(7)
C(23)-C(22)-C(26)	108.7(11)		C(121)-C(120)-Fe(8)	69.7(7)
C(23)-C(22)-Fe(2)	71.5(7)		C(119)-C(120)-H(120)	125.5
C(26)-C(22)-Fe(2)	69.6(7)		C(121)-C(120)-H(120)	125.5
C(23)-C(22)-H(22)	125.7		Fe(8)-C(120)-H(120)	125.9
C(26)-C(22)-H(22)	125.7		C(120)-C(121)-C(122)	107.0(12)
Fe(2)-C(22)-H(22)	124.8		C(120)-C(121)-Fe(8)	69.9(7)
C(24)-C(23)-C(22)	106.9(11)		C(122)-C(121)-Fe(8)	68.6(7)
C(24)-C(23)-Fe(2)	69.9(7)		C(120)-C(121)-H(121)	126.5
C(22)-C(23)-Fe(2)	67.7(7)		C(122)-C(121)-H(121)	126.5
C(24)-C(23)-H(23B)	126.6		Fe(8)-C(121)-H(121)	126.5
C(22)-C(23)-H(23B)	126.6		C(118)-C(122)-C(121)	107.8(11)
Fe(2)-C(23)-H(23B)	127.4		C(118)-C(122)-C(123)	128.0(12)
C(23)-C(24)-C(25)	110.0(11)		C(121)-C(122)-C(123)	124.0(12)
C(23)-C(24)-Fe(2)	69.9(7)		C(118)-C(122)-Fe(8)	70.1(7)
C(25)-C(24)-Fe(2)	69.4(7)		C(121)-C(122)-Fe(8)	69.6(6)
C(23)-C(24)-H(24)	125.0		C(123)-C(122)-Fe(8)	122.4(8)
C(25)-C(24)-H(24)	125.0		O(22)-C(123)-C(124)	122.2(12)
Fe(2)-C(24)-H(24)	127.3		O(22)-C(123)-C(122)	118.0(11)

C(24)-C(25)-C(26)	106.4(11)		C(124)-C(123)-C(122)	119.7(12)
C(24)-C(25)-Fe(2)	70.2(7)		C(125)-C(124)-C(123)	121.0(14)
C(26)-C(25)-Fe(2)	68.2(7)		C(125)-C(124)-H(124)	119.5
C(24)-C(25)-H(25)	126.8		C(123)-C(124)-H(124)	119.5
C(26)-C(25)-H(25)	126.8		O(23)-C(125)-C(124)	120.3(13)
Fe(2)-C(25)-H(25)	126.4		O(23)-C(125)-C(126)	115.6(12)
C(22)-C(26)-C(25)	108.1(11)		C(124)-C(125)-C(126)	124.1(14)
C(22)-C(26)-C(27)	126.2(11)		C(125)-C(126)-C(127)	114.6(13)
C(25)-C(26)-C(27)	125.6(11)		C(125)-C(126)-H(12G)	108.6
C(22)-C(26)-Fe(2)	69.1(7)		C(127)-C(126)-H(12G)	108.6
C(25)-C(26)-Fe(2)	70.5(6)		C(125)-C(126)-H(12H)	108.6
C(27)-C(26)-Fe(2)	122.6(8)		C(127)-C(126)-H(12H)	108.6
O(4)-C(27)-C(28)	121.8(12)		H(12G)-C(126)-H(12H)	107.6
O(4)-C(27)-C(26)	117.1(11)		C(126)-C(127)-C(28A)	115.0(15)
C(28)-C(27)-C(26)	121.1(11)		C(126)-C(127)-H(12J)	108.5
C(29)-C(28)-C(27)	119.0(13)		C(28A)-C(127)-H(12J)	108.5
C(29)-C(28)-H(28)	120.5		C(126)-C(127)-H(12K)	108.6
C(27)-C(28)-H(28)	120.5		C(28A)-C(127)-H(12K)	108.5
O(5)-C(29)-C(28)	122.0(12)		H(12J)-C(127)-H(12K)	107.5
O(5)-C(29)-C(30)	117.1(12)		O(24A)-C(28A)-C(127)	118.9(17)
C(28)-C(29)-C(30)	120.9(13)		O(24A)-C(28A)-H(12L)	107.7
C(31)-C(30)-C(29)	112.2(12)		C(127)-C(28A)-H(12L)	107.6
C(31)-C(30)-H(30A)	109.2		O(24A)-C(28A)-H(12M)	107.5
C(29)-C(30)-H(30A)	109.2		C(127)-C(28A)-H(12M)	107.6
C(31)-C(30)-H(30B)	109.1		H(12L)-C(28A)-H(12M)	107.0

Table A.4: Anisotropic displacement parameters ($Å^2 x\ 10^3$) for $FcCOCH_2CO(CH_2)_3OH$. The anisotropic displacement factor exponent takes the form: $-2\pi^2[\ h^2 a^{*2} U^{11} + ... + 2\ h\ k\ a^*\ b^*\ U^{12}\ ]$

U^{11}	U^{22}		U^{33}	U^{23}	U^{13}	U^{12}
Fe(1)	25(1)	19(1)	24(1)	0(1)	-3(1)	-2(1)
Fe(2)	26(1)	19(1)	25(1)	-2(1)	-1(1)	-1(1)
Fe(3)	19(1)	20(1)	23(1)	0(1)	-3(1)	0(1)
Fe(4)	26(1)	19(1)	25(1)	-1(1)	-3(1)	3(1)
Fe(5)	21(1)	21(1)	21(1)	2(1)	-1(1)	2(1)
Fe(6)	22(1)	17(1)	25(1)	1(1)	-4(1)	-1(1)
Fe(7)	25(1)	20(1)	27(1)	-2(1)	-5(1)	1(1)
Fe(8)	26(1)	19(1)	27(1)	-2(1)	1(1)	1(1)
O(1)	32(5)	36(5)	29(4)	7(4)	-1(4)	3(4)
O(2)	27(5)	36(5)	43(6)	13(4)	4(4)	1(4)
O(3A)	60(20)	43(6)	44(10)	7(6)	-6(17)	23(12)
O(3B)	60(20)	43(6)	44(10)	7(6)	-6(17)	23(12)
O(4)	27(5)	28(5)	44(6)	2(4)	3(4)	4(4)
O(5)	41(6)	30(5)	39(6)	6(4)	4(4)	4(4)
O(6A)	68(13)	41(12)	100(18)	32(12)	-24(12)	-18(10)
O(6B)	80(20)	44(11)	54(16)	2(12)	-2(14)	-38(14)
O(7)	22(5)	33(5)	30(5)	8(4)	-3(4)	-1(4)
O(8)	39(6)	36(5)	37(5)	12(4)	-1(4)	-1(4)
O(9A)	110(30)	33(7)	55(13)	-3(8)	8(14)	-17(11)
O(9B)	50(50)	60(30)	20(20)	-15(19)	-10(20)	-20(30)
O(10)	33(6)	26(5)	45(6)	4(4)	6(4)	4(4)
O(11)	31(5)	30(5)	43(6)	12(4)	-1(4)	4(4)
O(12A)	100(20)	42(10)	83(17)	0(11)	3(15)	25(12)
O(12B)	80(16)	21(11)	44(13)	15(9)	10(11)	10(10)
O(13)	20(5)	36(5)	42(5)	-1(4)	-2(4)	3(4)
O(14)	28(5)	40(6)	42(6)	-8(4)	-6(4)	-5(4)
O(15A)	60(50)	44(12)	60(20)	11(12)	20(30)	14(18)
O(15B)	20(20)	35(8)	47(13)	-4(8)	12(14)	12(10)

O(16)	16(5)	35(5)	40(5)	-4(4)	-1(4)	2(4)
O(17)	42(6)	39(6)	33(6)	-1(4)	3(5)	0(4)
O(18A)	43(16)	48(10)	73(16)	-19(10)	-21(11)	-19(10)
O(18B)	31(12)	39(12)	66(15)	-18(10)	1(9)	-5(9)
O(19)	21(5)	41(5)	35(5)	-9(4)	-1(4)	-1(4)
O(20)	43(6)	39(6)	43(6)	-11(5)	9(5)	2(4)
O(21A)	10(10)	31(5)	45(7)	-2(5)	-13(8)	5(6)
O(21B)	10(10)	31(5)	45(7)	-2(5)	-13(8)	5(6)
O(22)	26(5)	33(5)	42(6)	6(4)	-13(4)	8(4)
O(23)	53(6)	27(5)	41(6)	3(4)	-6(5)	-5(4)
O(24A)	70(15)	35(12)	71(17)	29(11)	-40(13)	-10(11)
O(24B)	110(30)	44(10)	90(19)	14(12)	-26(16)	-24(13)
C(1)	36(8)	25(5)	37(7)	-6(5)	2(5)	-19(5)
C(2)	36(7)	21(5)	37(7)	-4(4)	3(6)	-2(5)
C(3)	22(7)	30(6)	27(5)	-1(4)	-6(5)	1(5)
C(4)	22(7)	39(7)	25(5)	-4(5)	-9(5)	0(5)
C(5)	27(7)	49(8)	35(7)	-18(6)	0(5)	-18(5)
C(6)	18(6)	28(6)	22(5)	1(4)	-3(4)	-3(4)
C(7)	34(7)	24(6)	24(6)	2(4)	-7(5)	-6(4)
C(8)	29(7)	17(5)	31(6)	1(4)	-7(5)	-1(4)
C(9)	17(6)	24(5)	32(6)	-2(4)	-9(5)	-3(4)
C(10)	15(6)	26(6)	25(5)	-4(4)	-4(4)	0(4)
C(11)	29(7)	23(6)	19(5)	-8(4)	-2(5)	5(5)
C(12)	17(7)	34(7)	29(6)	-2(5)	-1(5)	0(5)
C(13)	24(7)	30(7)	27(6)	-6(5)	3(5)	3(5)
C(14)	29(8)	38(7)	31(6)	6(5)	5(5)	5(6)
C(15)	54(10)	34(7)	35(7)	-2(6)	-9(6)	11(6)
C(16A)	76(13)	50(8)	33(8)	-2(6)	-18(8)	13(8)
C(16B)	76(13)	50(8)	33(8)	-2(6)	-18(8)	13(8)
C(17)	38(8)	29(6)	25(5)	-3(5)	0(5)	-2(5)
C(18)	29(7)	36(7)	24(6)	-4(5)	5(5)	-6(5)
C(19)	43(8)	36(7)	28(6)	-3(5)	1(5)	14(5)
C(20)	58(9)	19(5)	39(7)	-6(4)	16(6)	-12(5)
C(21)	32(7)	33(7)	37(7)	-15(5)	1(5)	-11(5)
C(22)	18(6)	26(6)	38(6)	-11(4)	-5(5)	-6(5)
C(23)	27(7)	33(6)	24(5)	-6(4)	-8(5)	8(5)
C(24)	34(7)	31(6)	20(5)	1(4)	1(4)	0(5)
C(25)	15(6)	26(6)	34(6)	-2(5)	6(4)	4(4)
C(26)	22(7)	20(5)	32(6)	-3(4)	0(4)	-3(4)
C(27)	13(6)	22(5)	32(6)	-5(4)	4(5)	5(4)
C(28)	23(7)	30(6)	35(7)	-3(5)	2(5)	0(5)
C(29)	38(8)	28(6)	30(6)	-8(5)	1(5)	5(5)
C(30)	58(10)	29(7)	40(7)	-4(6)	-4(7)	-11(6)
C(31)	79(12)	37(8)	39(7)	2(7)	-1(8)	-22(8)
C(32A)	61(11)	49(8)	50(9)	2(7)	-4(7)	-25(8)
C(32B)	61(11)	49(8)	50(9)	2(7)	-4(7)	-25(8)
C(33)	32(7)	24(5)	32(6)	-10(4)	-6(5)	-2(5)
C(34)	29(7)	28(6)	32(6)	-7(5)	1(5)	-6(4)
C(35)	26(7)	27(6)	35(6)	-5(4)	-17(5)	0(5)
C(36)	26(7)	33(6)	26(5)	-6(4)	-5(5)	-3(5)
C(37)	30(7)	37(7)	31(6)	-11(5)	-2(5)	4(5)
C(38)	38(7)	24(6)	19(5)	0(4)	-4(5)	2(5)
C(39)	21(6)	24(5)	27(6)	1(4)	0(5)	1(4)
C(40)	36(8)	17(5)	33(7)	4(4)	1(5)	-3(4)
C(41)	14(6)	27(6)	29(6)	-2(4)	-6(4)	-6(4)
C(42)	27(7)	21(5)	24(5)	-3(4)	-9(4)	-4(4)
C(43)	16(6)	22(6)	20(5)	-7(4)	-6(4)	1(4)
C(44)	12(6)	35(6)	23(6)	-2(4)	0(4)	1(4)
C(45)	25(7)	24(6)	29(6)	-1(5)	-13(5)	-4(5)
C(46)	26(8)	36(7)	41(7)	10(6)	-11(6)	-7(5)

C(47)	73(13)	71(10)	41(8)	-11(8)	8(8)	-39(9)
C(48A)	59(11)	42(8)	38(8)	-8(7)	12(7)	-13(7)
C(48B)	59(11)	42(8)	38(8)	-8(7)	12(7)	-13(7)
C(49)	36(8)	25(6)	27(5)	-1(5)	-5(5)	1(5)
C(50)	27(7)	34(7)	33(6)	1(5)	-16(5)	-2(5)
C(51)	39(8)	33(7)	30(7)	-9(5)	-1(5)	-11(5)
C(52)	41(8)	23(5)	34(7)	-5(4)	-3(6)	5(5)
C(53)	44(8)	26(6)	33(6)	-8(5)	4(5)	9(5)
C(54)	27(7)	25(6)	31(6)	-8(4)	0(5)	8(5)
C(55)	33(8)	29(7)	31(5)	-4(5)	-4(5)	-6(5)
C(56)	46(8)	27(6)	24(5)	1(5)	-13(5)	4(5)
C(57)	32(7)	27(6)	27(6)	-4(4)	-6(5)	3(5)
C(58)	21(7)	22(5)	29(6)	0(4)	-6(5)	4(4)
C(59)	29(7)	18(5)	30(6)	-5(4)	0(5)	4(4)
C(60)	23(7)	32(6)	34(7)	1(5)	-3(5)	8(5)
C(61)	32(8)	32(7)	35(7)	-4(5)	-1(6)	9(5)
C(62)	33(8)	32(7)	37(7)	2(6)	-1(6)	2(6)
C(63)	84(14)	49(10)	39(8)	-3(8)	-10(8)	29(9)
C(64A)	72(12)	55(9)	37(8)	5(7)	-4(7)	18(8)
C(64B)	72(12)	55(9)	37(8)	5(7)	-4(7)	18(8)
C(65)	35(8)	23(5)	45(7)	9(5)	-14(6)	-1(5)
C(66)	31(8)	40(7)	44(7)	24(5)	5(6)	2(5)
C(67)	27(8)	47(8)	22(5)	8(5)	-3(5)	16(6)
C(68)	33(7)	34(6)	26(6)	0(5)	-18(5)	9(5)
C(69)	17(6)	25(6)	37(6)	1(5)	-6(5)	15(4)
C(70)	19(6)	27(6)	21(5)	3(4)	-2(4)	1(4)
C(71)	37(7)	21(5)	28(6)	-1(4)	0(5)	-8(5)
C(72)	28(8)	28(6)	32(7)	2(5)	-6(5)	16(5)
C(73)	11(6)	32(6)	32(6)	7(5)	-7(4)	10(4)
C(74)	17(6)	29(6)	16(5)	7(4)	-5(4)	-1(4)
C(75)	17(6)	23(6)	26(6)	9(4)	-2(5)	-2(4)
C(76)	22(7)	21(6)	36(7)	5(4)	-6(5)	7(5)
C(77)	6(6)	32(7)	33(6)	4(5)	-2(5)	3(5)
C(78)	21(7)	31(7)	31(6)	-1(5)	-6(5)	-2(5)
C(79)	62(12)	42(7)	37(7)	9(6)	9(7)	19(7)
C(80A)	50(10)	40(7)	31(7)	-1(6)	0(6)	10(6)
C(80B)	50(10)	40(7)	31(7)	-1(6)	0(6)	10(6)
C(81)	33(7)	30(6)	27(6)	2(5)	-11(5)	-1(5)
C(82)	18(6)	26(6)	34(7)	1(5)	-8(5)	5(4)
C(83)	29(7)	27(5)	35(7)	8(4)	-4(5)	3(5)
C(84)	26(7)	40(7)	30(6)	13(5)	3(5)	2(5)
C(85)	41(8)	38(7)	20(5)	5(5)	-2(5)	5(6)
C(86)	7(6)	37(6)	25(6)	0(4)	-6(4)	3(4)
C(87)	28(7)	33(6)	23(5)	2(5)	-12(4)	2(5)
C(88)	39(8)	27(6)	24(5)	0(4)	10(5)	4(5)
C(89)	33(7)	21(5)	29(6)	5(4)	2(5)	-2(5)
C(90)	21(7)	25(5)	28(6)	6(4)	-3(5)	3(4)
C(91)	14(6)	24(5)	31(6)	8(4)	-5(5)	11(4)
C(92)	33(8)	29(6)	35(7)	-2(5)	-4(5)	-7(5)
C(93)	39(8)	27(6)	32(7)	8(5)	-3(6)	1(5)
C(94)	69(11)	37(8)	39(7)	-5(6)	1(7)	-15(7)
C(95)	66(13)	72(11)	46(8)	8(8)	-12(9)	-36(9)
C(96A)	42(10)	62(9)	50(9)	-8(8)	0(7)	-18(8)
C(96B)	42(10)	62(9)	50(9)	-8(8)	0(7)	-18(8)
C(97)	60(10)	35(6)	43(8)	9(5)	9(7)	20(6)
C(98)	42(8)	28(6)	34(7)	1(4)	-4(6)	-8(5)
C(99)	47(8)	38(7)	26(6)	3(4)	4(5)	8(6)
C(100)	53(9)	36(7)	34(6)	7(5)	-26(6)	-7(6)
C(101)	21(7)	66(9)	59(9)	31(7)	-8(6)	10(6)
C(102)	28(7)	29(6)	27(6)	1(4)	-6(4)	0(5)

C(103)	33(7)	24(6)	34(7)	-1(5)	-7(5)	10(5)
C(104)	52(9)	24(5)	35(7)	0(5)	-12(6)	-4(5)
C(105)	24(7)	25(6)	35(6)	2(4)	-12(5)	-7(5)
C(106)	22(7)	24(5)	24(5)	3(4)	-5(4)	-1(4)
C(107)	29(7)	30(7)	26(6)	3(5)	-7(5)	4(5)
C(108)	7(6)	25(6)	33(6)	-1(4)	-4(5)	1(4)
C(109)	29(7)	18(6)	32(6)	4(4)	-4(5)	4(5)
C(110)	39(8)	24(6)	27(6)	0(5)	1(5)	-3(5)
C(111)	61(11)	27(6)	35(7)	9(5)	-22(6)	-7(6)
C(12A)	48(11)	32(7)	47(8)	-4(6)	-22(7)	0(6)
C(12B)	48(11)	32(7)	47(8)	-4(6)	-22(7)	0(6)
C(113)	34(7)	39(7)	30(6)	-3(5)	11(5)	-3(6)
C(114)	23(7)	34(7)	30(5)	-4(5)	-4(5)	7(5)
C(115)	27(7)	38(7)	48(7)	-22(5)	5(5)	-8(5)
C(116)	65(10)	18(5)	38(7)	-9(4)	22(7)	-1(5)
C(117)	45(8)	37(7)	29(7)	-3(5)	-1(6)	18(5)
C(118)	32(7)	29(6)	29(6)	-7(4)	-3(5)	-3(5)
C(119)	35(7)	28(7)	25(5)	-8(4)	-7(5)	6(5)
C(120)	30(7)	31(6)	28(5)	-6(5)	7(5)	2(5)
C(121)	27(7)	27(6)	33(6)	-10(5)	2(5)	3(5)
C(122)	28(7)	21(5)	31(6)	-8(4)	0(5)	-2(4)
C(123)	24(7)	23(5)	35(7)	-7(4)	3(5)	4(5)
C(124)	30(7)	29(6)	38(7)	-4(5)	4(5)	-2(5)
C(125)	49(9)	34(7)	29(7)	-7(5)	-3(6)	-3(6)
C(126)	44(9)	27(7)	45(8)	-8(6)	2(7)	1(6)
C(127)	70(13)	58(10)	47(9)	-5(8)	12(9)	-26(9)
C(28A)	60(11)	56(9)	53(9)	11(7)	-9(7)	-27(8)
C(28B)	60(11)	56(9)	53(9)	11(7)	-9(7)	-27(8)

I, Lydia Siegert, declare that the dissertation/thesis hereby handed in for the qualification Magister Scientiae in Chemistry at the University of the Free State is my own independent work and that I have not previously submitted the same work for a qualification at/in another university/faculty. I furthermore cede copyright of the thesis in favour of the University of the Free State.

Ek, Lydia Siegert, verklaar dat die verhandeling wat hierby vir die kwalifikasie Magistergraad (Chemie) aan die Universiteit van die Vrystaat deur my ingedien word, my selfstandige werk is en nie voorheen deur my vir 'n graad aan 'n ander universiteit / fakulteit ingedien is nie. Ek doen voorts afstand van die outeursreg in die verhandeling ten gunste van die Universiteit van die Vrystaat.

Lydia Siegert

1 February 2016